Nanoemulsion-like Polymersomes for Nanoreactors

A DISSERTATION
SUBMITTED TO THE FACULTY OF THE GRADUATE SCHOOL
OF THE UNIVERSITY OF MINNESOTA
BY

Soonyong So

IN PARTIAL FULFILLMENT OF THE REQUIREMENTS
FOR THE DEGREE OF
DOCTOR OF PHILOSOPHY

Advisor: Timothy P. Lodge

July 2015

Acknowledgements

The past five years of my life has been a journey of emotions, strength and learning. It was a tragic moment when I had to experience the loss of my grandfather. Moreover, my father's severe illness at the time period made me go through a rough phase. My faith in God has helped me recover from this difficult time, but without the help and support from some important people in my life, I would not have been able to stand where I am today.

First and foremost, I wish to express my sincere gratitude to my advisor, Professor Timothy P. Lodge, for his patience, guidance and encouragement through all of my graduate studies. Through him, I have learn how to conduct scientific research, and how to be a good researcher and leader. I will never forget the time he encouraged and helped me, when I was overwhelmed and frustrated by difficulties and surrounding pressures. It has been a great honor to learn from him. I also appreciate the thoughtful comments of preliminary and final exam committees, Professors Christopher W. Macosko, Joseph A. Zasadzinski, Marc A. Hillmyer and Kevin D. Dorfman.

I would like to thank Letitia J. Yao for helping me conduct NMR experiments. She has been a great support in resolving technical issues as well as guiding me through NMR analysis and answering any questions that I had. I also would like to thank Itaru Asano, Takeshi Ueki and Sujay Chopade for the great collaborations.

Being a part of the polymer group and the Lodge group, has enhanced my graduate school experience. All the helpful discussions and interactions with the members of the aforementioned groups, have been very educative and productive. Zhifeng Bai patiently mentored me in my project during my first year in graduate school. I thank Keun Hyung Lee, Lucas McIntosh, Sangwoo Lee, Yuanyan Gu, Sangwon Lee, Intaek Lee, Karen Haman and Sipei Zhang for their tremendous help in the lab during my first year in

graduate school. I have also greatly benefited from the helpful discussions and support from Matt Irwin, Robert Hickey, Jae-Hong Choi, Jennifer Laaser, In-Woo Cheong, Joseph Lott, Seyoung Jung, Yuanchi Ma, and other former and current members. I am also glad to have become great friends with Jie Lu, Christopher Thurber and John McAllister. We started as first years in the Lodge group and it has been a memorable experience to share this journey together. Itaru Asano, Sujay Chopade, Yiming Zhang and Aakriti Kharel have been good friends with me. I thank you all for a lot of good memories spent together.

I also would like to thank Pastors Lowell Busman and Kathleen Macosko at Stadium Village Church for their encouragement and prayers.

In the end, I would like to thank my parents, sisters and my brother for their tremendous love and support. Without their prayers and support, I would not have been able to accomplish this journey. Therefore, I dedicate this thesis to them.

To my family

Abstract

Self-assembly of block copolymers in various selective solvents provides a means to control nanostructures. Among selective solvents, ionic liquids (ILs) are of great interest as reaction media, with the possibility of replacing organic solvents. However, the implementation ILs is limited by their high viscosity and cost. Phase transfer of IL-filled polymer vesicles (polymersomes) from the IL phase to water produces a very stable kind of "nanoemulsion." Nanoemulsion-like polymersomes have great potential as they confine a catalyst within the interiors, thus mitigating the mass transfer limitations of ILs while simultaneously providing a facile route to quantitative catalyst recovery

The issues in the nanoreactor system and the mechanism of the phase transfer in the biphasic system are discussed. First, a new reversible reaction process with the thermo-responsive shuttling of the IL-filled polymersomes between the phases was designed. In nanoreactor applications, a narrowly distributed, small vesicle size is required. The size of polymersomes having rubbery and glassy membranes was controlled through mechanical and kinetic approaches. In the mechanical approach, the extrusion method was employed. For the kinetic approach, the amount of co-solvent and the hydrophilic fraction of amphiphilic block copolymer were varied and its effects on the size and dispersity were studied. Transport phenomena across the glassy and rubbery bilayer membranes was elucidated by NMR techniques to quantify the mobility inside and outside the polymersomes, plus the rate of exchange through the membrane. The dependence of the membrane thickness, glass transition temperature of the membranes and the partition coefficient of tracer molecules in the IL/water were also examined. We demonstrated a general boundary for the phase transfer of polymersomes in terms of a reduced tethering density for poly(ethylene oxide) (PEO), and analyzed the phenomena thermodynamically. The tethering density can be increased by increasing the block length

of PEO and the size of the polymersomes, and the increased tethering density induces the phase transfer. Interfacial tension-related phase transfer led to develop a novel separation method in the biphasic system of the IL and water. By controlling the interfacial tension between the hydrophobic membrane and water, worm-like micelles and polymersomes were successfully separated.

Table of Contents

List of Figures

List of Tables

List of Schemes

Chapter 1

Introduction

1.1 Nanoreactors

A nanoreactor is defined as a confined container for chemical reactions, less than 1 μm in diameter.[1] Reactions in nanoscale compartments can be found abundantly in nature. For example, a cell has more than 20 of organelles more than 20 including lysosomes, ribosomes, endoplasmic reticulum, and mitochondria.[2] Each of the organelles has their own intricate functions, and works together for a living cell under contact with the cytosol.[3] Reactions in biological systems are well controlled in terms of efficiency and precision by selective transportation of substances for membrane-enclosed organelles like lysosome, and by site-specific reactions for protein complexes like ribosomes.[1,4]

Biomimetic nanoscale reactors are highly desirable to understand the biological reactions better,[5] and to utilize the advantages of nature's nanoreactors that enable the synthetic reactions to be maximized in terms of the precision and efficiency.[6–8] Self-assembled micelles and vesicles,[9–11] dendrimers,[12] and inorganic nanocarriers[13] are examples of biomimetic nanoreactors recently developed. Compartmentalization and confinement of reaction components is a key feature of the nanoreactors, which can improve reaction efficiency and selectivity by preventing interference from other substances. For example, the semi-permeable shell compartment (*e.g.* bilayer membrane of polymersomes) of the nanoreactors can allow transmembrane diffusion of small reagents and products while keeping the large catalysts inside. These size exclusive membranes are beneficial towards biological and conventional chemical reactions because they can confine the chemical reaction space within the nanoreactors and protect

the catalytic activity from the environment. Anisur *et al*. developed a hollow silica nanosphere having 1 nm pores, and a manganese oxide catalyst layer on the inner surface of the hollow.[5] They showed that the reaction was significantly reactant-size selective, as consequence of size exclusive permeation of reactant molecules through the nanosphere-like molecular sieve. When the R group of aldehyde was changed from phenyl to 3,5-dibenzyloxyphenyl group, the reaction yield was less than 10%, whereas the yield was over 95% with benzaldehyde.

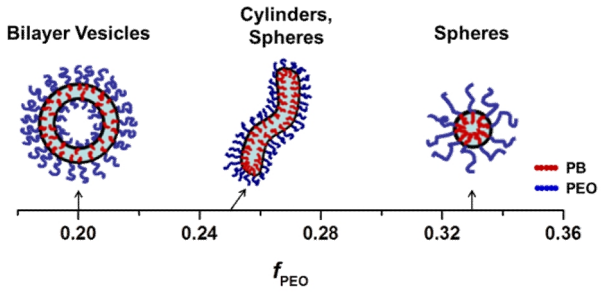

Figure 1–1. Phase diagram with morphology schemes depending on volume fraction of hydrophilic poly(ethylene oxide) block for 1,2-polybutadiene-*b*-poly(ethylene oxide) (PB–PEO) having 9 kDa PB block in an ionic liquid (1.0 wt %) at 25 °C.[14]

Another remarkable feature of nanoreactors is the high surface-to-volume ratio from nano-sized confined reactor. The large surface-to-volume ratio of the nanosized container is effective in heat exchange with its environment when the nanoreactors are dispersed in media,[15] and increases the reaction rate by shortened mean free path within the container which generates more frequent collisions with molecules.[2,16] Chiu *et al*. studied the collision frequency of two hard spheres, representing a single substrate and a single enzyme, as a function of vesicle size by a Brownian dynamics Monte Carlo simulation.[25] The collision frequency increased by a factor of 10, when the radius of vesicle decreased from around 35 to around 20 nm. As a consequence of increased collision frequency, higher reaction rate can be expected with reduced size of nanoreactors.[17] In polymer

vesicles, the rate constant of enzyme catalyzed reactions, which follow Michaelis–Menten kinetics, increased as the size of vesicle decreased due to increased collision frequency between catalysts and substrates.[18–21]

Polymeric nanoreactors, consisting of amphiphilic block copolymers, have attracted increased attention for nanoreactors due to the tunable function and morphology by designing of block copolymer chemistry.[22–26] Depending on the volume fraction of the hydrophilic block, various assemblies can be formed in a selective solvent. For example, the amphiphilic block copolymer, 1,2-polybutadiene-*b*-poly(ethylene oxide) (PB–PEO) in an ionic liquid varies from micelles to vesicles as the fraction of PEO block decreases, as shown in Figure 1–1. The hydrophilic block stabilizes the nano-assemblies as a dispersed phase, and the hydrophobic block provides hydrophobic core for micelles, and physical membrane exhibiting confined interiors providing room to load hydrophobic active substances, *e.g.* catalysts, and reactants.[27,28] Furthermore, the compartmentalized internal space of vesicles can be used to encapsulate and deliver hydrophilic active materials.[29–31] The use of polymer micelles and vesicles in nanoreactor applications is related to the way their core properties (*i.e.* permeability for vesicles), which can be controlled and tuned by a precise molecular design of the constituting blocks. In this regard, polymeric nanoreactors have flexibility and versatility from readily tunable parameters such as block length, chemical structure, and functionality.[32]

Block copolymers assemblies have been applied as "designer" nanoreactors, and widely studied for many reactions from small molecule organic reactions to polymerization. In general, catalyst is confined into the nanostructure, and reactants and products in the dispersed medium diffuse into nanoreactors, then diffuse out after the reaction. Lipshutz and co-workers demonstrated a micellar nanoreactor composed of hydrophilic and hydrophobic blocks linked by a moiety capable of covalent linkage to a pendant catalyst for various reactions, such as ring-closing metathesis,[33] Heck-coupling

reactions.[34,35] The isolated core for reaction, and confined catalyst yield higher conversion of the reaction, and increased cycle number of catalyst. Polymerization was also demonstrated in an aqueous micelle solution of poly(dimethylacrylamide)-*b*-poly(*N*-isopropylacrylamide) (PDMA–PNIPAm).[36] Polystyrene (PS) nanoparticles were produced through reversible addition-fragmentation chain transfer (RAFT) with a PNIPAm macro chain transfer agent (PNIPAm–CTA). Narrowly dispersed PS around $Đ \sim 1.1$ could be obtained with the controlled molecular weight. One of the noticeable features of this system is the thermoresponsive PNIPAm block. Lower critical solution temperature (LCST) behavior of PNIPAm in water enable the reactants to be loaded into the reactor effectively above the LCST, and the product, PS nanoparticles to be separated and stabilized in water after the reaction below the LCST.[37]

Stimuli-responsive moieties in nanoreactors provide an additional feature, in that the nanoreactors can communicate with their environment effectively to regulate reactions by controlling the permeation behavior of molecules. At specific conditions (*i.e.* pH,[38] temperature,[39] concentration[40]), the stimuli-responsive blocks alter their solubility, leading to morphology or permeability changes. Yu and co-workers demonstrated pH sensitive polymer vesicles with poly(ethylene oxide)-*b*-polystyrene-*b*-poly(2-diethyl aminoethyl methacrylate) (PEO-*b*-PS-*b*-PDEA) block copolymers.[41] The PDEA block is soluble in acidic water, but it is not soluble when the pH exceeds the neutral range. This pH sensitive PDEA block in the vesicle membrane swelled under acidic conditions, and the permeation of H^+ was allowed through the polymer membrane. The acidic condition of vesicle interiors can be controlled simply with the pH of medium. Multiple stimuli-responsive vesicles have been also proposed by incorporating pH sensitive, and sugar reactive poly(styrene boronic acid) (PSBA) blocks into membrane of PS–PEO vesicles.[42] The solubility of PSBA in water increases after the transformation of boronic acid group to boronate group under high pH, or in the presence of sugar, such as

D-glucose. pH and sugar sensitive PSBA were removed from the vesicles for the molecular level holes in the vesicle membrane. The vesicles with the small holes were used to demonstrate enzyme catalyzed hydrolysis. Since the hole size is in the molecular level, only substrates permeated through the membrane, while relatively big enzyme was well protected even by etched membranes.

Nanoreactors, especially vesicle nanoreactors, in the aqueous phase extensively studied with heterogeneous, and enzyme catalysis, because they cannot accommodate water insoluble catalyst, such as transition metal catalyst, into the interiors, which is aqueous as the medium.[23,43] Therefore, canonical vesicles have limitations both in terms of type of reactions, and in product separation after reaction. Conventionally, a catalyst can be loaded into vesicles during the self-assembly of amphiphilic surfactants in an aqueous solvent, and the catalyst for the reaction can reside in both interior and exterior of the vesicles.[44] Effective encapsulation of catalysts is required for the nanoreactor system to avoid undesired reaction in the vesicle exterior. For effective loading into the interior, filtration or dialysis is used as an additional process to remove the active species in the medium of vesicle solution, so that the reaction is conducted only in the confined interior of the nanosized vesicles. Moreover, the products should be selectively separated from the aqueous catalysis phase because the reaction locus is also aqueous.

In this thesis, a new nanoreactor system, which is potentially applicable in versatile chemical reactions, is proposed with combinations of ionic liquid and thermoresponsive block copolymers.

1.2 Ionic Liquids as Reaction Media

Environmentally benign and cost effective processes are in high demand for the chemical industry. One of the key parameters to quantify the eco-efficiency of a process is the

environmental waste factor (E factor). It is defined as the amount of waste produced relative to the desired material.[45] Typical E factors for fine-chemical and pharmaceutical industries are in the range of 5 to 100, largely attributable to volatile organic solvents and catalyst waste.[46] The E-factor can be reduced by reusing catalysts, or replacing organic solvent based system to supercritical fluid based,[47] water-based or dry-media-based (solvent-free) reactions.[48] Ionic liquids (ILs) are non-volatile near ambient temperatures and therefore are promising candidates to replace volatile organic solvents, though recently it has been reported that some aprotic IL can be distilled at high temperatures (200 – 300 °C) and very low pressure (< 0.07 mbar).[49] Chemical processes implementing non-volatile ILs would minimize the pollution arising from the use of the organic solvents.

ILs are known as molten salts because they have low melting points (T_m), often below 100 °C, and are composed only of ions.[50] The interaction between the bulky, charge delocalized cations and anions of IL is relatively weak compared to generic salts like NaCl. Wilkes and co-workers investigated T_m of a series of salts by varying the alkyl chain length of dialkylimidazolium. NaCl melts at about 800 °C, but by replacing the cation with 1-ethyl-3-methylimidazolium ([EMIM]), and 1-butyl-3-methyl-imidazolium ([BMIM]), the melting point of the resultant salt decreases to around 85 and 67 °C, respectively.[51] ILs with [BMIM] cation and polyatomic anions, such as PF_6^-, CF_3COO^- ([triflate]), and $(CF_3SO_2)_2N^-$ ([TFSI]) exhibit lower melting points of 11, 13, –2 °C, respectively.[52] The difference between the T_m of [triflate] and [TFSI] can be explained by the delocalization of the electrons in [TFSI], which is absent in the non-symmetric [triflate] anion.[53] It is difficult to predict the exact physical properties of an IL system, including melting point, owing to the multiple interactions such as Coulombic interaction, van der Waals interaction, and also hydrogen bonds.[54] However, various

room temperature ILs can be designed or synthesized by combining typical organic cation and polyatomic anions, as shown in Figure 1–2.

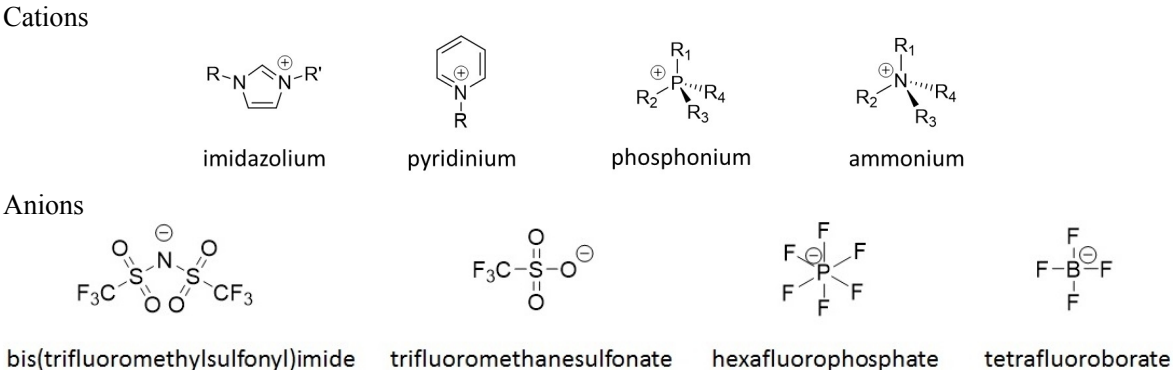

Figure 1–2. Chemical structures of typical cations and anions for ILs.

Besides the favorable non-volatile character, ILs offer wide processing temperature windows (up to ~ 400 °C), high tunability by the selection of cation and anion, versatile solvation ability from organic to inorganic compounds, and high polarity and viscosity. In many chemical reactions, such as acylation and esterification, ILs serve as catalyst in addition to being a solvent for the reaction system. Furthermore, ILs can also form biphasic or multiphasic systems with water and organic solvents.

Careful selection of the cations and the anions allows tuning the intermolecular interactions between ILs and solutes, including dipolar, dispersive, ionic interaction and hydrogen bonding, and thereby improving the solvation ability of the IL. For example, the anion affects the water–IL miscibility. Water is not miscible with [BMIM][PF_6], [BMIM][TFSI], and [EMIM][TFSI],[55] but water dissolves well in [BMIM][Cl], [BMIM][BF_4], and [EMIM][triflate].[56,57] Cammarata *et al.* demonstrated that hydrogen bonding strength between anions and water is the main origin of miscibility.[58] Cations, however, can tune the polarity of ILs, and longer alkyl chains on cations can dissolve less

polar organic solvent.[59] There are methods, such as solvatochromism of Reichardt's dye[60,61] and Rohrschneider-McReynolds gas-liquid chromatography to scale the polarity of ILs,[62] which is generally considered as a parameter to determine the solvation ability of the solvents. However, most of the ILs fall into the polarity range of alcohols,[63] which is not sufficient to explain the different solvation behavior of ILs.[64] Anderson and co-workers used the solvation model suggested by Abraham with three interaction parameters, dipolarity, hydrogen bond, and dispersion forces to characterize the solvation interactions of various ILs.[65] The Abraham model categorizes the ILs based on their interaction parameters and explains the experimental results that cannot be explained by examining polarity alone.

The solvation of catalysts in ILs to perform various organic reactions is particularly interesting. Due to the polar and electronic characters of ILs, many transition metal complexes can be dissolved in ILs at sufficient concentration for homogenous catalysis.[66] In 1972, Parshall first reported hydrogenation of ethylene and cyclododecatriene in tetraalkylammonium based ILs with $PtCl_2$ as catalyst.[67] Then, various catalytic schemes have been demonstrated, such as Friedel-Craft reactions,[68] hydrogenation,[69] Diels-Alder reactions,[70] Baylis–Hillman reactions,[71] palladium-catalyzed Suzuki cross-coupling reactions,[72] catalytic oxidation, and acid-base catalyzed reactions.[64] In many cases, ILs can stabilize the transition state of catalysts, and lead to better performance in terms of reaction rate, and selectivity of product. Furthermore, it was reported that certain enzymes can be dissolved in ILs, and sometimes shows better reaction yields than in organic solvent.[73] Unlike in polar solvents such as methanol, polar enzymes are not deactivated in ILs, even though the polarity of ILs are similar to methanol.[74] Catalysis in ILs has another advantage that they can form bi-, or multiple phasic systems with water and other organic solvents, whereby recycling of catalyst and IL are possible.

As water or organic solvent soluble materials can be easily extracted and separated from the IL phase, the immobilized homogeneous catalysts in ILs are recyclable.[75,76] Peng *et al*. reported hydroxylation of benzene to phenol in a biphasic system of IL and water.[77] The oxidant hydrogen peroxide was dissolved in the aqueous phase, but the catalyst, dodecanesulfonate salt with Fe^{3+}, Co^{2+}, Cu^{2+}, and Ni^{2+} cations, was only isolated in the IL phase. Two immiscible phases were stirred, and phase-separated after the reaction. The water-favorable product phenol stayed in the aqueous phase, but the catalyst was recovered from the IL. In addition to the enhanced reaction conversion, and selectivity of desired product compared to the system with organic solvent, biphasic catalysis with ILs has the notable advantages that the recovery of catalysis in IL, and the separation of the product can be conducted simultaneously without the use of volatile organic solvents. The simply separated catalyst in IL can be recycled many times with the constant catalytic performance without any modification of chemical structures, which is necessary for immobilized catalysts.[78]

Immobilization of IL is another way to utilize a biphasic system.[79,80] The Buchmeiser group developed a continuous process with an immobilized IL, 1-butyl-2,3-dimethylimidazolium tetrafluoroborateionic ([BDMIM][BF_4]) for ring-closing metathesis with high turnover numbers. [BDMIM][BF_4] containing Ru complex catalyst was adsorbed on monolithic supports and immobilized in a packed column.[81] Through the column, the IL immiscible organic phase containing reactants flew continuously, and the final product eluted with the organic flow after the reaction in the IL phase without leaching out the IL.

There are also disadvantages of ILs as reaction media. Most ILs are expensive, and their viscosity is high (10 – 10^3 mPa·s at 25 °C), which decreases rates of mass transfer in catalytic applications and charge movement in electrochemical applications.[82] Diffusion

in ILs (~ 10^{-11} m^2/s) is usually 100 times slower than in the aqueous and organic solvents (~ 10^{-9} m^2/s).[83,84]

ILs, however, still have significant advantages not only for chemical reactions, but also for other applications, such as electrochemical applications, separation processes, lubricants, and bio-related applications due to their advantages discussed in this section. Furthermore, using high tunablility, various studies are on-going to solve toxicity, high viscosity, and expense of ILs. Recently, it was reported that the IL aggregates can be stabilized by block copolymer surfactants in water, whereby the viscosity of the system decreased significantly by requiring less volume of the IL.[85]

1.3 Phase Transfer of Micelles and Vesicles

In a biphasic system composing of two immiscible fluids, the distribution of a dissolved or a well-dispersed compound is determined by the partition coefficient of the species between the two fluids.[86,87] The compound can transfer from one phase to the other phase, if the partitioning is reversed, and it is called "phase transfer," or "shuttle" when it is reversible.[88–90]

A commercial example is phase transfer catalysis using a quaternary ammonium or phosphonium cation (Q^+) for applications in organic synthesis, pharmaceuticals, and agrochemicals.[91,92] For instance, two reactants namely aqueous sodium cyanide (NaCN) and 1-bromooctane (RBr) are immiscible and therefore require vigorous stirring at high temperature to react.[93] However, the displacement reaction between the reactants can be accelerated by introducing of phase transfer catalyst, QBr. In the aqueous phase, QBr reacts with NaCN to produce QCN. Q^+, which is soluble in the organic phase, delivers CN^- to the organic phase containing RBr, and thus dramatically accelerates the displacement reaction. Thereafter, the phase transfer agent Q^+ migrates to the aqueous

phase with Br^- for further reactions. As an example of the phase transfer catalyst, the phase transfer of molecules, nanoparticles, or polymer assemblies can deliver non-transferrable materials to the other phase, and facilitate reactions in the phase with the materials.[94–96]

The phase transfer is usually triggered by a stimulus, such as temperature variation,[97,98] UV radiation,[99] pH change,[100–102] and interfacial tension with stimuli-sensitive moieties.[103] The stimulus change the functionality of moieties in the solvents, and thus leads to phase transfer by an affinity change for the two immiscible solvents. Chechik and co-workers reported the phase transfer behavior of amine-terminated poly(amidoamine) dendrimers between aqueous solution and a non-polar toluene phase in the presence of dodecanoic acid.[104] Hydrophilic dendrimers were converted to hydrophobic dendrimers via the formation of ion pairs between the functional groups of dodecanoic acid and the dendrimers. Because ion pairs are based on acid-base interactions, the dendrimers could transfer back to the aqueous phase simply by adding HCl to the toluene phase. They also showed that the dendrimers can encapsulate hydrophilic methyl orange, or non-soluble nanoparticles into their interiors, and effectively deliver them to the organic phase. Wang and co-workers also used a similar strategy for phase transfer with amine-functionalized silicate nanocomposites.[100] Depending on the pH of the aqueous phase, the phase transfer of the particles was controlled. In addition, without any additives, nanoparticles having UV sensitive spiropyran groups can transfer between toluene and water phases by UV irradiation, and polymer micelles having PEO, or poly(2-ethyl-2- oxazoline) groups as coronas show the phase transfer behavior triggered by temperature in a water/IL biphasic system.[99]

Thermoresponsive polymer micelle shuttle between water and IL phase is of great interest due to high tunability of both polymer and ILs, with the interesting properties of ILs discussed in Chapter 1.2.[85,105,106] He and Lodge developed the micelle shuttle using

an amphiphilic block copolymer, 1,2-polybutadiene-*b*-poly(ethylene oxide) (PB–PEO) in a hydrophobic IL, [BMIM][PF_6].[97] Because PEO is well soluble in the IL and water, but PB is not, the morphology and even the dimensional characteristics of the micelles with PB as core block and PEO as corona were retained during the round trip between two immiscible phases. The affinity of the micelles changes with temperature. Below the transfer temperature (T_t), which is around 70 ~ 80 °C, the micelles prefer the water phase, but above the T_t, they prefer to stay in the IL phase. Bai and Lodge demonstrated that T_t is well correlated with the lower critical solution temperature (LCST) of PEO in water, thus indicating the affinity change of PEO corona is the origin of this phenomenon.[107] In addition, they reported that the phase transfer upon heating from water to the IL is an entropy driven process, which is well supported in other studies, and the phase behavior of PEO in water.[105]

Bai and co-workers demonstrated a multi-thermosensitive system including the phase transfer of micelles of poly(*N*-isopropylacrylamide)-*b*-poly(ethylene oxide) (PNIPAm –PEO) in the biphasic system of water and [BMIM][PF_6].[108] Since the PNIPAm block has an LCST in water,[109] but an upper critical solution temperature (UCST) in [BMIM][PF_6],[110] micellization in the aqueous phase was possible after the phase transfer of the polymers above the LCST of PNIPAm in water, and demicellization processes after the phase transfer of PNIPAm–PEO micelles was conducted above UCST of PNIPAm in the IL.

Bai and Lodge have expanded the interesting shuttle of polymer micelles in the biphasic system of water and ILs to the formation of a “nanoemulsion-like” system.[85] Polymer vesicles (polymersomes) were initially formed from PB–PEO in the IL, [EMIM][TFSI], and therefore polymersome interiors were filled with the IL. Then, the polymersomes migrated into the aqueous phase under contact with water as PB–PEO micelles. The most interesting finding was that the IL interiors were maintained without

leaking during the phase transfer and even after the transfer, and the nanoemulsion-like vesicle solution was produced. The phase transfer of polymersomes having IL interiors is potentially applicable to the areas of delivery, extraction, and catalysis. This new catalysis process with the phase transfer of polymersomes with IL interiors will be further described below.

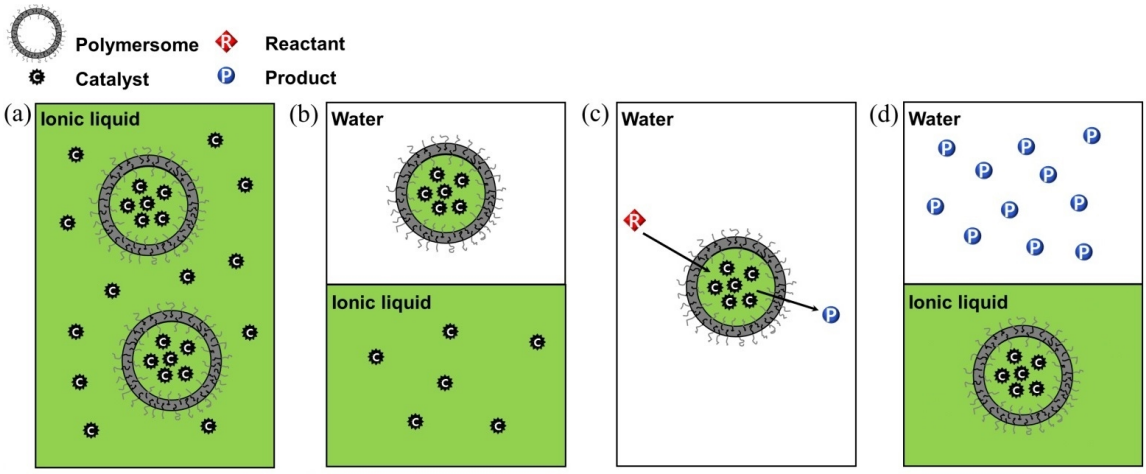

Scheme 1–1. The proposed reaction process with the polymersome nanoreactors. (a) preparing the polymersomes in the IL solution of catalyst, (b) transfer of the polymersomes to the aqueous phase at the temperature below the transfer temperature (T_t), (c) conducting the reaction by adding reactants to the aqueous phase, (d) recovering the polymersomes and separating the products above T_t.

1.4 Design of a Reaction Process with Polymersomes Shuttle

An ideal reaction process with polymersome nanoreactors is illustrated based on the system of thermoresponsive polymersomes with a hydrophobic IL interior in a biphasic water/IL system (e.g. PB–PEO polymersomes in water/[EMIM][TFSI]).[85, 111] The polymersomes prefer to reside in the aqueous phase below T_t, whereas above T_t the polymersomes move to the water–IL interface and start to diffuse into the IL phase. Reversibly, below the T_t the polymersomes cream to the interface and diffuse into the

aqueous phase. The reaction process with the thermoresponsive polymersomes is designed according to Scheme 1–1. This process will be examined in the following order: 1) Loading the catalyst into the polymersomes in an IL, 2) Transfer of the polymersomes to the aqueous phase, 3) Reactions in the confined space consisting of the IL in the aqueous phase, 4) Selective separation of products and the catalyst loaded polymersomes via reverse transfer of the polymersomes from the aqueous phase.

The polymersomes are prepared in an IL solution containing a catalyst that is selectively soluble in the IL. The catalyst is encapsulated in the interior of the resultant polymersomes (Scheme 1–1a). Upon adding water to the IL solution at a temperature below T_t, the loaded polymersomes partition to the aqueous phase, however the encapsulated catalyst is still retained in the polymersome interior. This process produces a reaction system consisting of a homogeneous reaction solution segregated by polymersome membranes, dispersed in another medium heterogeneously (Scheme 1–1b). The aqueous phase containing polymersomes is separated to prevent any interference from the IL and uncapsulated catalyst. Reactants are added to the aqueous medium and the target reaction initiates and proceeds by the diffusion of reactants and products (Scheme 1–1c). The polymersomes are transferred to the IL phase by increasing the temperature above the T_t, leaving behind the preferentially hydrophilic products in the aqueous phase. The aqueous phase containing the products and the catalyst and the IL in the polymersomes can be recovered easily (Scheme 1–1d) owing to the biphasic formation between the IL and the aqueous phase. Moreover, the collected polymersomes can be recycled for the additional reaction cycles by adding the aqueous phase to the IL phase.

However, in order to realize the proposed process with polymersomes, several requirements are necessary. Reactants should be soluble in water and permeable through the polymersomes membrane, products must diffuse through membranes and be

selectively soluble in water, and catalysts should reside in the polymersome interiors and be impermeable across the membranes.

As a result of these requirements, this system may have certain limitations due to the unfavorable partition ratio between reactants, products, and catalysts in the aqueous phase, IL phase, and bilayer membrane.

1.5 Overview

To this end, I demonstrate a new nanoreactors, polymersomes with IL interior dispersed in an aqueous phase controlled by the thermal stimuli. To apply the system to reactions, prerequisite studies are necessary: (i) polymersome size should be controlled, (ii) molecular transportation behavior through polymersome membrane should be demonstrated with various molecules, (iii) the phase transfer mechanism of the polymersomes needs to be understood. The thesis is focused on the prerequisite studies for the nanoreactors.

In Chapter 2, methods to control the size of polymersomes with glassy and rubbery bilayers are discussed. Two approaches, namely extrusion and the co-solvent method, are employed. For the mechanical process, extrusion through a polycarbonate membrane is employed and the dispersity and size evolution with the number of passes is invesitigated. In the co-solvent method, we find that the size and dispersity of all polymersomes with rubbery and glassy hydrophobic blocks are highly sensitive to assembly conditions. The co-solvent content and the volume fraction of hydrophilic block affect the polymersome size and dispersity. The size and dispersity dependence are confirmed directly by cryogenic transmission electron microscopy (cryo-TEM), and the size distribution is analyzed by dynamic light scattering (DLS).

In Chapter 3, the permeation of molecules is investigated by nuclear magnetic resonance spectroscopy (NMR) techniques: 1-D ^{1}H NMR spectroscopy, and pulsed field gradient NMR (PFG-NMR). We find that imidazole derivatives show different chemical shift when they are in the IL pool than the aqueous phase, due to a magnetic susceptibility difference. The shifted peaks were confirmed to be from the IL interiors by varying the polymersome concentration. This difference in ^{1}H NMR gives direct evidence of molecular permeation, and the mole fraction of the tracer molecules within the polymersomes versus in the aqueous exterior. The effect of molecular charge status on the permeation is quantitatively examined with similarly sized charged and neutral molecules by PFG-NMR. The escape and entry rates of tracer molecules are obtained by fitting the echo-decay curves (PFG–NMR results) with a two-site exchange model from Fick's second law with exchange terms. In addition, polymersome concentration effects on the rates are also examined. Additionally, in the Appendices, the PFG-NMR technique is expanded to investigate the exchange rate of the tracer molecule having opposite partitioning with the molecules in Chapter 3, and the polymersome membrane-forming block is modified for permeability control with temperature.

In Chapter 4, we closely investigate factors affecting phase transfer of polymersomes from water and a water immiscible IL with PS–PEO diblock copolymers by varying the molecular weight of PS as well as varying the volume fraction of PEO. Interestingly, it is found that the tethering density of PEO in the membrane critically governs the phase transfer, and the minimum tethering density for the transfer is independent of the molecular weight of the hydrophobic PS. The phase transfer is also analyzed in terms of the free energy of polymersomes in the biphasic system. We propose the phase transfer is a competing process between the interfacial tension penalty and the negative PEO free energy terms. In addition, the quality of the aqueous phase, which affects the interfacial tension of the PS membrane, influenced the phase transfer.

In Chapter 5, we show extraction of polymersomes from a mixture of polymersomes and worm-like micelles in a hydrophobic IL to water using the interfacial-tension-controlled phase transfer shown in Chapter 4. First, the interfacial tension penalty for the phase transfer is controlled by adding a salt to the aqueous phase, and the critical tethering density of PEO is shifted to the point where only larger polymersomes can transfer to the aqueous phase. Then, using the relationship between the salt concentration and the critical tethering density, a mixture of cylindrical micelles and polymersomes are successfully separated into two different phases. This fractionation is a novel and simple separation process without any special apparatus, and would help to prepare monodispersed polymersomes and separate unwanted morphologies and size.

1.6 References

1. Renggli, K.; Baumann, P.; Langowska, K.; Onaca, O.; Bruns, N.; Meier, W. *Adv. Funct. Mater.* **2011**, *21*, 1241–1259.
2. Ostafin, A.; Landfester, K. *Nanoreactor engineering for life sciences and medicine*; Artech House: MA, USA, 2009.
3. Rafelski, S. M.; Marshall, W. F. *Nature Review* **2008**, *9*, 593–602.
4. Weng, G.; Bhalla, U. S.; Iyengar, R. *Science* **1999**, *284*, 92–96.
5. Karlsson, M.; Davidson, M.; Karlsson, R.; Karlsson, A.; Bergenholtz, J.; Konkoli, Z.; Jesorka, A.; Lobovkina, T.; Hurtig, J.; Voinova, M.; Orwar, O. *Annu. Rev. Phys. Chem.* **2004**, *55*, 613–649.
6. Anisur, R. M.; Shin, J.; Choi, H. H.; Yeo, K. M.; Kang, E. J.; Lee, I. S. *J. Mater. Chem.* **2010**, *20*, 10615–10621.
7. Nardin, C.; Thoeni, S.; Widmer, J.; Winterhalter, M.; Meier, W. *Chem. Commun.* **2000**, 1433–1434.
8. Peters, R. J. R.; Louzao, I.; van Hest, J. C. M. *Chem. Sci.* **2012**, *3*, 335–342.
9. Bolinger, P.-Y.; Stamou, D.; Vogel, H. *Angew. Chem. Int. Ed.* **2008**, *47*, 5544–5549.
10. Lan, Y.; Zhang, M.; Zhang, W.; Yang, L. *Chem. Eur. J.* **2009**, *15*, 3670–3673.
11. Dong, R.; Liu, W.; Hao, J. *Acc. Chem. Res.* **2012**, *45*, 504–513.
12. Chen, G.; Guan, Z. *J. Am. Chem. Soc.* **2004**, *126*, 2662–2663.
13. Miletic, N.; Abetz, V.; Ebert, K.; Loos, K. *Macromol. Rapid. Commun.* **2010**, *31*, 71–74.
14. Simone, P. M.; Lodge, T. P. *Macromolecules* **2008**, *41*, 1753–1759.
15. Odian, G. *Principles of Polymerization*; John Wiley & Sons: Hoboken, 2004.
16. Chiu, D. T.; Wilson, C. F.; Karlsson, A.; Danielsson, A.; Lundqvist, A.; Stromberg, A.; Ryttsen, F.; Davidson, M.; Nordholm, S.; Orwar, O.; Zare, R. N. *Chem. Phys.* **1999**, *247*, 133–139.

17. Ostafin, A.; Chen, Y.-C. *Kirk-Othmer Encyclopedia of Chemical Technology* **2009**, 1–18.
18. Chen, Q.; Schönherr, H.; Vancso, G. J. *Small* **2009**, *5*, 1436–1445.
19. Chen, Q.; Rausch, K. G.; Schönherr, H.; Vancso, G. J. *Chem. Phys. Chem.* **2010**, *11*, 3534–3540.
20. Ud-Dean, S. M. M. *IET Nanobiotechnol.* **2009**, *3*, 65–70.
21. Stano, P.; Luigi, P. *Reactions in Liposomes, in Molecular Encapsulation: Organic Reactions in Constrained Systems*; John Wiley & Sons, Ltd: Chichester, UK. 2010.
22. Peters, R. J. R. W.; Marguet, M.; Marais, S.; Fraaije, M. W.; van Hest, J. C. M.; Lecommandoux, S. *Angew. Chem.* **2014**, *126*, 150–154.
23. Spulber, M.; Baumann, P.; Saxer, S. S.; Pieles, U.; Meier, W.; Bruns. N. *Biomacromolecules* **2014**, *15*, 1469–1475.
24. Chuanoi, S.; Anraku, Y.; Hori, M.; Kishimura, A.; Kataoka, K. *Biomacromolecules* **2014**, *15*, 2389–2397.
25. Jain, S.; Bates, F. S. *Science* **2003**, *300*, 460–464.
26. Jain, S.; Bates, F. S. *Macromolecules*, **2004**, *37*, 1511–1523.
27. Lee, J. C. M.; Bermudez, H.; Discher, B. M.; Sheehan, M. A.; Won, Y. Y.; Bates, F. S.; Discher, D. E. *Biotechnol. Bioeng.* **2001**, *73*, 135–145.
28. Mueller, W.; Koynov, K.; Fischer, K.; Hartmann, S.; Pierrat, S.; Basche, T.; Maskos, M. *Macromolecules* **2009**, *42*, 357–361.
29. Meng, F.; Zhong, Z.; Feijen, J. *Biomacromolecules* **2009**, *10*, 197–209.
30. Watanabe, K.; Takizawa, S.-Y.; Murata, S. *Chem. Lett.* **2011**, *40*, 345–347.
31. Yow, H. N.; Routh, A. F. *Soft Matter* **2006**, *2*, 940–949.
32. Discher, D. E.; Eisenberg, A. *Science* **2002**, *297*, 967–973.
33. Lipshutz, B. H.; Ghorai, S. *Org. Lett.* **2009**, *11*, 705–708.
34. Lipshutz, B. H.; Taft, B. R. *Org. Lett.* **2008**, *10*, 1329–1332.

35. Lipshutz, B. H.; Ghorai, S.; Abela, A. R.; Moser, R.; Nishikata, T.; Duplais, C.; Krasovskiy, A. *J. Org. Chem.* **2011**, *76*, 4379–4391.

36. Urbani, C. N.; Monteiro, M. J. *Macromolecules* **2009**, *42*, 3884–3886.

37. Monteiro, M. J. *Macromolecules* **2010**, *43*, 1159–1168.

38. Doyagüez, E. G.; Rodríguez-Hernández, J.; Corrales, G.; Fernández-Mayoralas, A. *Macromolecules* **2012**, *45*, 7676–7683.

39. Li, S.; Ge, Y.; Tiwari, A.; Cao, S. *Small* **2010**, *6*, 2453–2459.

40. Wilson, D. A.; Nolte, R. J. M.; van Hest, J. C. M. *Nat. Chem.* **2012**, *4*, 268–274.

41. Yu, S.; Azzam, T.; Rouiller, I.; Eisenberg, A. *J. Am. Chem. Soc.* **2009**, *131*, 10557–10566.

42. Kim, K. T.; Cornelissen, J. J. L. M.; Nolte, R. J. M.; van Hest, J. C. M. *Adv. Mater.* **2009**, *21*, 2787–2791.

43. Du, J.; O'Reilly, R. K. *Soft Matter* **2009**, *5*, 3544–3561.

44. Choucair, A.; Soo, P. L.; Eisenberg, A. *Langmuir* **2005**, *21*, 9308–9313.

45. Lipshutz, B. H.; Ghorai, S. *Green Chem.* **2014**, *16*, 3660–3679.

46. Lipshutz, B. H.; Isley, N. A.; Fennewald, J. C.; Slack, E. D. *Angew. Chem. Int. Ed.* **2013**, *52*, 10952–10958.

47. Johnston, K. P; Haynes, C. *AIChE J.* **1987**, *33*, 2017–2026.

48. Enache, D. I.; Edwards, J. K.; Landon, P.; Solsona-Espriu, B.; Carley, A. F.; Herzing, A. A.; Watanabe, M.; Kiely, C. J.; Knight, D. W.; Hutchings, G. J. *Science* **2006**, *311*, 362–365.

49. Earle, M. J.; Esperanca, J. M. S. S.; Gilea, M. A.; Canongia Lopes, J. N.; Rebelo, L. P. N.; Magee, J. W.; Seddon, K. R.; Widegren, J. A. *Nature* **2006**, *439*, 831–834.

50. Garcia, B.; Lavallée, S.; Perron, G.; Michot, C.; Armand, M. *Electrochim. Acta* **2004**, *49*, 4583–4588.

51. Wilkes, J. S.; Levisky, J. A.; Wilson, R. A.; Hussey, C. L. *Inorg. Chem.* **1982**, *21*,

1263–1264.

52. Fredlake, C. P.; Crosthwaite, J. M.; Hert, D. G.; Aki, S. N. V. K.; Brennecke, J. F. *J. Chem. Eng. Data* **2004**, *49*, 954–964.

53. Huddleston, J. G.; Visser, A. E.; Reichert, W. M.; Willauer, H. D.; Broker, G. A.; Rogers, R. D. *Green Chem.* **2001**, *3*, 156–164

54. Dupont, J.; *J. Braz. Chem. Soc.* **2004**, *15*, 341–350.

55. Wolfson, A.; Vankelecom, I. F. J.; Jacobs, P. A. *Tetrahedron Lett.* **2005**, *46*, 2513–2516.

56. Rivera-Rubero, S.; Baldelli, S. *J. Phys. Chem. B* **2006**, *110*, 15499–15505.

57. Orchilles, A. V.; Miguel, P. J.; Vercher, E.; Martinez-Andreu, A. *J. Chem. Eng. Data* **2008**, *53*, 2426–2431.

58. Cammarata, L.; Kazarian, S. G.; Salter, P. A.; Welton, T. *Phys. Chem. Chem. Phys.* **2001**, *3*, 5192–5200.

59. Welton, T. *Chem. Rev*. **1999**, *99*, 2071–2084.

60. Liptay, W. *Angew. Chem.* **1969**, *81*, 161–188.

61. Papaiconomou, N.; Yakelis, N.; Salminen, J.; Bergman, R.; Prausnitz, J. M. *J. Chem. Eng. Data* **2006**, *51*, 1389–1393.

62. Armstrong, D. W.; He, L.; Liu, Y.-S. *Anal. Chem.* **1999**, *71*, 3873–3876.

63. Dzyuba, S. V.; Bartsch, R. A. *Tetrahedron Lett.* **2002**, *43*, 4657–4659.

64. Hallet, J. P.; Welton, T. *Chem. Rev.* **2011**, *111*, 3508–3576.

65. Anderson, J. L.; Ding, J.; Welton, T.; Armstrong, D. W. *J. Am. Chem. Soc.* **2002**, *124*, 14247–14254.

66. Wasserscheid, P.; Stark, A. *Handbook of Green Chemistry, Vol. 6, Ionic Liquids*; Wiley-VCH-Verlag: Weinheim, Germany, 2010.

67. Parshall, G. W. J. *Am. Chem. Soc.* **1972**, *94*, 8716–8719.

68. Boon, J. A.; Levisky, J. A.; Pflug, J. L.; Wilkes, J. S. *J. Org. Chem.* **1986**, *51*,

480–483.

69. Ghavre, M.; Morrissey, S.; Gathergood, N. *Ionic Liquids: Applications and Perspectives: Theory and Practice*; *Hydrogenation in Ionic Liquids*: InTech, 2011.
70. Earle, M.; McCormac, P. B.; Seddon, K. R. *Green Chem.* **1999**, *1*, 23–25.
71. Jeong, Y.; Ryu, J.-S. *J. Org. Chem.* **2010**, *75*, 4183–4191.
72. McLachlan, F.; Mathews, C. J.; Smith, P. J.; Welton, T. *Organometallics* **2003**, *22*, 5350–5357.
73. Kragl, U.; Eckstein, M.; Kaftzik, N. *Curr. Opin. Biotech.* **2002**, *13*, 565–571.
74. Park, S.; Kazlauskas, R. J. *Curr. Opin. Biotech.* **2003**, *14*, 432–437.
75. Luo, H. M.; Li, Y. Q.; Zheng, W. J. *Chinese Chem. Lett.* **2005**, *16*, 906–908.
76. Wolfson, A.; Vankelecom, I. F. J.; Jacobs, P. A. *Tetrahedron Lett*. **2005**, *46*, 2513–2516.
77. Peng, J.; Shi, F.; Gu, Y.; Deng, Y. *Green Chem.* **2003**, *5*, 224–226.
78. Lee, H.; Lee, J. S.; Ahn, B. S.; Kim, H. S. *J. Korean Ind. Eng. Chem.* **2005**, *16*, 595–602.
79. Riisager, A. Wasserscheid, P. van Hal, R.; Fehmann, R. *J. Catal.* **2003**, *219*, 452–455.
80. Riisager, A.; Fehrmann, R.; Flicker, S.; van Hal, R.; Haumann, M.; Wasserscheid, P. *Angew. Chem. Int. Ed.* **2005**, *44*, 815–819.
81. Autenrieth, B.; Frey, W.; Buchmeiser, M. R. *Chem. Eur. J.* **2012**, 18, 14069–14078.
82. Froba, A. P.; Kremer, H.; Leipertz, A. *J. Phys. Chem. B* **2008**, *112*, 12420–12430.
83. Mills, R. *J. Phys. Chem.* **1973**, *77*, 685–688.
84. Noda, A.; Hayamizu, K.; Watanabe, M. *J. Phys. Chem. B* **2001**, *105*, 4603–4610.
85. Bai, Z.; Lodge, T. P. *J. Am. Chem. Soc.* **2010**, *132*, 16265–16270.
86. Spitzer, M.; Sabadini, E.; Loh, W. *J. Phys. Chem. B* **2002**, *106*, 12448–12452.
87. Rogers, R. D.; Willauer, H. D.; Griffin, S. T.; Huddleston, J. G. *J. Chromatogr. B*

Biomed. Sci. Appl. **1998**, *711*, 255–263.

88. Tian, H.; Chen, X.; Lin, H.; Deng, C.; Zhang, P.; Wei, Y.; Jing, X. *Chem. Eur. J.* **2006**, *12*, 4305–4312.
89. Gittins, D. I.; Caruso, F. *Angew. Chem. Int. Ed.* **2001**, *40*, 3001–3004.
90. Edwards, E. W.; Chanana, M.; Wang, D.; Möhwald, H. *Angew. Chem. Int. Ed.* **2008**, *47*, 320–323.
91. Halpern, M. *Ullmann's Encyclopedia of Industrial Chemistry* **2000**, *26*, 495–501**.**
92. Metzger, J. O. *Angew. Chem. Int. Ed.* **1998**, *37*, 2975–2978.
93. Starks, C. M. *J. Am. Chem. Soc.* **1971**, *93*, 196–199.
94. Zuwei, X.; Ning, Z.; Yu, S.; Kunlan, L. *Science* **2001**, *292*, 1139–1141.
95. Dorokhin, D.; Tomczak, N.; Han, M.; Reinhoudt, D. N.; Velders, A. H.; Vansco, G. J. *ACS Nano* **2009**, *3*, 661–667.
96. Qin, B.; Zhao, Z.; Song, R.; Shanbhag, S.; Tang, Z. *Angew. Chem.* 2008, *120*, 10023–10026.
97. He, Y.; Lodge, T. P. *J. Am. Chem. Soc.* **2006**, *128*, 12666–12667.
98. Guerrero-Sanchez, C.; Wouters, D.; Hoeppener, S.; Hoogenboom, R.; Schubert, U. S. *Soft Matter* **2011**, *7*, 3827–3831.
99. Wu, Y.; Zhang, C.; Qu, X.; Liu, Z.; Yang, Z. *Langmuir* **2010**, *26*, 9442–9448.
100. Wang, H.; Yang, H.; Liu, H.; Yu, Y.; Xin, H. *Langmuir* **2013**, *29*, 6687–6696.
101. Popescu, M.-T.; Tasis, D.; Tsitsilianis, C. *ACS Macro Lett.* **2014**, *3*, 981–984.
102. Wang, Y.; Leng, W.; Gao, Y.; Guo, J. *ACS Appl. Mater. Interfaces* **2014**, *6*, 4143–4148.
103. So, S.; Lodge, T. P. *Langmuir* **2015**, *31*, 594–601.
104. Chechick, V.; Zhao, M.; Crooks, R. M. *J. Am. Chem. Soc.* **1999**, *121*, 4910–4911.
105. Bai, Z.; Lodge, T. P. *J. Phys. Chem. B* **2009**, *113*, 14151–14157.
106. Ueki, T.; Sawamura, S.; Nakamura, Y.; Kitazawa, Y.; Kokubo, H.; Watanabe, M.

Langmuir **2013**, *29*, 13661–13665.

107. Bai, Z.; Nagy, M. W.; Zhao, B.; Lodge T. P. *Langmuir* **2014**, *30*, 8201–8208.

108. Bai, Z.; He, Y.; Young, N. P.; Lodge, T. P. *Macromolecules* **2008**, *41*, 6615–6617.

109. Heskins, M.; Guillet, J. E. *J. Macromol. Sci. A* **1968**, *2*, 1441–1455.

110. Ueki, T.; Watanabe, M. *Chem. Lett.* **2006**, *35*, 964–965.

111. So, S.; Lodge, T. P. *J. Phys. Chem. C* **2014**, *118*, 21140–21147.

Chapter 2

Size Control of Polymersomes with Glassy and Rubbery Bilayer Membranes in an Ionic Liquid

2.1 Introduction

Ionic liquids (IL), also known as molten salts, are of great interest as media for chemical and biochemical reactions, and pharmaceutical and biotechnological applications due to their remarkable properties, such as negligible vapor pressure, low melting point, and wide range of solvation ability.[1–4] ILs are composed of bulky and asymmetric ions and have low melting points, usually below 100 °C. Typical organic cations include N-alkylpyridinium, and N,N′-dialkylimidazolium, and common polyatomic anions are PF_6^-, BF_4^-, CF_3COO^-, and $(CF_3SO_2)_2N^-$.[5,6] Compared to traditional volatile organic solvents, ILs have negligible vapor pressure and high thermal stability (often decomposing only above 400 °C).[7] In addition, the properties of ILs can be tuned for a specific application by developing new ions or combining different type of cations and anions.[8] ILs are good solvents for a wide range of organic, inorganic and organometallic compounds due to a suite of intermolecular interactions between ILs and solutes, including dipolar, dispersive, ionic, and hydrogen bonding.[9] These characteristics make ILs potentially environmentally friendly media for separation processes, electrochemical applications (fuel cells, lithium ion batteries, *etc.*), catalytic processes, and for biological applications such as gene delivery and enzyme catalyzed reactions.[10–14]

Self-assembly of block copolymers in ILs is being actively studied.[15,16] Since both ILs and block copolymers are highly tunable, a system can be optimized for a wide

variety of applications, such as gel electrolyte membranes, supercapacitors, and separation media.[17–19] In particular, polymersomes (vesicles self-assembled from amphiphilic block copolymers) with both confined interiors and membranes, have potential to serve as "nanoreactors" for catalysis, as well as transport vehicles for controlled delivery and separation applications.[20–22] Precise control of polymersome diameter is desirable because polymersome size is an important parameter in determining the performance of a designed system. For instance, in biological applications, the size distribution of vesicles is important for the efficiency of delivery because the circulation time of vesicles and the release rate of cargo are size-dependent.[23] In nanoreactor applications, a narrowly distributed, small vesicle size is required to simplify the analysis and characterization. Similarly, it facilitates achieving higher reaction rates and better catalytic performance through higher collision frequencies among the reactants, catalysts and the wall of the vesicle interior.[24,25]

Various strategies have been utilized to prepare narrowly dispersed polymersomes with controlled size. Mechanical approaches such as extrusion involve rupture of large polymersomes, which are then forced through a membrane with well-controlled pore size and thus transformed into smaller polymersomes. The extrusion method is widely used because it is a relatively rapid way to produce monodispersed polymersomes without the introduction of contaminants.[26–28] Other methods, such as inkjet printing, microfluidics, and nanoprecipitation involve a co-solvent, which can dissolve both vesicle forming polymers and a selective solvent.[29–31] The basic mechanism for polymersome formation is the same as the solvent-switch or co-solvent (CS) method.[32] Homogeneously dispersed droplets are produced in the selective solvent by the listed methods. Then, as the co-solvent in the droplets is removed, amphiphilic block copolymers self-assemble into polymersomes under quasi-equilibrium conditions, and narrowly-sized polymersomes can be produced.

Here, two types of diblock copolymers, one possessing a rubbery and one a glassy membrane-forming block, were employed for polymersome preparation, and the size and dispersity of polymersomes was controlled in the IL. Using two methods, extrusion and co-solvent, we disclose environmentally friendly and facile approaches for fabricating nanosized polymersomes of 1,2-polybutadiene-*b*-poly(ethylene oxide) (PB–PEO) and polystyrene-*b*-poly(ethylene oxide) (PS–PEO), exploiting the non-volatility and highly thermal stability of the IL. Furthermore, the number of extrusion passes in the mechanical approach, and the content of co-solvent and hydrophilic block length in the co-solvent protocol were varied, and the concomitant effects on the size and distribution of polymersomes were studied.

2.2 Experimental Section

2.2.1 Materials. 1,2-Polybutadiene-*b*-poly(ethylene oxide) (PB–PEO) and polystyrene-*b*-poly(ethylene oxide) (PS–PEO) block copolymers were prepared via sequential anionic polymerization. Hydroxyl-terminated 1,2-polybutadiene (PB-OH) and polystyrene (PS-OH) homopolymers were synthesized in anhydrous tetrahydrofuran (THF) at –60 °C and cyclohexane at 40 °C, respectively, with *sec*-butyllithium as initiator. The homopolymers were end-capped with hydroxyl groups by adding ethylene oxide approximately 10 times molar excess of the growing chains followed by adding deoxidized methanol. The PEO block was grown from PB-OH and PS-OH in the same manner. Homopolymers were dissolved in anhydrous THF and converted to the macroinitiators using electron transfer agents (diphenylmethyl potassium or potassium naphthalenide). Then, purified ethylene oxide monomer in *n*-butyllithium was added and reacted for 24 h at 45 °C. The polymer chains were terminated with concentrated deoxidized methanol at room temperature. The number average molecular weight (M_n)

was obtained by ^{1}H NMR spectroscopy, and the dispersity ($Đ = M_w/M_n$) was measured by size exclusion chromatography (SEC), where M_w is the weight-average molecular weight. Polymers used in this study are listed in Table 2–1. The ionic liquid 1-ethyl-3-methylimidazolium bis(trifluoromethylsulfonyl) imide ([EMIM][TFSI]) was prepared by combining 1-ethyl-3-methylimidazolium bromide ([EMIM][Br], Io-Li-Tec, 99%) and lithium bis(trifluoromethylsulfonyl)imide ([Li][TFSI], HQ115) in water. An equimolar mixture of [EMIM][Br] and [Li][TFSI] was allowed to react at 70 °C for a day. The separation of the water-immiscible product was followed by washing with deionized water at least 3 times. The [EMIM][TFSI] was purified via alumina (Al_2O_3) column, dried under vacuum at 60 °C for 3 days, and stored in a desiccator before use. The co-solvent, dichloromethane (Stabilized/Certified ACS) (DCM) was purchased from Fischer Scientific and used as received.

2.2.2 Size-Controlled Polymersome Preparation. For the mechanical approach, polymersomes were prepared through the thin film (TF) method. TFs of polymers (PB–PEO(9–3) and PS–PEO(14–2.5)) were prepared by drying the polymer solution in DCM under nitrogen purge and further dried under vacuum at 50 °C for 24 h to remove the remaining DCM. In order to produce an 0.5 wt % polymersome solution, weighed [EMIM][TFSI] was added to the TF and stirred vigorously at 150 °C under an argon atmosphere overnight, and the solution was slowly cooled down to room temperature. Diluted polymersome solutions (0.1 wt % of PB–PEO(9–3) and PS–PEO(14–2.5)) from the TF method were extruded and pressed 1 – 25 times by using an extrusion device (LiposoFast-Basic Extruder, Avestin) through polycarbonate membranes with defined pore sizes of 200 nm diameter. For PS–PEO(14–2.5) polymersomes, 10 vol % of DCM of the solution was added as plasticizer for the glassy polystyrene membrane. In the kinetic approach, the solvent-switch or CS method was used. The weighed polymers were dissolved in DCM followed by adding [EMIM][TFSI] to the solution. Consecutively, the

volatile DCM was selectively removed by N_2 purging and drying under vacuum for a day at room temperature. It is known that the homogeneous conditions of the CS method favors the formation of relatively monodisperse polymersomes compared to the TF method.[31,33] However, even with the CS method, the size and dispersity depend on the ratio of CS to the selective solvent and the relative length of the hydrophilic block. To study the effect of CS content, the initial content of DCM was varied from 17 vol % to 60 vol % for PS–PEO(14–2.5) and from 30 vol % to 60 vol % for PB–PEO(9–3). Three PS–PEO block copolymers with a common PS block length (M_n = 18 kg/mol), but different lengths of the PEO block (M_n = 2.5, 3.0, 3.6 kg/mol), were used to study the effect of PEO block length on the polymersome size and distribution. The polymersomes from PS–PEO(18–2.5), PS–PEO(18–3), and PS–PEO(18–3.6) were prepared through the CS protocol with initial DCM content of 60 vol %.

2.2.3 Dynamic Light Scattering (DLS). The mean size and dispersity of the polymersomes were analyzed by DLS with a Brookhaven BI-200SM goniometer and a Brookhaven BI-9000AT correlator. Measurements were performed at seven different angles between 60° and 120° at λ = 637 nm and 25 °C. The average hydrodynamic radius ($<R_h>$) and the dispersity (μ_2/Γ^2) were evaluated from the average decay rate ($\Gamma = D_m \cdot q^2$, where D_m is a mutual diffusion coefficient, and q is the scattering vector) and the second cumulant (μ_2) values, which were obtained from cumulant fitting of the normalized auto correlation function, $g^{(2)}(q, t)$. The distribution of size can also be obtained via Laplace inversion, in this case using REPES (Regularized Positive Exponential Sum).[34] All samples for DLS were diluted to 0.01 wt % and filtered through a syringe filter (Millex-SV 5.0 μm) prior to the measurements.

2.2.4 Cryogenic Transmission Electron Microscopy (cryo-TEM). About 0.3 μL of polymersome solution (0.1 or 0.5 wt % in [EMIM][TFSI]) was placed on a carbon-coated and lacey film-supported copper TEM grid at room temperature and vitrified in liquid

ethane (~ –180 °C) in a FEI Vitrobot Mark III vitrification robot. A sample grid was carefully transferred to a single tilt liquid nitrogen cryotransfer holder (Gatan), and then the images were taken by using a FEI Tecnai G2 Spirit BioTWIN, operating at 120 kV under liquid N_2 cryo conditions with an Eagle 4 mega pixel CCD camera.

Table 2–1. Molecular characterization of PB–PEO and PS–PEO diblock copolymers.

Sample Code	M_n[a] (kg/mol)	M_{PEO}[b] (kg/mol)	$Đ$[c]	f_{PEO}[d]
PB–PEO(9–3)[e]	9.0	2.5	1.07	0.17
PS–PEO(14–2.5)	14.1	2.6	1.04	0.16
PS–PEO(18–2.5)	18.4	2.5	1.01	0.13
PS–PEO(18–3)	18.4	2.9	1.03	0.14
PS–PEO(18–3.6)	18.4	3.6	1.01	0.17

[a] Number average molecular weight of the ω-hydroxyl polybutadiene (PB-OH) and polystyrene (PS-OH) homopolymers determined by ^{1}H NMR spectroscopy. [b] Number average molecular weight of PEO block from ^{1}H NMR spectroscopy and the M_n of PB-OH or PS-OH. [c] Dispersity (M_w/M_n) of PB–PEO and PS–PEO determined by SEC (Agilent Technologies 1260 Infinity) equipped with a multiangle light scattering detector (Wyatt Technology Dawn Heleos-II), where M_w is weight average molecular weight. [d] Volume fraction of PEO block from M_n of each block and the bulk densities: ρ_{PB} = 0.87 g/cm^3, ρ_{PS} = 1.05 g/cm^3, ρ_{PEO} = 1.13 g/cm^3. [e] The fraction of 1,2-addition of PB-OH was 91%.

2.3 Results and Discussion

It has been demonstrated that amphiphilic block copolymers, such as polystyrene -*b*-poly(methyl methacrylate), poly(*N*-isopropylacrylamide)-*b*-poly(ethylene oxide), PB–PEO, and PS–PEO can self-assemble into micelles or vesicles in ILs.[35–37] Especially, amphiphilic diblock copolymers with low volume fractions of the hydrophilic block

preferentially form vesicles in order to minimize the interfacial area between the membrane forming block and the selective solvent.[38] The polymers in this study have low volume fractions of PEO, ≤ 0.2, and self-assemble into vesicles in [EMIM][TFSI].

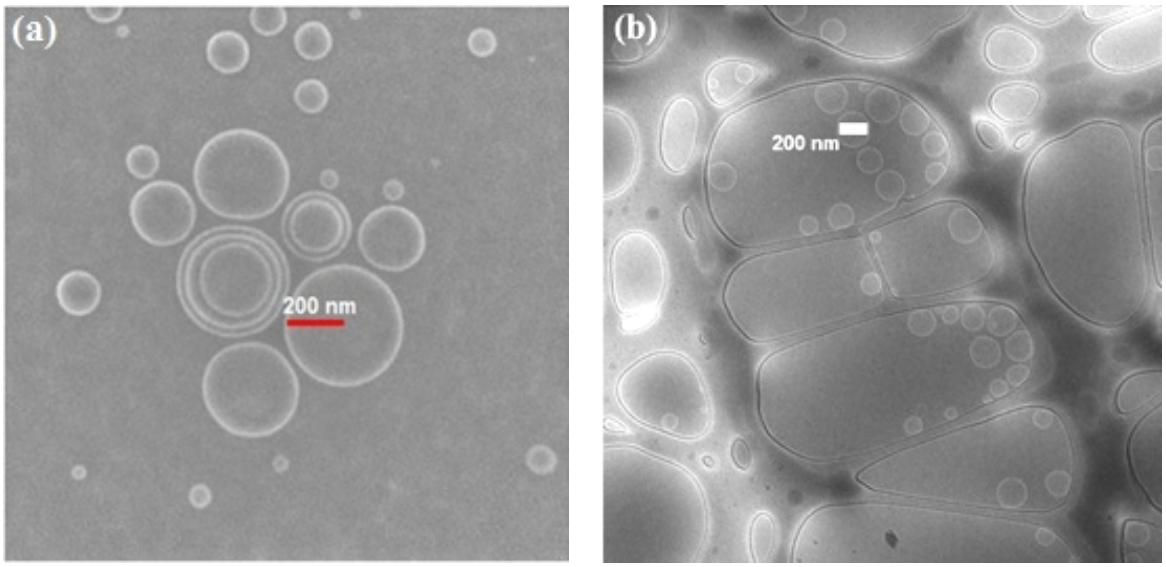

Figure 2–1. Cryo-TEM image of PB–PEO(9–3) polymersomes in [EMIM][TFSI] (a) from the TF method, and (b) after 25 passes (0.1 wt%) through the extruder membrane with pore radius of 100 nm.

The self-assembled nanostructure of PB–PEO(9–3) in [EMIM][TFSI] from the TF method is shown in Figure 2–1a. The vesicular structure was observed with bright circular regions, which represent the PB membranes in the dark IL matrix (phase contrast of PB–PEO(9–3) polymersomes also can be seen in Figure 2–1b). The phase contrast can be attributed to the electron density difference between the PB membrane and [EMIM][TFSI].[20, 39, 40] Similar phase contrast was also observed in the PS–PEO polymersomes. In the bright-field cryo-TEM images, the probability of scattering is a primary source for the intensity (brightness) difference.[41] The intensity increases as the probability of scattering by the specimen, which is proportional to the electron density and the thickness of species, decreases. Since the PB and PS membranes scatter fewer

electrons than the IL, the membranes appear brighter than the interior and exterior of the polymersomes. In the cryo-TEM images of PB–PEO(9–3) (Figure 2–1a), the polymersomes are polydisperse, with the size ranging from about 50 to 400 nm in diameter. Most of the vesicles observed are unilamellar vesicles (ULVs) consisting of a single closed bilayer, however, a few multilamellar vesicles (MLVs) having an indefinite number of concentric bilayers are also observed. The broad size distribution is also reflected in the DLS results. Cumulant fitting shows that $\mu_2/\Gamma^2 \approx 0.41$ with $\langle R_h \rangle \approx 172$ nm. The relatively large value of μ_2/Γ^2 indicates a broad distribution of polymersome sizes (when the particles are monodisperse, $\mu_2/\Gamma^2 = 0$) as shown in Figure 2–2b.

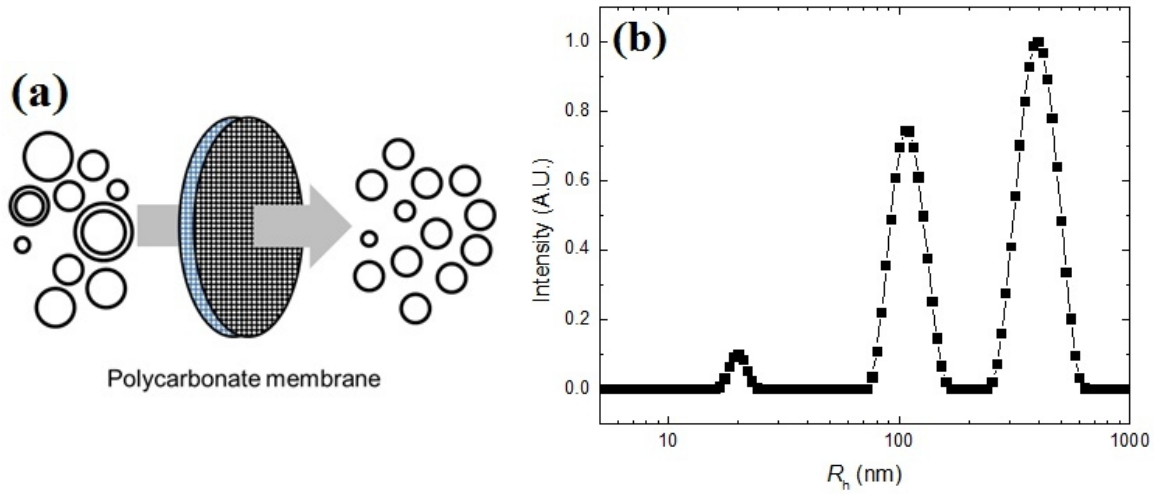

Figure 2–2. (a) Schematic description of polymersome extrusion through the membrane, and (b) Size distribution of PB–PEO(9–3) polymersomes in [EMIM][TFSI] prepared by TF method.

Extrusion through the membrane was conducted with the PB–PEO(9–3) solution from the TF method. As depicted in Figure 2–2a, an extrusion device was employed to extrude the solution through polycarbonate membranes with defined pore sizes of 100 nm in radius. This process was repeated up to 25 times to determine the optimum number of passes. As polymersome solutions from the TF method were driven through the

polycarbonate membranes, the relatively large polymersomes were broken up into smaller ones, and the width of the size distribution also decreases with subsequent passes. The nanostructure of PB–PEO(9–3) is retained even after 25 passes, and the sizes of all polymersomes are comparable to the radius of the membrane pores (100 nm) (see Figure 2–1b). Figure 2–3 summarizes the variation in $\langle R_h \rangle$ and μ_2/Γ^2 with the number of passes through the membrane. At the first pass, $\langle R_h \rangle$ and μ_2 / Γ^2 decrease significantly from 172 to 113 nm and from 0.41 to 0.11, and then level off to roughly constant values ($\langle R_h \rangle \sim 99$ nm, $\mu_2/\Gamma^2 \sim 0.1$) after *ca*. 3 passes through the extruder.

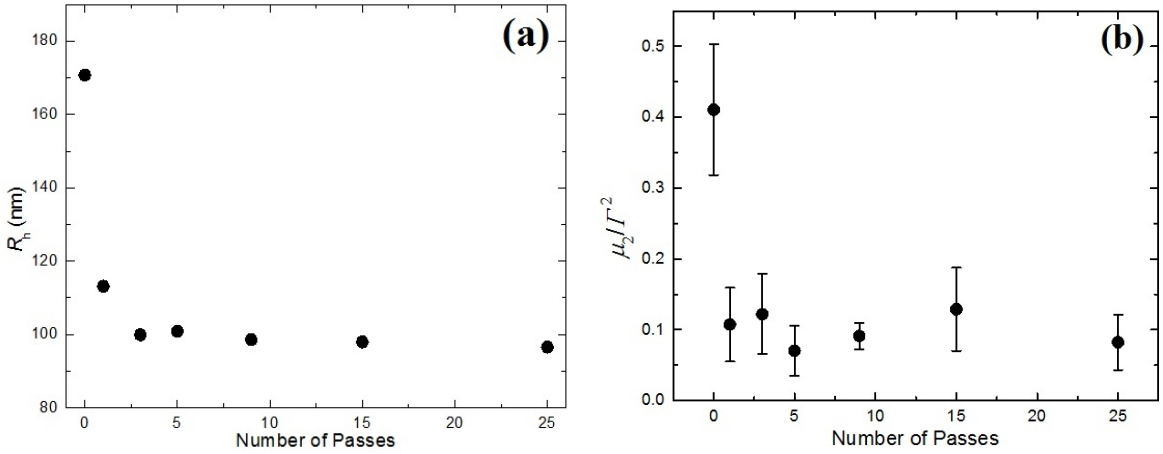

Figure 2–3. (a) Evolution of hydrodynamic radius (R_h) and (b) size dispersity (μ_2/Γ^2) of PB–PEO(9–3) with the number of passes through the 100 nm radius pore, which were measured by DLS at the angle of 90°.

While the PB–PEO(9–3) polymersomes with rubbery PB bilayer membranes did pass through the extruder under manually applied pressure at room temperature, it was not possible to extrude PS–PEO(14–2.5) polymersomes with glassy hydrophobic segments. The estimated glass transition temperature (T_g) of 14 kg/mol PS homopolymers is around 90 °C.[42] When the PS–PEO(14–2.5) solution was driven through the extruder membrane, the cloudy solution turned optically clear, indicating loss of the polymer material.

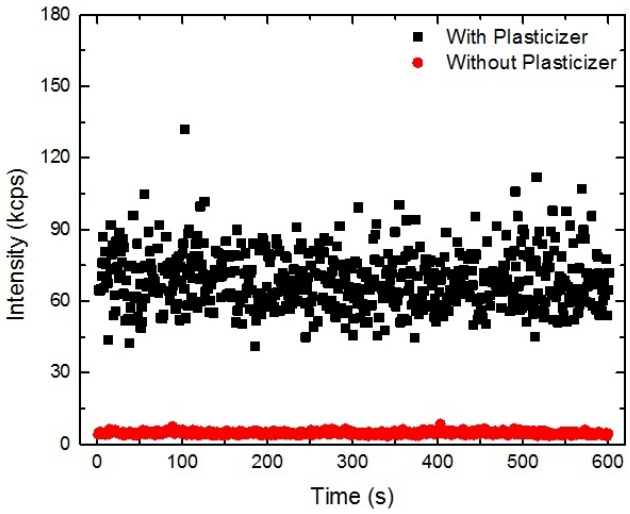

Figure 2–4. Scattering intensity comparison of the extruded solution of PS–PEO(14–2.5) with 10 vol % of dichloromethane as plasticizer (■) and without plasticizer (●).

However, when 10 vol % of DCM was added to the PS–PEO(14–2.5) solution as a plasticizer for the PS bilayer membrane, the solution remained cloudy even after several passes, and the scattering intensity of the extruded solution actually increased compared to the pristine solution as shown in Figure 2–4. The scattering result indicates that the plasticization decreases the T_g of the PS membrane, consequently the polymersomes are ruptured through the extrusion process rather than filtered out. The fluidity of the polymersome membrane is an important factor to consider during extrusion, since the large polymersomes need to be ruptured when they are extruded through the pores.[43] The fluidity of the membrane is governed by the molecular weight and the glass transition temperature (T_g) of the membrane forming block.[44,45] Since T_g of the PS membrane is higher than room temperature, the minimum required force to overcome the line tension of the polymersomes might be much higher than the PB–PEO(9–3) counterpart. The extrusion of PS–PEO(14–2.5) polymersomes with DCM added produced narrowly dispersed polymersomes with size comparable to the extruder membrane. The $<R_h>$

decreased from around 300 nm to 110 nm, and μ_2/Γ^2 also significantly decreased from 0.53 to 0.13, after 9 passes, as shown in Figure 2–5.

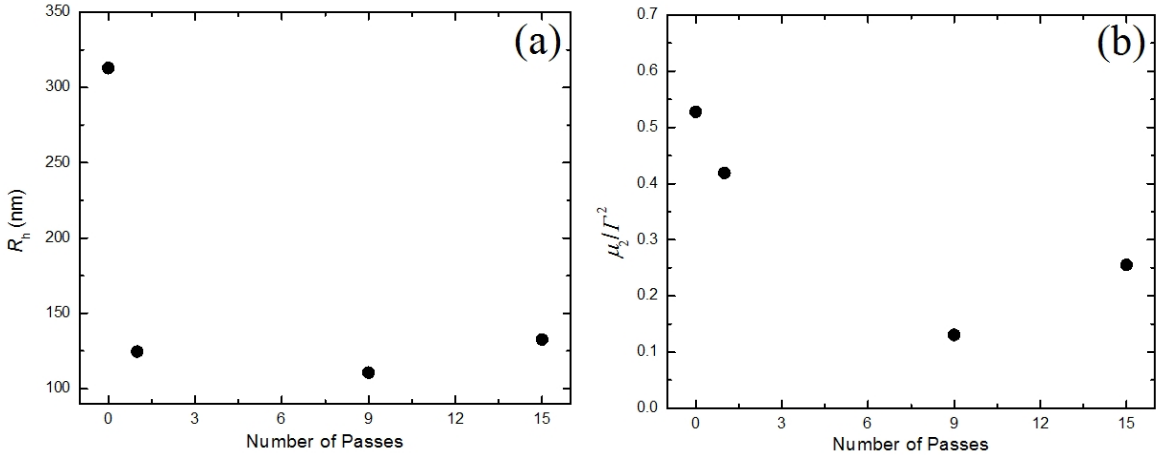

Figure 2–5. (a) Evolution of hydrodynamic radius (R_h) and (b) size dispersity (μ_2/Γ^2) of DCM added PS–PEO(14–2.5) polymersomes with the number of passes increases through the 100 nm radius pore, which were measured by DLS at the angle of 90°.

Interestingly, some of the extruded PS–PEO (14–2.5) polymersomes exhibited prolate shapes. Figure 2–6a shows PS–PEO(14–2.5) polymersomes after 9 extrusion passes. Many of polymersomes in the images have elliptical shapes, including dumbbells, and the measured aspect ratio ranges from 1.1 to 2.3. The length of the minor axis ranged from *ca.* 100 nm to 200 nm. These cryo-TEM results indicate that the size of the polymersomes was decreased, but the deformed shape did not completely recover to a spherical form after passing through the membrane pore, which has an aspect ratio of 30. This frozen shape of the polymersomes is presumably also due to the high T_g of the PS membranes. In other words, the CS made the PS membranes sufficiently compliant to enter the pores, but by the time they exited at the downstream end the kinetics of shape recovery was too slow. However, the spherical shape could be restored by annealing the solution at 100 °C for 8 h, as shown in Figure 2–6b.

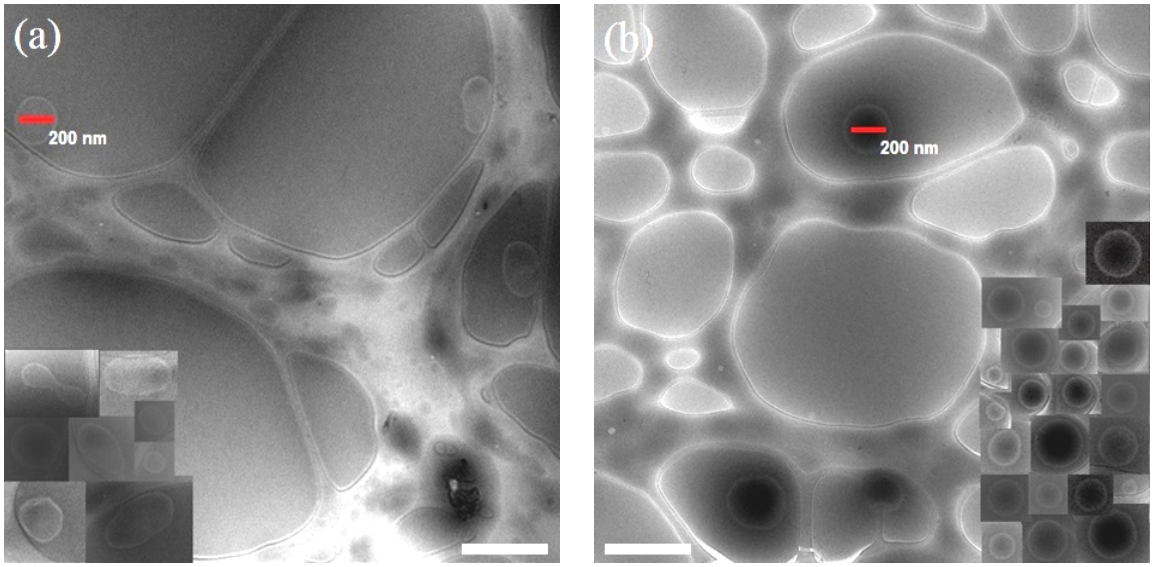

Figure 2–6. Cryo-TEM images of (a) PS–PEO(14–2.5) polymersomes in [EMIM][TFSI] after 9 times extrusion with 10 vol % of DCM, and (b) the polymersomes after being annealed at 100 °C after the extrusion. Images of PS–PEO(14–2.5) polymersomes were collected and pasted on the image with the same scale. Scale bars 500 nm.

The main disadvantage of extrusion is the loss of solution during the process.[46] Furthermore, the extruder membrane failure can occur by building up of high pressure, owing to the blockage of the polycarbonate membrane pores by the polymersomes.[47] Accordingly, longer processing times and higher pressures are needed. Despite these disadvantages, extrusion is still a powerful tool to obtain a desired polymersome size. Especially, the extrusion with ILs can be applied to various polymers regardless of their T_g. A crucial prerequisite for the extrusion is relatively larger polymersomes than the pore size of the extruder membrane. Block copolymers having a high T_g block (*e.g.* PS) cannot form polymersomes through the TF method, which can make relatively large polymersomes,[48,49] because the diffusion process of solvent into high T_g polymer film is significantly reduced. In ILs, however, the process temperature can be set well above the T_g of the glassy segments to accelerate the solvent diffusion, since the IL is a stable liquid

even at high temperature (the melting temperature of [EMIM][TFSI] is −12 °C, and the degradation occurs above 400 °C[50]).

In the TF method, the thin film is swollen by a selective solvent, and polymersomes form and diffuse into the IL.[51,52] In contrast, the polymersomes through the CS method are homogeneously and instantaneously formed, when the amount of a selective solvent drops to the point where the solution turns cloudy.[53] Therefore, the quality and content of a co-solvent in the solution can affect the dimension of the formed polymersomes.

The samples prepared by the CS method have an additional number in their labels. The number after the polymer code is the initial volume fraction of DCM in the solution. For example, PS–PEO(14–2.5)-60 means that the polymersomes in [EMIM][TFSI] were prepared for PS–PEO(14–2.5) and the initial solution contained by 60 vol % of DCM and 40 vol % of [EMIM][TFSI]. The final solution, however, had no DCM, which was removed under vacuum. The critical concentration of [EMIM][TFSI] at which the polymers start to self-assemble was determined by laser scattering. The solution turned cloudy at the point where the DCM content decreased to less than about 70 vol %, as shown in Figure 2–7. [EMIM][TFSI] was gradually added to the polymer solution in DCM to control the initial DCM content from 17 vol % up to 60 vol %. Figure 2–8 shows the size distribution of each sample, and illustrates the effect of co-solvent content on the polymersome size and dispersity. As the initial DCM content increased, the size and dispersity decreased for both PS–PEO(14–2.5) and PB–PEO(9–3) polymersomes. For example, $\langle R_h \rangle$ of PS–PEO(14–2.5)-17 was 457 nm with μ_2/Γ^2 = 0.35, but that of PS–PEO(14–2.5)-60 was 68 nm with a dispersity (μ_2/Γ^2) of 0.11. This trend was the same for PB–PEO(9–3) with rubbery bilayer membranes. The cumulant fitting gave $\langle R_h \rangle$ = 253 nm, μ_2/Γ^2 = 0.37 for PB–PEO(9–3)-30, but $\langle R_h \rangle$ = 67 nm, μ_2/Γ^2 = 0.13 for PB–PEO(9–3)-60. Cryo-TEM images of PS–PEO(14–2.5)-20 and PS–PEO(14–2.5)-60 in Figure 2–9 clearly show the effect of the DCM content on the size and dispersity.

Whereas the size of the PS–PEO(14–2.5)-20 polymersomes varies from 87 nm to 275 nm in radius in Figure 2–9a, Figure 2–9b from PS–PEO(14–2.5)-60 shows relatively smaller (mean radius is 74 nm) and more narrowly dispersed (standard deviation of radius, σ = 14 nm) polymersomes. The effect of CS content on the size of polymersomes also can be seen in the case of PB–PEO(9–3) as shown in Figure 2–10.

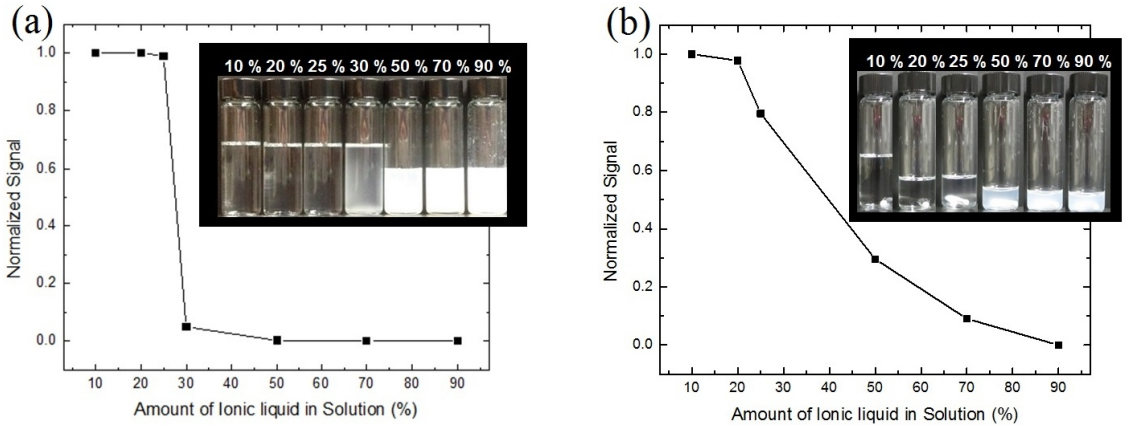

Figure 2–7. Transmittance measurement of (a) PS–PEO(14–2.5) and (b) PB–PEO(9–3) in DCM and [EMIM][TFSI] solution at various [EMIM][TFSI] volume contents. The final concentration of polymers was 0.5 wt % in [EMIM][TFSI] after the co-solvent evaporation. The inset experimental images are PS–PEO(14–2.5) and PB–PEO(9–3) in the mixtures of DCM and [EMIM][TFSI].

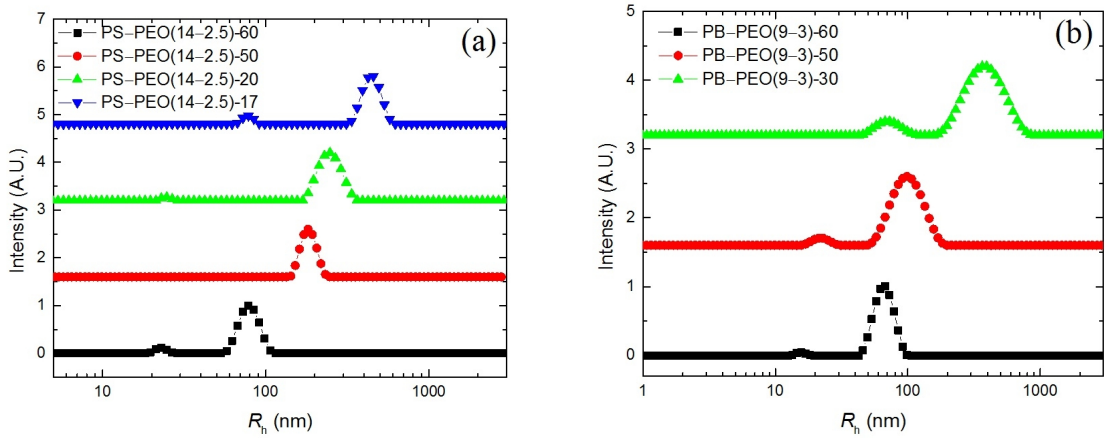

Figure 2–8. Hydrodynamic radius (R_h) distribution of (a) PS–PEO(14–2.5) and (b) PB–PEO(9–3) at different initial content of DCM. R_h increases, as the initial DCM content decreases.

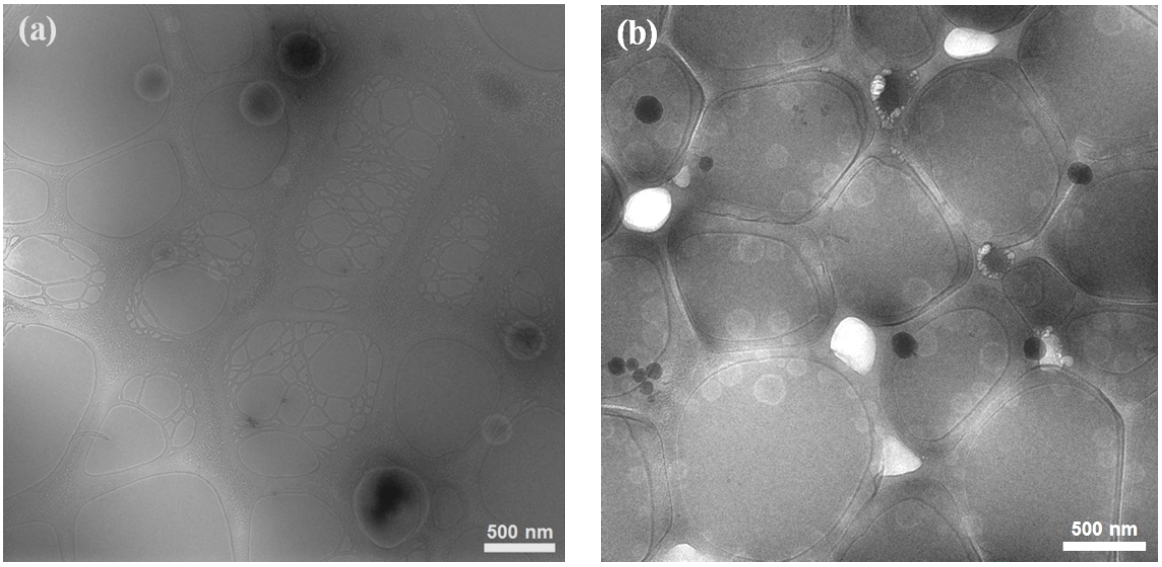

Figure 2–9. Cryo-TEM images of PS–PEO(14–2.5) polymersomes in [EMIM][TFSI] (0.5 wt %); (a) PS–PEO(14–2.5)-20, (b) PS–PEO(14–2.5)-60. Scale bars 500 nm.

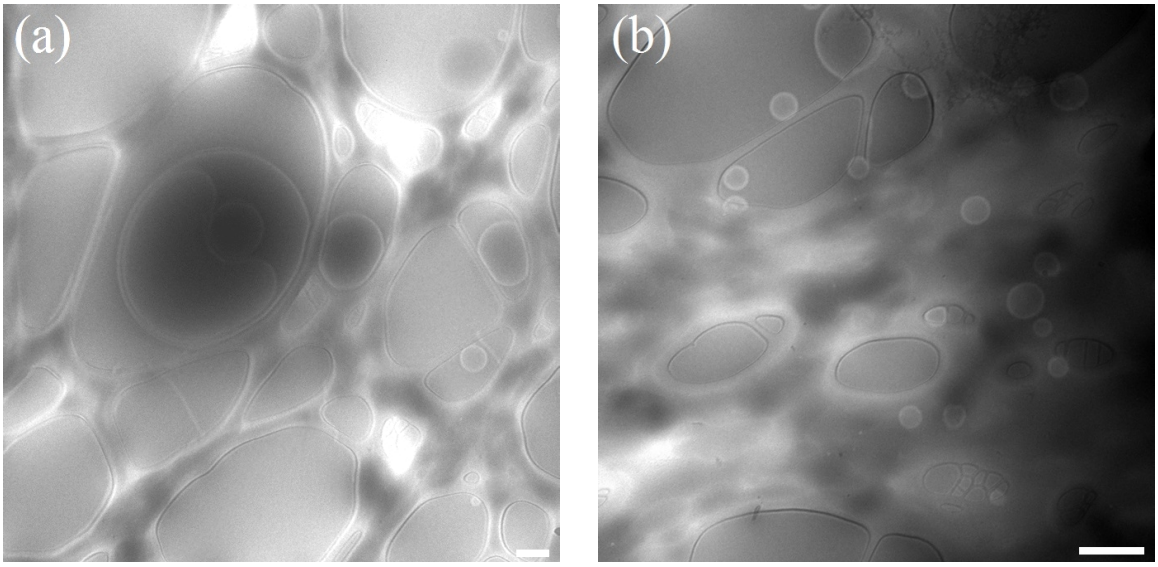

Figure 2–10. Cryo-TEM images of PB–PEO(9–3) polymersomes in [EMIM][TFSI] (0.5 wt %); (a) PB–PEO(9–3)-30, (b) PB–PEO(9–3)-60. Scales bars: 200 nm.

These changes are due to the solvent quality toward the membrane forming blocks, PS and PB. The solvent quality can be understood via solubility parameter (δ) differences between the two components, which is directly related to the interfacial tension. The solubility parameters of PS (δ_{PS}) and PB (δ_{PB}) are 18.6 $MPa^{1/2}$ and 17.1 $MPa^{1/2}$ close to 20.2 $MPa^{1/2}$ of DCM, but the solubility parameter of the IL, δ_{IL} is 27.6 $MPa^{1/2}$.[54,55] Therefore, the increase of [EMIM][TFSI] content to the amount of DCM should increase the interfacial tension between the bilayer membranes and the solvent mixture. Since the total interfacial energy is proportional to the surface area of the polymersomes, the polymersome size should be larger in order to reduce the surface area per chain when more [EMIM][TFSI] is added. Similar observations were also made by Luo and Eisenberg.[56] They studied the size changes of polystyrene-*b*-poly(acrylic acid) (PS–PAA) assemblies by varying the THF/dioxane content from 43.3% to 80% in mixtures with water. THF/dioxane was used as a co-solvent, and water was a selective solvent for the polymers. As water content increased, the vesicle size also increased. They also demonstrated that the larger vesicles had higher size dispersity due to less size dependent total interfacial energy change, which is proportional to $-1/R^2$.

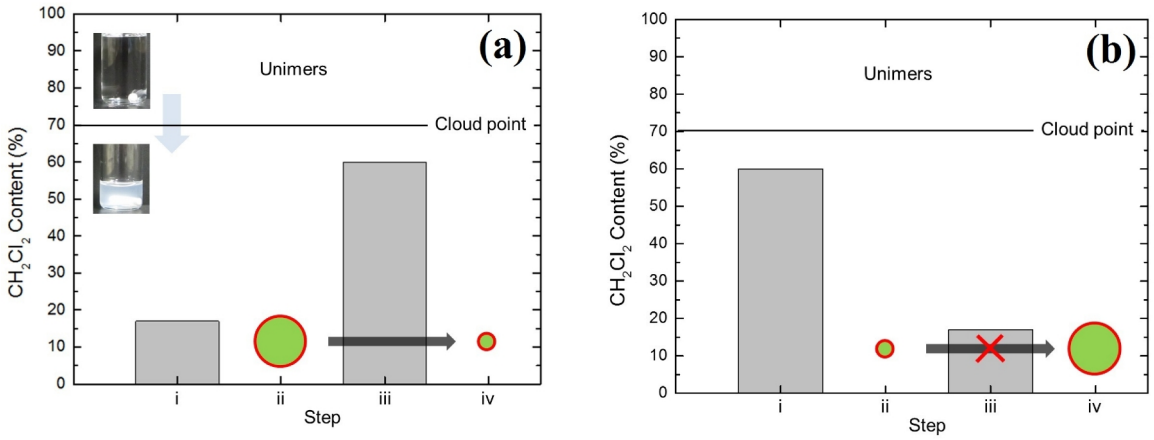

Figure 2–11. Phase diagrams of PS–PEO and PB–PEO polymers, and the DCM content along with the each step for the reversibility test for (a) PS–PEO(14–2.5)-17 to PS–PEO(14–2.5)-17-to-60, and (b) PS–PEO(14–2.5)-60 to PS–PEO(14–2.5)-60-to-17.

PS–PAA polymersomes showed reversible size change with solvent composition within the time scale of a minute. The larger polymersomes could become smaller, and the smaller ones could grow through fission and fusion mechanisms, by adding water or THF/dioxane, respectively. Here, in contrast, the size of the PS–PEO and PB–PEO polymersomes was not reversible. The reversibility was tested as shown in Figure 2–11. In step (i), [EMIM][TFSI] was added to the polymer solution, then the solution turned cloudy as described in the inset image of Figure 2–11a. Thereafter all the DCM was removed as depicted in step (ii) of Figure 2–11a and 2–11b. Depending on the DCM content in step (i), different sizes of polymersomes were prepared. In step (iii), even more DCM was added to the solution of the larger polymersomes (Figure 2 –11a), however the amount of DCM was less compared to the case of smaller polymersomes (Figure 2 –11b). Then all of DCM in the solution was evaporated as depicted in step (iv). The final samples after these four steps were named and differentiated with the initial samples by adding '-to-(vol % of DCM in step (iii))'. If this size change was thermodynamically reversible, the bigger vesicles should shrink, and vice versa. But as shown in the size distributions (Figure 2–12a), smaller vesicles did not grow even when the polymersome solution was interrupted by addition of CS, whereas bigger vesicles diminished in size and the dispersity in the time scale of mixing of about 5 h at step (iii). These observations indicate that the size change was not thermodynamically reversible. The size of PS–PEO(14–2.5)-17 was significantly decreased from 457 nm to 86 nm in radius, and the dispersity was also reduced from μ_2/Γ^2 = 0.35 to 0.12. However, PS–PEO(14–2.5)-60-to-17 had the same dimensions with PS–PEO (14–2.5)-60 as $<R_h>$ = 68 nm, μ_2/Γ^2 = 0.13. Figure 2–12b shows a cryo-TEM image of PS–PEO(14–2.5)-17-to-60 polymersomes. Compared to the image of PS–PEO (14–2.5)-20 polymersomes (Figure 2–9a), the size and dispersity of PS–PEO (14–2.5)-17-to-60 polymersomes significantly diminished. The average radius in the image is 75 nm (± 16 nm), which is close to that of

PS–PEO(14–2.5)-60. It is known that the chain exchange rate (k (s^{-1})) of amphiphilic chains in a solution is proportional to $exp(-\gamma)$, where γ is interfacial tension between hydrophobic part and a solvent.[57] Therefore, the size irreversibility of PS–PEO polymersomes is due to kinetically locked-in structure when the IL content is dominant. At low DCM concentration, γ is not changed much, consequently the polymersomes are frozen without size or morphology changes, whereas the size can change at high DCM concentration due to the increased mobility of PS membrane.

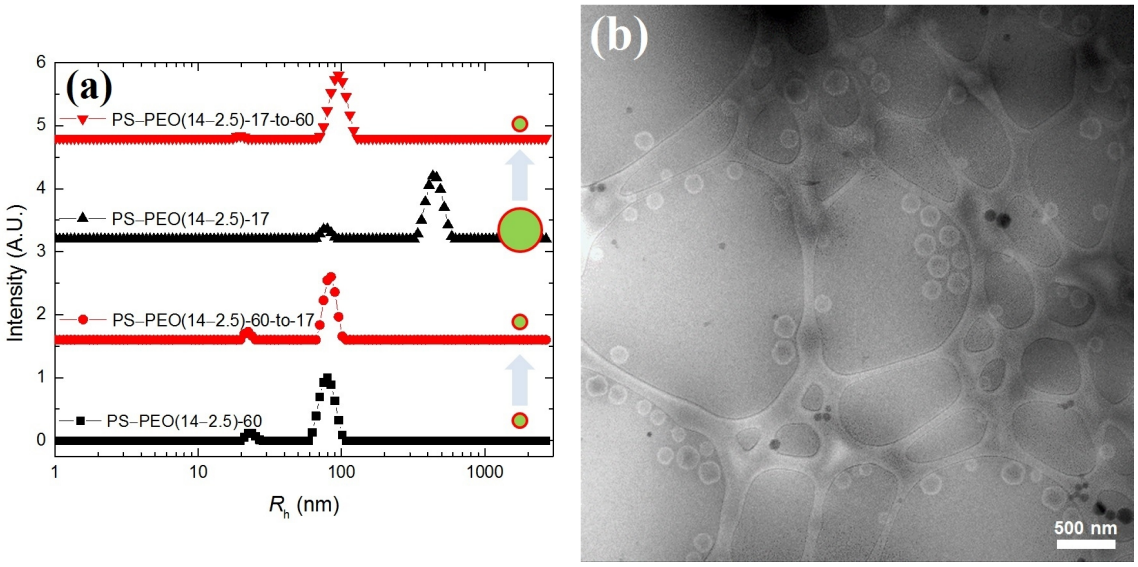

Figure 2–12. Size change of PS–PEO(14–2.5) polymersomes when [EMIM][TFSI] content is changed from 83% to 40%.; (a) Size distribution change measured by DLS, and (b) Cryo-TEM image of PS–PEO(14–2.5)-17-to-60 in [EMIM][TFSI].

Meli *et al.* studied the path-dependent morphology change of PB–PEO and PS–PEO micelles in ionic liquids.[54] Through the CS method, small and narrowly dispersed spherical micelles were obtained, but through the TF method or direct dissolution (DD) method, large and broadly dispersed micelles formed. By annealing the solutions at 170 °C, the micelles from the TF and DD protocols achieved their equilibrium size, while the micelles from the CS protocol failed to attain the equilibrium size, which is larger than

the original. The authors concluded that the partial equilibration can be explained by the aggregation number (Q) difference of a system from the aggregation number at equilibrium (Q_{eq}), as proposed by Dormidontova.[58] When $Q > 1.5Q_{eq}$, micelles fission into smaller micelles, but when Q is close to Q_{eq}, size of the micelles does not change. In the current study, the irreversibility of PB–PEO and PS–PEO polymersomes resulted in size change only towards the minimal size of the polymersomes. The smaller polymersomes could not grow into the bigger ones. According to vesicle formation mechanism, the minimal vesicle size (R_{min}) can be determined by the energy balance between the surface tension from the edge of bilayer disks and the bending energy of vesicles.[32,59] R_{min} is $2k_c/(\gamma d)$, where k_c is the bending modulus of the membrane, γ is the surface tension of the membrane in a solvent, and d is the thickness of the membrane. A vesicle having curvature will be spontaneously formed when the bending energy is less than the surface energy of the disk, and will have the radius larger than R_{min}. The estimated R_{min} of a PB–PEO(9–3) polymersome is around 40 nm after accounting for the membrane thickness and the corona length. (k_c of PB membrane is around 5.4×10^{-18} J, γ of PB-water is assumed same as γ of a pure hydrocarbon-water interface, which is around 26 mJ /m^2, and d_m is 22 nm from the d_m of PB–PEO(9–3) polymersomes.[60,61]) There is no specific equilibrium radius in terms of bending and surface tension energy since the vesicle formation is favorable when R is larger than R_{min}, but as in lipid vesicle system, the equilibrium radius of polymersomes can be defined with the balance between the entropy of mixing and the curvature energy. Therefore, unless the chain exchange or fusion and fission are limited by kinetically frozen membranes, there should be an equilibrium state for equilibrium radius, R_{eq}. R_{eq} can be accessible under high CS content, at where the polymersomes can have highly mobilized membranes. If R_{eq} is close to R_{min}, this irreversibility is on the same line with the study of Meli *et al.*, and Dormidontova. At high DCM content condition, the polymersomes are expected to be under thermodynamic

equilibrium, which leads to small size and narrow dispersity. As DCM evaporates, the interfacial tension between the membrane and the solvent increases and the polymersomes are locked in the size at the initial equilibrium state, since this effect can be attributed to the dramatic decrease in the molecular exchange rate between polymersomes or the polymersome fission and fusion process. However, at low DCM content, the equilibrium could not be achieved because the polymersomes were formed instantaneously and frozen after adding the selective solvent. After the second DCM addition process, the size of large polymersomes decreased to the equilibrium value since the polymersomes with low DCM content were far from the R_{eq}, while those with high DCM content was near at the equilibrium value.

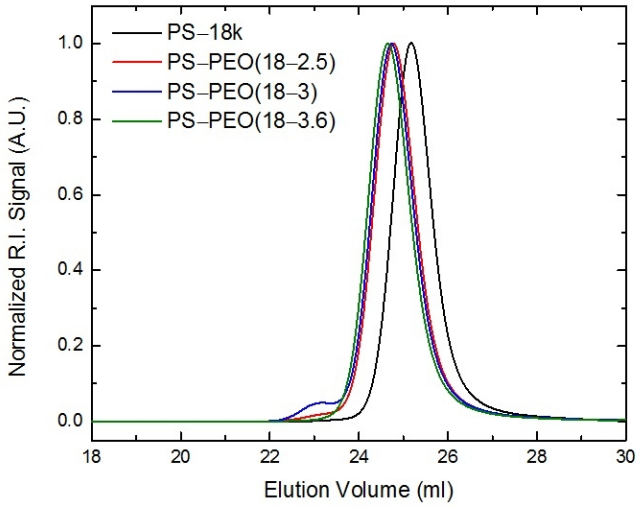

Figure 2–13. SEC traces of polystyrene ($M_{n,PS}$ = 18 kg/mol) and PS–PEO block copolymers having different PEO block length ($M_{n,PEO}$ = 2.5 kg/mol, 3 kg/mol, 3.6 kg/mol).

Moreover, the effect of hydrophilic block length was studied by systemically varying the PEO block length with a constant 18 kg/mol of PS-OH. With three different PS–PEO(18–2.5), PS–PEO(18–3), and PS–PEO(18–3.6) (see the SEC traces of PS–PEO

polymers in Figure 2–13), the CS method was used for the polymersome preparation. The initial DCM content was fixed at 60 vol % for all polymers. As shown in Figure 2–14, as the PEO length is increased, the size of polymersomes decreased; (cryo-TEM images are shown in Figure 2–15). The longer PEO block can accommodate more volume to prevent the contact with PS membrane from the exposure to the IL or IL/DCM mixture. Therefore the curvature of the polymersomes should be larger with longer PEO block.

The size and dispersity of the polymersomes could be controlled kinetically by varying the CS content and the length of PEO block of PS-PEO. Both approaches successfully produced small and monodispersed polymersomes in the IL. Compared to other systems with water as a selective solvent, the CS protocol with the IL is more efficient and environmentally friendly due to non-volatile IL. The organic CS, DCM, was effectively removed under vacuum, and the time for preparing the organic solvent free polymersomes was much reduced because there was no additional steps, such as dialysis.

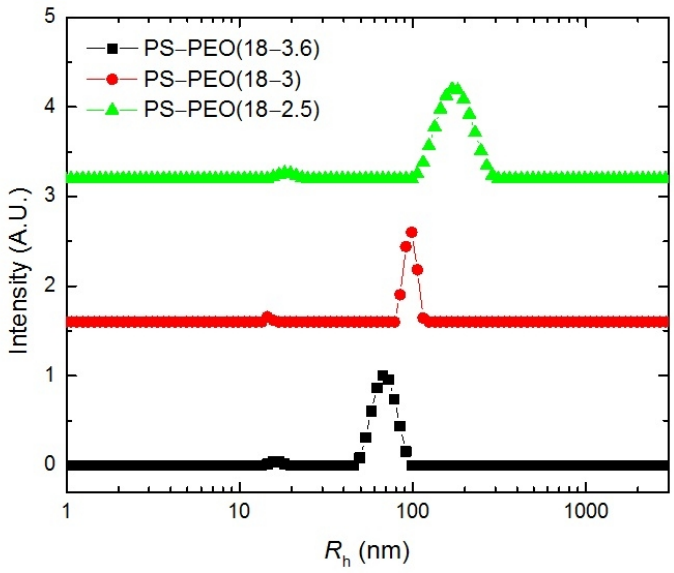

Figure 2–14. Effect of PEO block length on the size of PS–PEO polymersomes. The initial content of [EMIM][TFSI] was 40% for all polymers.

2.4 Conclusions

In summary, the size and dispersity of PS–PEO and PB–PEO polymersomes in [EMIM][TFSI] were controlled by mechanical extrusion or by changing the methodology of the polymersome formation. The rather precisely controlled size ($<R_h> \approx 100$ nm) with fairly narrow size distribution (less than $\mu_2/\Gamma^2 \approx 0.2$) of the polymersomes was obtained by several passes through polycarbonate membranes. Through the kinetic control, relatively monodisperse small polymersomes (($<R_h> \approx 70$ nm, $\mu_2/\Gamma^2 \approx 0.1$) were obtained with an organic solvent at high CS content. Non-volatile IL directly led to the organic solvent free polymersomes with a single step under vacuum. Increasing the CS concentration and the PEO block length, the diameter and size dispersity of the polymersomes decreased. Furthermore, as-assembled polymersomes using the co-solvent method showed irreversible size change with additional DCM.

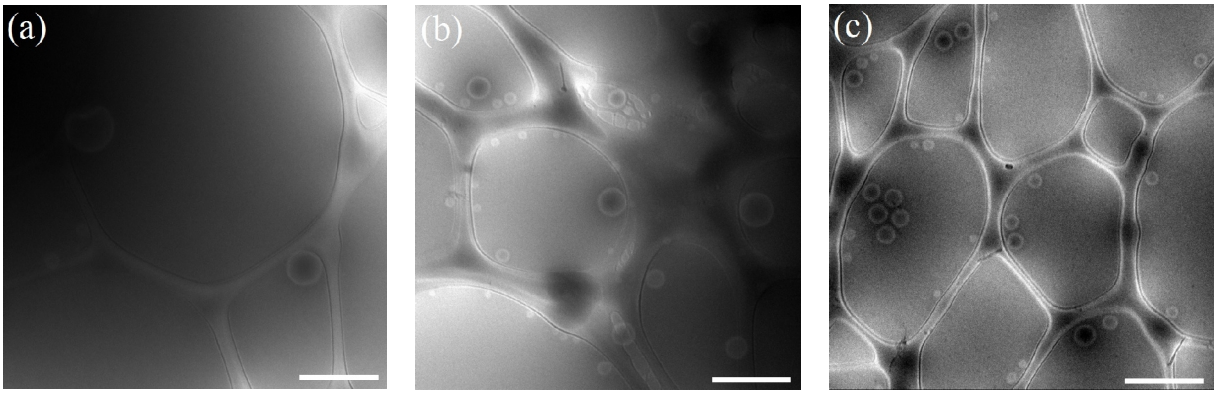

Figure 2–15. Cryo-TEM images of PS–PEO polymersomes having 18 kg/mol of PS block, but different length of PEO in [EMIM][TFSI] (0.5 wt %); (a) PS–PEO(18–2.5), (b) PS–PEO(18–3), (c) PS–PEO(18–3.6) with 60 vol % of initial dichloromethane. Scale bars: 500 nm.

2.5 References

1. Oliver-Bourbigou, H.; Magna, L.; Morvan, D. *Appl. Catal. A* **2010**, *373*, 1–56.
2. Wei, D.; Ivaska, A. *Anal. Chim. Acta.* **2008**, *607*, 126–135.
3. Stoimenovski, J.; MacFarlane, D. R. *Chem. Commun.* **2011**, *47*, 11429–11431.
4. Sekhon, B. S. *Asian J. Pharm. Biol. Res.* **2011**, *1*, 395–411.
5. Chiappe, C.; Pieraccini, D. *J. Phys. Org. Chem.* **2005**, *18*, 275–297.
6. Shin, W. S. *News & information for chemical engineers* **2007**, *25*, 286–291.
7. Sheldon, R. *Chem. Commun.* **2001**, 2399–2407.
8. Rogers, R. D.; Seddon, K. R. *Science* **2003**, *302*, 792–793.
9. Welton, T. *Chem. Rev.* **1999**, *99*, 2071–2084.
10. Appetecchi, G. B.; Scaccia, S.; Tizzani, C.; Alessandrini, F.; Passerini, S. *J. Electrochem. Soc.* **2006**, *153*, A1685–A1691.
11. Luo, H. M.; Li, Y. Q.; Zheng, W. J. A *Chinese Chem. Lett.* **2005**, *16*, 906–908.
12. Wolfson, A.; Vankelecom, I. F. J.; Jacobs, P. A. *Tetrahedron Lett.* **2005**, *46*, 2513–2516.
13. Zhang, Y.; Chen, X.; Lan, J.; You, J.; Chen, L. *Chem. Biol. Drug. Des.* **2009**, *74*, 282–288.
14. Kragl, U.; Eckstein, M.; Kaftzik, N. *Curr. Opin. Biotech.* **2002**, *13*, 565–571.
15. Lodge, T. P. *Science* **2008**, *321*, 50–51.
16. Ueki, T.; Watanabe, M. *Macromolecules* **2008**, *41*, 3739–3749.
17. Schulze, M. W.; McIntosh, L. D., Hillmyer, M. A.; Lodge, T. P. *Nano Lett.* **2014**, *14*, 122–126.
18. Cho, J. H.; Lee, J.; Xia, Y.; Kim, B.; He, Y.; Renn, M. J.; Lodge, T. P.; Frisbie, C. D. *Nat. Mater.* **2008**, *7*, 900–906.
19. Gu, Y.; Cussler, E. L.; Lodge, T. P. *J. Membr. Sci.* **2012**, *423–424*, 20–26.
20. Bai, Z.; Lodge, T. P. *J. Am. Chem. Soc.* **2010**, *132*, 16265–16270.

21. Ueki, T.; Sawamura, S.; Nakamura, Y.; Kitazawa, Y.; Kokubo, H.; Watanabe, M. *Langmuir* **2013**, *29*, 13661–13665.
22. Bai, Z.; Lodge, T. P. *Langmuir* **2010**, *26*, 8887–8892.
23. Wong, B.; Boyer, C.; Steinbeck, C.; Peters, D.; Schmidt, J.; van Zanten, R.; Chmelka, B.; Zasadzinski, J. A. *Adv. Mater.* **2011**, *23*, 2320–2325.
24. Antonietti, M.; Förster, S. *Adv. Mater.* **2003**, *15*, 1323–1333.
25. Chen, Q.; Schonherr, H.; Vancso, G. J. *Small* **2009**, *5*, 1436–1445.
26. Hunter, D. G.; Frisken, B. J. *Biophys. J.* **1998**, *74*, 2996–3002.
27. Hope, M. J.; Bally, M. B.; Webb, G.; Cullis, P. R. *Biochim. Biophys. Acta* **1985**, *812*, 55–65.
28. Patty, P. J.; Frisken, B. *Biophys. J.* **2003**, *85*, 996–1004.
29. Hauschild, S.; Lipprandt, U.; Rumplecker, A.; Borchert, U.; Rank, A.; Schubert, R.; Föster, S. *Small* **2005**, *1*, 1177–1180.
30. Thiele, J.; Steinhauser, D.; Pfohl, T.; Förster, S. *Langmuir* **2010**, *26*, 6860–6863.
31. Sanson, C.; Schatz, C.; Le Meins, J.-F.; Brûlet, A.; Soum, A.; Lecommandoux, S. *Langmuir* **2010**, *26*, 2751–2760.
32. Le Meins, J.-F., Sandre, O.; Lecommandoux, S. *Eur. Phys. J. E* **2011**, *34*, 1–17.
33. Meli, L.; Lodge, T. P. *Macromolecules* **2009**, *42*, 580–583
34. Jakes, J. *Collect. Czech. Chem. Commun.* **1995**, *60*, 1781–1797.
35. Mok, M. M.; Lodge, T. P. *J. Polym. Sci. B* **2012**, 50, 500–515.
36. Simone, P. M.; Lodge, T. P. *Macromol. Chem. Phys.* **2007**, *208*, 339–348.
37. Bai, Z.; He, Y.; Young, N. P.; Lodge, T. P. *Macromolecules* **2008**, *41*, 6615–6617.
38. Simone, P. M.; Lodge, T. P. *Macromolecules* **2008**, *41*, 1753–1759.
39. He, Y. Y.; Li, Z. B.; Simone, P.; Lodge, T. P. *J. Am. Chem. Soc*. **2006**, *128*, 2745–2750.
40. Kesselman, E.; Talmon, Y.; Bang, J.; Abbas, S.; Li, Z.; Lodge, T. P. *Macromolecules*

2005, *38*, 6779–6781.

41. Williams, D. B.; Carter, C. B. *Transmission Electron Microscopy, Imaging III*; Plenum Press: New York, 1996.
42. Hiemenz, P. C.; Lodge, T. P. *Polymer Chemistry*; 2nd ed; CRC Press: Boca Raton, London, New York, 2007
43. Nayar, R.; Hope, M. J.; Cullis, P. R. *Biochim. Biophys. Acta* **1989**, *986*, 200–206.
44. Aranda-Espinoza, H.; Bermudez, H.; Bates, F. S.; Discher, D. E. *Phys. Rev. Lett.* **2011**, *87*, 208301-1–208301-4.
45. Plazek, D. J.; O'Rourke, V. M. *J. Polym. Sci. A-2 Polym. Phys.* **1971**, *9*, 209–243.
46. Wagner, A.; Vorauser-Uhl, K. *J. Drug Deliv.* **2011**, 591325.
47. Frisken, B. J.; Asman, C.; Patty, P. J. *Langmuir* **2000**, *16*, 928–933.
48. Kim, K. T.; Zhu, J.; Meeuwissen, S. A.; Cornelissen, J. J. M.; Pochan, D. J.; Nolte, R. J. M.; van Hest, J. C. M. *J. Am. Chem. Soc.* **2010**, *132*, 12522–12524.
49. Mai, Y.; Eisenberg, A. *Chem. Soc. Rev.* **2012**, *41*, 5969–5985.
50. Garcia, B.; Lavallée, S.; Perron, G.; Michot, C.; Armand, M. *Electrochim. Acta* **2004**, *49*, 4583–4588.
51. Battaglia, G.; Ryan, A. J. *J. Phys. Chem. B* **2006**, *110*, 10272–10279.
52. LoPresti, C.; Lomas, H. Massignani, M.; Smart, T.; Battalia, G. *J. Mater. Chem.* **2009**, *19*, 3576–3590.
53. Choucair, A.; Lavigueur, C.; Eisenberg, A. *Langmuir* **2004**, *20*, 3894–3900.
54. Meli, L.; Santiago, J. M.; Lodge, T. P. *Macromolecules* **2010**, *43*, 2018–2027.
55. Ovalles, C.; Rogel, E.; Moir, M.; Thomas, L.; Pradhan, A. *Energy Fuels* **2012**, *26*, 549–556.
56. Luo, L.; Eisenberg, A. *Langmuir* **2011**, *17*, 6804–6811.
57. Förster, S.; Borchert, K. Polymer Vesicles. *Encyclopedia of Polymer Science and Technology,* 2005.

58. Lund, R.; Willner, L.; Richter, D.; Dormidontova, E. E. *Macromolcelus* **2006**, *39*, 4566–4575.

59. Sackmann, E. *FEBS Lett.* **1994,** *346*, 3–16.

60. Bermudez, H.; Brannan, A. K.; Hammer, D. A.; Bates, F. S.; Discher, D. E. *Macromolecules* **2002**, *35*, 8203–8208.

61. Discher, B. M.; Won, Y.; Ege, D. S.; Lee, J. C-M.; Bates, F. S.; Discher, D. E.; Hammer, D. A. *Science* **1999**, *284*, 1143–1146.

Chapter 3

Rate of Molecular Exchange Through the Membranes of Ionic Liquid Filled Polymersomes Dispersed in Water by NMR Techniques*

3.1 Introduction

Polymeric vesicles prepared from amphiphilic block copolymers, or polymersomes, have attracted increased attention as potential "nanoreactors", due to tunability of their building blocks and similarity to biological cell structures. Vesicles exhibit both confined interiors and membranes that provide enough room to load active substances.[1] For example, the internal space of vesicles can be used to encapsulate and deliver active materials, *e.g.* fragrances, drugs, catalysts, and reactants.[2–4] The use of vesicles in such applications depends on their membrane properties (*e.g.*, permeability and stability), which can be controlled and tuned by precise molecular design of the constituting blocks.[5] In this regard, polymersomes have greater flexibility and versatility via readily tuned parameters such as block length and chemical structure, compared to liposomes prepared from low molecular weight phospholipids.[6]

Recently, Bai and Lodge developed a new kind of polymersome solution or "nanoemulsion", in which a water-immiscible ionic liquid (IL) is compartmentalized within water.[7] The polymersomes, dispersed in water, from 1,2-polybutadiene-*b*-

* This chapter is reproduced in part with permission from So, S.; Lodge, T. P. *J. Phys. Chem. C* **2014**, *118*, 21140–21147.

poly(ethylene oxide) (PB–PEO) contained 1-ethyl-3-methylimidazolium bis(trifluoro-methyl-sulfonyl)imide ([EMIM][TFSI]). The IL-filled polymersomes are distinct from canonical vesicles, which have the same fluid inside and outside.[1,6,8] They offer an opportunity to design new reaction processes by installing appropriate catalysts within the IL interiors, while maintaining the facile molecular transport, low viscosity, and cost-effectiveness of an aqueous majority phase.[9,10] These vesicles are prepared via a thermoresponsive polymersome "shuttling" in the biphasic system of water and IL. After transfer of the polymersomes from a hydrophobic IL to water, the IL inside the polymersomes remains segregated and stabilized from the aqueous phase by the hydrophobic and IL-phobic bilayer PB core.[11]

This reversible shuttle of the IL-filled polymersomes exhibits characteristics of both homogeneous and heterogeneous catalysis. Since the locus of the reaction is the liquid interior of the polymersomes, the reaction is potentially homogeneous, yet this system resembles heterogeneous catalysis in that facile and quantitative recovery of the polymersome nanoreactors and catalyst can be conducted via the reverse thermoresponsive shuttle. The properties of such nanoemulsion-like polymersomes have not been studied extensively, and particularly the rate of molecular transfer into and out of the polymersomes has not been characterized; clearly the rate of molecular transport across the membrane will be an important factor in any reaction system design.[12] Especially, when polymersomes have completely different phases across the membranes, the permeability has not been explored. The change of chemical potential for a reagent or product molecule at each interface (IL-membrane or water-membrane) is not the same, in contrast to conventional vesicles, which have symmetric interfaces across the membrane. The permeation rate can be affected by the partitioning of a probe molecule between the two fluids, in addition to the solubility and diffusivity of the probe molecules in the

membrane, and the time scale of molecular permeation for each direction needs to be understood to optimize the system for nanoreactor applications.

Quantification of permeability is not straightforward compared to conventional polymersome systems. Previous studies of vesicle permeation have employed fluorescence or UV-Vis spectroscopy. Through these methods, the amount of molecules released from the vesicles or loaded to the vesicles can be quantified, and the permeability can be obtained. However, there are limitations in the selection of permeants in order to use either fluorescence or UV-Vis spectroscopy. [13–21] For example, Battaglia *et al.* studied the molecular permeability through the membranes of poly(ethylene oxide)-*b*-poly(butylene oxide) vesicles with an UV-detectable bimolecular reaction.[19] One of the reactants should be in the vesicles without permeation out of the vesicles, and the product should be UV-detectable, and stay in the vesicle interiors, for accurate results. In particular, tracer molecules should have partition coefficients between vesicle interior and exterior fluids on the order of unity.

In this study, the molecular exchange of small molecules through the bilayer membrane is investigated by a combination of ^{1}H NMR spectroscopy and pulsed-field-gradient (PFG-NMR) techniques. NMR is a powerful tool because any molecule having an NMR-active nucleus can be used.[22–24] In the nanoemulsion solution, tracer molecules exhibit two diffusion coefficients in the two different environments, and are exchanged across the membranes between two immiscible phases. Three similarly sized probes, [EMIM], [BMIM], and 1-butylimidazole, were used in order to quantify the permeation through the hydrophobic membranes. As far as we are aware, this is the first example that resolves molecular permeation into and out of the polymersomes separately. The results demonstrate a powerful tool to analyze molecular transport in nanoemulsion-like polymersome solutions, whereby it is possible to quantify the rates of reagent entry and product escape from am IL-filled nanorector.

3.2 Experimental Section

3.2.1 Materials. A 1,2-polybutadiene-*b*-poly(ethylene oxide) (PB–PEO) block copolymer was synthesized via sequential anionic polymerization by adding ethylene oxide to *ω*-hydroxyl 1,2-polybutadiene homopolymer (PB-OH). First, the PB-OH was synthesized in anhydrous tetrahydrofuran (THF) at –60 °C with sec-butyllithium as initiator. The polymerization was capped by addition of one ethylene oxide unit, then terminated by adding deoxygenated methanol. Characterization by ^{1}H NMR spectroscopy and size exclusion chromatography (SEC) gave a number-average molecular weight (M_n) and dispersity ($Đ$) of 9.3 kg/mol and 1.04, respectively. The synthesized PB-OH was dissolved in anhydrous THF and converted into macroinitiator using diphenylmethyl potassium as an electron transfer agent. Weighed ethylene oxide was added to the reactor at room temperature, and the temperature was increased to 45 °C. After 24 h, the reaction was terminated in the same manner as PB-OH. The polymer was characterized by ^{1}H NMR spectroscopy and SEC to obtain M_n and $Đ$, as summarized in Table 3–1. The synthesized PB–PEO was designated PB–PEO(9–3) based on the M_n of the PB and PEO blocks (9.3 kDa and 2.5 kDa, respectively). [EMIM][TFSI] was synthesized by combining equal moles of 1-ethyl-3-methylimidazolium bromide ([EMIM][Br], Io-Li-Tec, 99%) and lithium bis(trifluoromethylsulfonyl)imide ([Li][TFSI], HQ115) with water, as described previously.[25] 1-Butylimidazole (98%), and 1-butyl-3-methyl-imidazolium chloride ([BMIM]Cl, 99%) were purchased from Aldrich, and Io-Li-Tec, respectively, and used as received.

3.2.2 Polymersome Solution Preparation. The polymersomes were prepared through a co-solvent method to obtain a narrow size distribution. PB–PEO(9–3) was first dissolved in dichloromethane, and then an equal mass of [EMIM][TFSI] was added. The solution was dried by N_2 purge to selectively remove dichloromethane. Vesicle formation was prompted by slow evaporation of the dichloromethane to yield an 0.5 wt % polymersome

solution in non-volatile [EMIM][TFSI]. The polymersomes with IL interiors were then allowed to migrate from the IL solution to an immiscible aqueous phase. A weighed amount of deuterium oxide (D_2O) was added to the [EMIM][TFSI] solution of polymersomes according to the target polymersome content in D_2O (0.5, 1.0, or 1.5 wt %). The polymersomes transferred to the aqueous phase at room temperature with stirring (~ 100 rpm). The two immiscible phases were in contact for at least 12 h at room temperature to allow complete transfer. After the transfer, the ionic liquid phase on the bottom turned clear, and the upper aqueous phase became cloudy, due to light scattering from the vesicles. The cloudy aqueous phase was then carefully removed for the NMR studies. The size and dispersity of the prepared polymersomes were measured by dynamic light scattering (DLS). For the exchange of [EMIM], the aqueous solution was used as prepared ($C_{[EMIM]}$ ~ 42 mM, which was calculated by using the solubility of [EMIM][TFSI] in water,[26] and the volume of the polymersomes). For 1-butylimidazole and [BMIM] studies, 50 mM of 1-butylimidazole or [BMIM]Cl was added to the aqueous polymersome dispersion, respectively, and the solution was stirred for at least one day to allow equilibration.

Table 3–1. Characteristics of polymer and vesicles with [EMIM][TFSI] interiors dispersed in D_2O.

Polymer	M_{PB}[a] (kg/mol)	M_{PEO}[b] (kg/mol)	$Đ$[c]	$\langle R_h \rangle$[d] (nm)	μ_2/Γ^2[e]
PB–PEO(9–3)	9.3	2.5	1.07	64	0.1

[a] Number average molecular weight of the ω-hydroxyl poly(butadiene) homopolymer (PB-OH) determined by ^{1}H NMR spectroscopy. The fraction of 1,2-addition was 91%. [b] Number average molecular weight of PEO block obtained from ^{1}H NMR spectroscopy and the PB-OH molecular weight. [c] Dispersity (M_w/M_n) of PB–PEO determined by SEC. [d] Average hydrodynamic radius and [e] dispersity of polymersomes determined by DLS.

3.2.3 NMR Measurements. A Bruker Avance III 500 MHz NMR spectrometer equipped with a 5 mm triple resonance broad band PFG probe was used for both ^{1}H NMR spectroscopy and pulsed-field-gradient NMR (PFG-NMR) at 25 °C. All PFG-NMR measurements were conducted on ^{1}H nuclei with DOSY (Diffusion Ordered Spectroscopy), using the "ledbpgp2s" pulse sequence (longitudinal eddy current delay experiment using bipolar gradients acquired in 2D mode).[27] Two gradient pulses with a strength G (ranging from 2% to 98% of the maximum gradient strength, 0.47 T/m) were applied for a duration (δ) in the pulse sequence. The intensity attenuation (I) of probe molecules with the gradient strength variation was recorded during a diffusion time (Δ), and processed by the Top Spin software package (version 3.1) in order to extract the translation diffusion coefficient (D). In the presence of free diffusion of probe molecules, the intensity (I) is attenuated with respect to the intensity (I_0) at $G = 0$ as

$$\frac{I}{I_0} = exp(-\gamma^2\delta^2G^2D(\Delta - \delta/3)), \qquad (3\text{–}1)$$

where γ is the proton gyromagnetic ratio (42.6 MHz/T). D can be evaluated from the slope of the linear plot of $\ln(I/I_0)$ vs. $(-\gamma^2\delta^2G^2(\Delta - \delta/3))$.

3.2.4 Cryogenic Transmission Electron Microscopy (cryo-TEM). The nanostructure of PB–PEO(9–3) in [EMIM][TFSI] was analyzed by cryo-TEM. Specimens were prepared in a FEI Vitrobot Mark III vitrification robot. In the climate chamber of the Vitrobot, 0.5 μL of the polymersome solution (0.5 wt %) was loaded onto a carbon-coated and lacey film-supported copper TEM grid, and then the grid was plunged into liquid ethane (~ –180 °C). The rapidly cooled samples were kept in liquid N_2 before measurements. Cryo-TEM imaging was performed using a FEI Tecnai G2 Spirit BioTWIN operating at 120 kV under liquid N_2 cryo conditions, and the images were

taken with an Eagle 4 mega pixel CCD camera. All images were obtained at an underfocus for adequate phase contrast (Figure 3–1a).

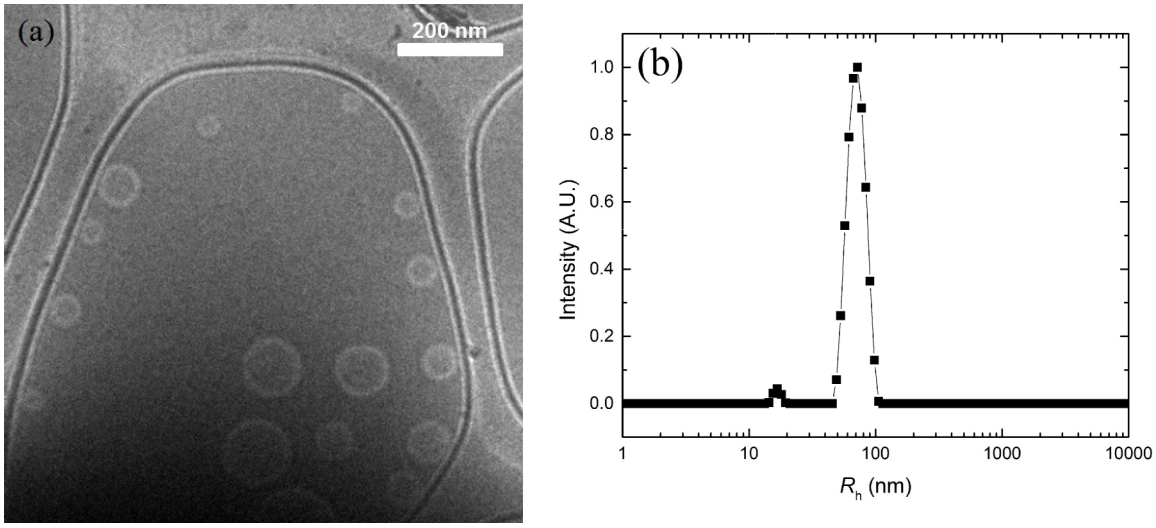

Figure 3–1. (a) Cryo-TEM images of 0.5 wt% PB–PEO(9–3) polymersomes in [EMIM][TFSI] (scale bar: 200 nm), and (b) Normalized hydrodynamic radius (R_h) distribution of 0.01 wt% PB–PEO(9–3) polymersomes in [EMIM][TFSI].

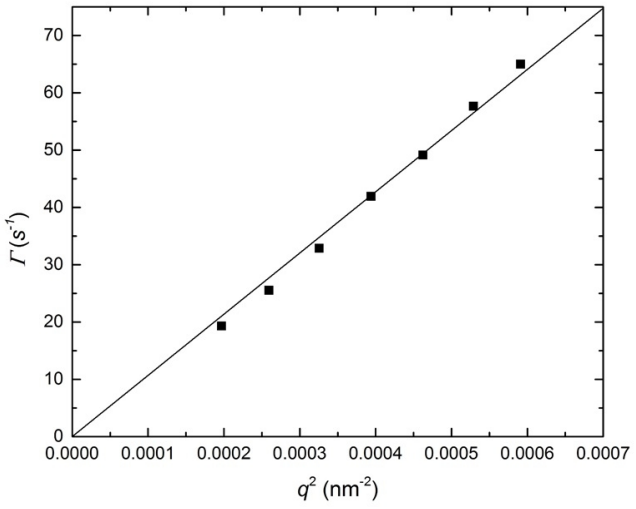

Figure 3–2. The linear fit of decay rate (Γ) vs. the square of the scattering vector (q^2) from DLS. Γ values were from the cumulant fitting of the correlation functions. The slope of the linear fit is diffusion coefficient of polymersomes in the solution.

3.2.5 Dynamic Light Scattering (DLS). DLS was performed over a range of angles (60 – 120°) with a Brookhaven BI-200SM goniometer and a Brookhaven BI-9000AT correlator at λ = 637 nm and 25 °C to obtain the average hydrodynamic radius $\langle R_h \rangle$. The dispersity of particle size was quantified by the reduced second cumulant μ_2 / Γ^2. The mean decay rate ($\Gamma = D_m q^2$, where D_m is the mutual diffusion coefficient and q is the scattering vector) and the μ_2 values were obtained from cumulant fitting of the normalized correlation function (Figure 3–2). The polymersome size distribution (Figure 3–1b) was also assessed through the Laplace inversion routine, REPES.[28] For the DLS measurement, polymersome solutions in [EMIM][TFSI] were diluted to 0.01 wt % by adding filtered [EMIM][TFSI] through a syringe filter (Millex-SV 5.0 μm).

3.3 Results and Discussion

3.3.1 Polymersome Characterization. A vesicle structure was observed in the ionic liquid solution of PB–PEO(9–3), consistent with previous PB–PEO block copolymers with low volume fractions of PEO (~ 0.2).[7,18,29,30] Polymersomes with mean radius less than 100 nm and narrowly dispersed in size are shown in the cryo-TEM image (Figure 3–1a). Relatively monodisperse small polymersomes were obtained using a volatile organic co-solvent, which can dissolve both PB and PEO blocks, and is miscible with the ionic liquid. The circular bright regions represent the PB membranes and appear brighter than the IL matrix due to lower electron density, while the solvated PEO coronas are invisible in the medium. Because both [EMIM][TFSI] and water are selective solvents for PB–PEO, and PEO shows a change in affinity with temperature in the biphasic system of [EMIM][TFSI] and water, upon adding D_2O (or water) to the IL solution at room temperature, the polymersomes moved spontaneously from the IL phase to the aqueous phase while retaining the vesicle structure and the IL interiors. Even after the transfer from the IL phase to the aqueous phase, the PB–PEO polymersomes retained

their structure and size (see Figure 3–3), as reported previously.[7] PB–PEO(9–3) polymersomes have essentially the same membrane thickness before and after the transfer, 21 (± 2) and 22 (± 2) nm, respectively, as measured by ImageJ software. This membrane thickness lies on the scaling line of $d \sim N^{0.6}$ of the membrane thickness of various PB–PEO vesicles in water, where d is the membrane thickness, and N is the degree of polymerization,[31] as shown in Figure 3–4. The size and dispersity of polymersomes in the ionic liquid were analyzed by DLS, and the mean hydrodynamic radius $\langle R_h \rangle$ = 67 nm with dispersity $\mu_2 / \Gamma^2 = 0.13$.

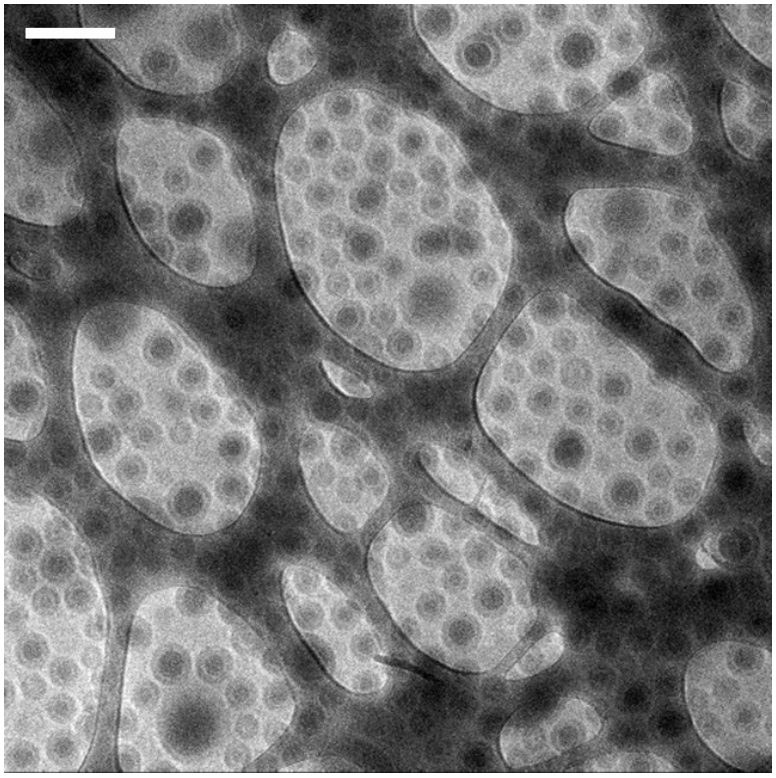

Figure 3–3. Cryo-TEM image of PB–PEO(9–3) polymersomes in D_2O (0.25 wt %). The dark interiors are the ionic liquid filled interiors, and the gray region around dark interiors are PB membranes (scale bar: 200 nm).

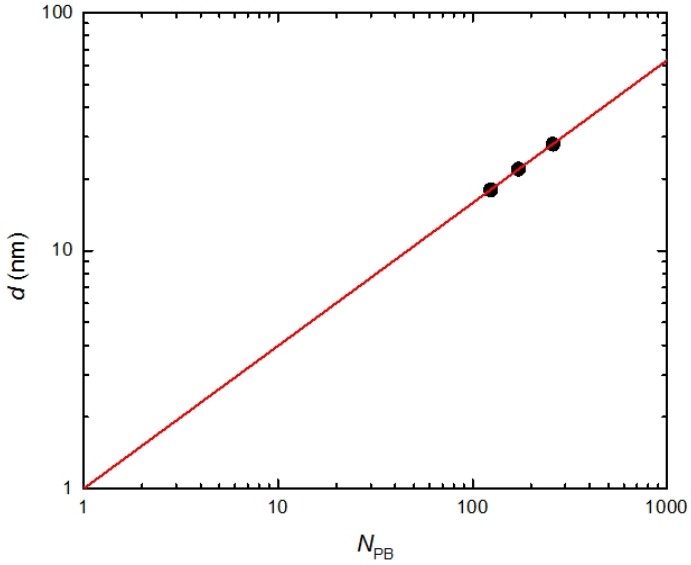

Figure 3–4. The membrane thickness (*d*) of PB–PEO polymersomes versus the degree of polymerization of PB (N_{PB}). *d* was obtained from cryo-TEM images.

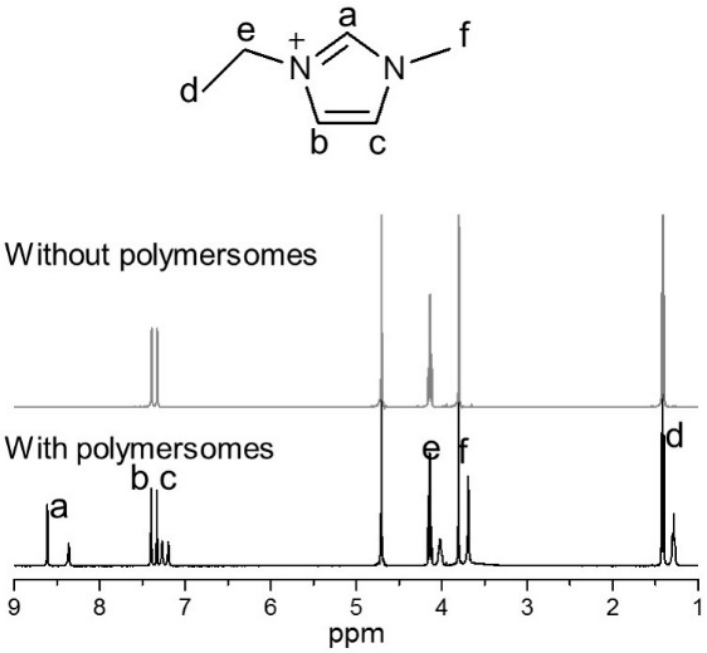

Figure 3–5. Chemical structure of [EMIM] and ^{1}H NMR spectrum of [EMIM] without and with PB–PEO(9–3) polymersomes. (Solvent peak at 4.7 ppm)

3.3.2 Equilibrium Partitioning of Imidazole Derivatives in Polymersome Solutions. ^{1}H NMR spectra of [EMIM][TFSI] in D_2O ([EMIM][TFSI] saturated), and in the polymersome solution, were measured in order to see the effect of polymersomes on the chemical shift of [EMIM] (Figure 3–5). The solution without polymersomes shows a single set of distinct peaks of [EMIM] protons in D_2O. (The signal for proton H_a was not observed due to hydrogen–deuterium exchange.[32]) The single peak around 4.7 ppm arises from protons of ^{1}HDO and ^1H_2O in D_2O. However, [EMIM] in the polymersome solution gives two sets of resonances. The two resolved sets are attributed to the population of the ionic liquid inside and outside the polymersomes. The smaller set of peaks is slightly upfield, and reflects [EMIM] in the vesicle interiors, as confirmed by comparing the experimental and theoretical mole fractions of [EMIM] in the interior, and observing the relative intensity by changing the concentration of the polymersomes from 0.5 wt % to 1.5 wt %. The values from the ^{1}H NMR spectra and from the theoretical calculation are consistent. The integrated fraction of the smaller peaks in the NMR is 0.21, and the mole fraction of the interior ionic liquid is 0.16. The theoretical mole fraction of the IL was calculated by using the solubility of [EMIM] in water (1.8 wt %) and the total volume fraction of the interior (estimated to be about 0.3%, based on the hydrodynamic radius and membrane thickness in this study). As shown in Figure 3–6, as the polymersome concentration increases, the fraction of smaller peaks also increases; this comparison clearly shows that satellite peaks are from the polymersome interiors. This chemical shift from the interiors was also observed for 1-butylimidazole (see Figure 3–11a) and [BMIM] (see Figure 3–7), which have diazole structures in common. The chemical shift is directly related to the magnetic field strength, which is a function of the magnetic susceptibility.[33] Since D_2O and [EMIM][TFSI] have different magnetic susceptibilities, the tracer molecules in this study showed two sets of peaks. Similar magnetic

susceptibility effects on chemical shifts have also been found in the case of suspensions of red blood cells and emulsion systems.[33,34]

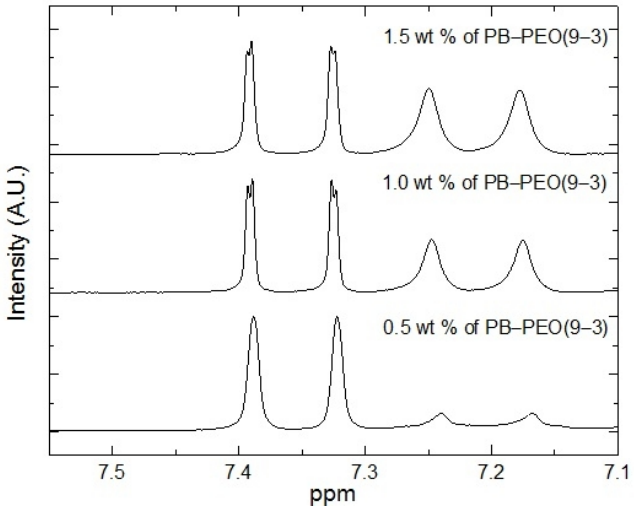

Figure 3–6. Normalized ^{1}H NMR spectra of polymersome solutions (0.5 wt %, 1.0 wt %, and 1.5 wt %). Two peaks between 7.4 ppm and 7.3 ppm are from the H_b and H_c of the free [EMIM], and smaller two peaks around 7.2 ppm from the H_b and H_c of the confined [EMIM] phase. As the polymersome content increases, the peaks around 7.2 ppm increases.

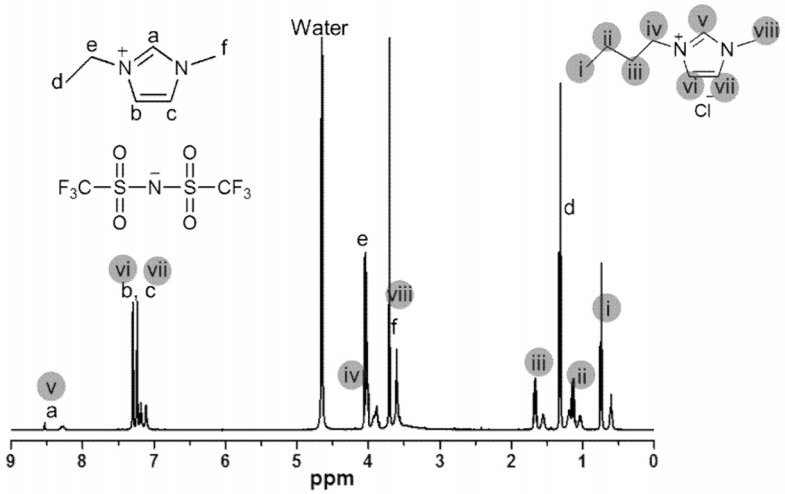

Figure 3–7. Chemical structure of [EMIM][TFSI] and [BMIM], and ^{1}H NMR spectrum of [BMIM] solution with PB–PEO(9–3) polymersome. As [EMIM], [BMIM] shows also two sets of chemical shifts. Many of peaks of [BMIM] are not completely distinguishable due to similar chemical structure with [EMIM].

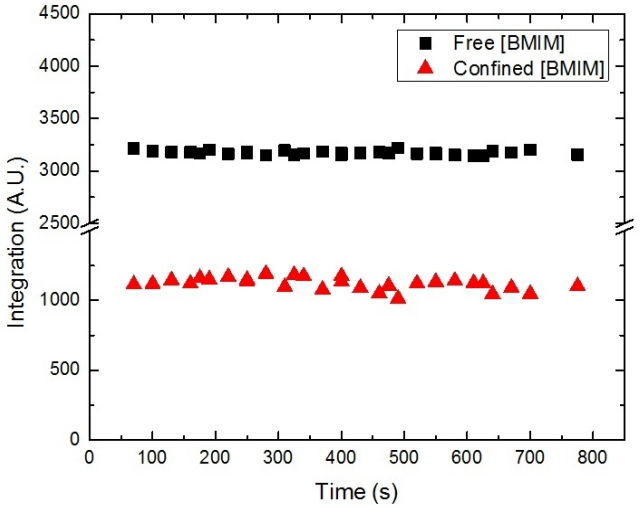

Figure 3–8. The kinetic experiment with transient ^{1}H NMR measurements. The charged molecules, [BMIM], which has similar structure with [EMIM], also shows two sets of peaks. H_i of [BMIM] (see Figure 3–7) from the exterior and the interiors were integrated separately with time. The intensity change of each peak cannot be found after 70 seconds.

While [EMIM] was initially loaded into the polymersomes, 1-butylimidazole and [BMIM]Cl were added to the dispersion in the aqueous solution; both 1-butylimidazole and [BMIM] also showed additional sets of peaks after reaching equilibrium. This result directly demonstrates the permeation of tracer molecules through the membranes, and also provides information on the population of the molecules in the interiors at equilibrium. If there was no permeation of the molecules, only a single set of peaks, from the exterior, should be evident in the spectra. By comparing the integrated areas of the free and confined peaks, the kinetics of permeation could potentially be monitored. After adding 50 mM of [BMIM]Cl to the polymersome solution, the integration of peaks for the exterior and interior molecules were monitored every 30 s. The transient results in Figure 3–8 shows that the integrations do not change with time. This indicates that even the charged [BMIM] molecules permeated through the hydrophobic PB membranes in well under 70 s. Kinetics at shorter times than 70 s could not be observed because at least

a minute was needed for the addition of [BMIM]Cl, NMR tube injection, and shimming and locking.

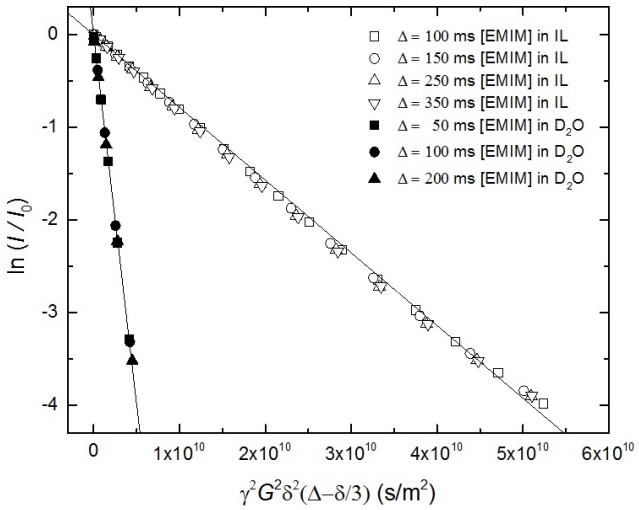

Figure 3–9. The echo decay curves of [EMIM] in D_2O and [EMIM][TFSI] with variation of the field-gradient-strength G for different diffusion times Δ with δ = 8 ms.

3.3.3 Self-Diffusion of [EMIM] in D_2O and [EMIM][TFSI]. If there is no geometrical restriction for diffusion, the attenuated intensity of an individual tracer should follow eqn 3–1, and the logarithm of normalized data points fall on a straight line with different diffusion times (Δ), as shown in Figure 3–9. The translation diffusion coefficient can be obtained from the slope. Figure 3–9 is the echo decay curve of [EMIM] in D_2O ([EMIM][TFSI] saturated), and in [EMIM][TFSI] (D_2O saturated). The solid lines are fits to eqn 3–1; the diffusion coefficient (D) of [EMIM] in D_2O is 7.9×10^{-10} m^2/s, and 7.9×10^{-11} m^2/s in [EMIM][TFSI]. These two values are close to the literature values.[35–37] According to the Stokes-Einstein equation ($D_{SE} = k_B T/(6\pi\eta R)$, where k_B is Boltzmann constant, T is the absolute temperature, η is the viscosity of a solvent, and R is the hydrodynamic radius), the diffusivity of objects should be proportional to the inverse of the solvent viscosity. However, in this case, this expectation is not realized. The

viscosities of D_2O and [EMIM][TFSI] at 25 °C are 1.1 mPa·s and 30.4 mPa·s, respectively, so the ratio of the inverse viscosities ($\eta_{[EMIM][TFSI]}/\eta_{heavy\ water}$) is around 28. In contrast, the ratio of the diffusivities for [EMIM] in water to that in the IL is around 10. This breakdown of this relation could be caused by several reasons. The calculated van der Waals radius of [EMIM] is 3 Å using the Hyperchem program.[38] Using the van der Waals radius as the hydrodynamic radius of [EMIM], the calculated D_{SE} values are 2.4×10^{-11} m^2/s in the IL and 6.5×10^{-10} m^2/s in D_2O, respectively. The actual diffusivity of [EMIM] is therefore greater in the IL, but slower in D_2O than the values of D_{SE}. When a large spherical particle moves randomly in a continuous and viscous solvent without specific interactions, such as hydrogen bonding, the motion of the particle follows the Stokes-Einstein relation.[39] However, in the IL, the size of [EMIM] is similar to that of the dissociated [EMIM] or [TFSI], and smaller than the associated [EMIM][TFSI]. In general for neutral molecules, the diffusivity of small solutes is enhanced relative to D_{SE}, as the size ratio of solute to solvent molecules decreases.[40–42] Even though [EMIM] in the IL can associate and dissociate with its counter ion,[36] [EMIM] showed an increased diffusivity due to the reduced friction as reported by Watanabe and Maroncelli groups.[35,36,43] These results are consistent with that of Edward.[40] In water, however, there are strong hydrogen bonding interactions between [EMIM] and water, which could reduce the diffusion coefficient.[37,44,45] The proton H_a is a good hydrogen bond donor, and there can be weak hydrogen bonding interaction between water and the protons of alkyl groups of [EMIM]. Nevertheless, the self-diffusion of [EMIM] in two saturated solutions suggests that the diffusion behavior is largely dictated by the viscosity of diffusion medium. In addition, with a single set of distinct peaks of [EMIM] protons in the NMR spectra, the single exponential echo decays in each phase imply that the ionic liquid and D_2O do not form long-lived aggregates in D_2O and the ionic liquid, respectively.

3.3.4 Escape and Entry Rates of [EMIM] and 1-Butylimidazole. Diffusion of probe molecules in the polymersome solution is not same as free diffusion, due to the restricted geometry, and thus cannot be simply described by eqn 3–1. For short diffusion times, the behavior is still within the range of the free diffusion. But over timescales where the mean displacement of the molecule is comparable to the dimension of the restricted geometry, the translation of the molecule in the laboratory frame is affected by the random walks of both the moving vesicles and the tracer molecules.[46] In the long time limit, the diffusion behavior of the tracer molecules confined in the vesicles should be similar to that of the vesicles, because the net displacement is much larger than the vesicle radius. For example, when an [EMIM] molecule and a vesicle (radius 100 nm) move with $D_{[EMIM]} = 1 \times 10^{-9}$ m^2/s and $D_{vesicle} = 1 \times 10^{-12}$ m^2/s by three dimensional random walks in water, the mean displacements, s during the observation time, t (*e.g.*, 100 ms) are about 25 μm and 0.8 μm, respectively, according to Einstein's relationship, $s = (6Dt)^{0.5}$. Since the mean displacement of the tracer molecule is two orders of magnitude larger than the radius of the polymersomes, the diffusion of molecules is restricted within the confined vesicles, and should have a similar displacement to the moving vesicle (see Scheme 3–1).[22] Moreover, the molecules in each site can be exchanged through the membranes. So the transmembrane exchange and the diffusion behavior should be described in a different way, and the two-site exchange approximation is a powerful tool to explain the exchange rate and the diffusion behavior.[47] In this model, exchange terms are added to Fick's second law of diffusion as shown in eqns 3–2 and 3–3,

$$\frac{\partial C_{\mathrm{i}}}{\partial t} = D_{\mathrm{i}}\nabla^2 C_{\mathrm{i}} - \frac{C_{\mathrm{i}}}{\tau_{\mathrm{i}}} + \frac{C_{\mathrm{e}}}{\tau_{\mathrm{e}}}, \tag{3–2}$$

$$\frac{\partial C_{\mathrm{e}}}{\partial t} = D_{\mathrm{e}}\nabla^2 C_{\mathrm{e}} - \frac{C_{\mathrm{e}}}{\tau_{\mathrm{e}}} + \frac{C_{\mathrm{i}}}{\tau_{\mathrm{i}}}, \tag{3–3}$$

where C_i, D_i and τ_i represent the concentration (mol/L), the diffusion coefficient (m^2/s) and residence time (s) of a tracer molecule in the interiors of polymersomes, respectively, and C_e, D_e and τ_e, represent the same parameters in the external aqueous medium.

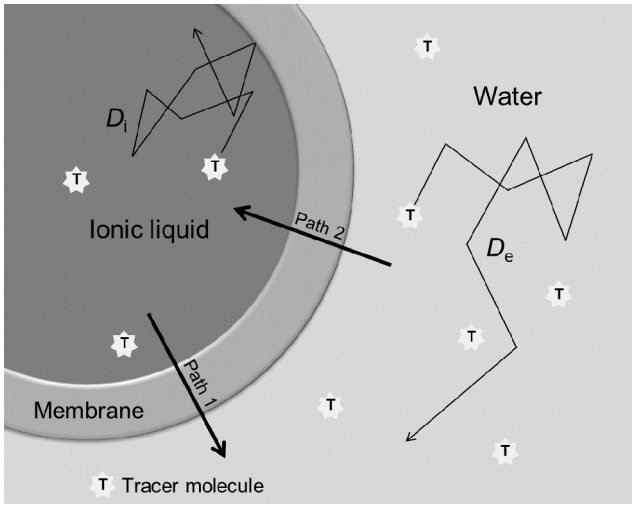

Scheme 3–1. Schematic of molecular diffusion in each phase, and transportation across the membrane of polymersome with IL interior dispersed in water. The tracer molecules move with diffusion coefficient D_i inside, and D_e outside of the polymersomes. Also, the molecules are exchangeable across the membranes through path 1 and path 2.

For the PFG-NMR experiment, the solution of eqns 3–2 and 3–3 is a bi-exponential function,

$$\frac{I}{I_0} = P_a^{'} \, exp(-k_a^{'}(\Delta - \delta/3)) + P_b^{'} \, exp(-k_b^{'}(\Delta - \delta/3)), \qquad (3\text{–}4)$$

where $P_a^{'}$, $P_b^{'}$, $k_a^{'}$, and $k_b^{'}$ are the apparent mole fraction of probe molecules and rate constants, which are functions of the real parameters, P_i, P_e, D_i, D_e, τ_i, τ_e, and effective relaxation times, T_e, T_i. P_i and P_e stand for the mole fraction of probe molecules in the encapsulated and free space ($P_i + P_e = 1$); τ_i and τ_e are the residence time at each phase,

and the inverse of the residence times represent the rate of escape ($1/\tau_i$, Path 1 in Scheme 3–1) and entry ($1/\tau_e$, Path 2 in Scheme 3–1), respectively. The residence times are also related by $\tau_e = (1 - P_i) \times \tau_i / P_i$. $k_a^{'}$ and $k_b^{'}$ can be described by two parameters, $Q_{1,2}$, which are defined in eqns 3–8 and 3–9,

$$k_{a,b}^{'} = Q_1 \mp Q_2 , \tag{3–5}$$

while $P_a^{'}$, and $P_b^{'}$ are defined by eqns 3–6 and 3–7.

$$P_a^{'} = 1 - P_b^{'} \tag{3–6}$$

$$P_b^{'} = \frac{1}{2} - \frac{\frac{1}{4}\left[\left(P_i - P_e\right)\left(k_e - k_i\right) + \frac{1}{\tau_e} + \frac{1}{\tau_i} + \frac{1}{T_e} + \frac{1}{T_i} \right]}{Q_2} \tag{3–7}$$

The parameters Q_1 and Q_2 are defined by k_i, k_e, τ_i, τ_e, T_e, and T_i,

$$Q_1 = \frac{1}{2}\left(k_e + k_i + \frac{1}{\tau_e} + \frac{1}{\tau_i} + \frac{1}{T_e} + \frac{1}{T_i} \right), \tag{3–8}$$

$$Q_2 = \frac{1}{2}\sqrt{\left(k_e - k_i + \frac{1}{\tau_e} - \frac{1}{\tau_i} + \frac{1}{T_e} - \frac{1}{T_i} \right)^2 + \frac{1}{\tau_e \tau_i}} , \tag{3–9}$$

where k_i and k_e are rate constants defined by γ, δ, G, and two diffusion coefficients, D_i, and D_e,

$$k_{\mathrm{i}} = \gamma^2 \delta^2 G^2 D_i , \tag{3–10}$$

$$k_{\mathrm{e}} = \gamma^2 \delta^2 G^2 D_{\mathrm{e}} , \tag{3–11}$$

The effective relaxation times, T_{i} and T_{e} are defined by eqns 3–12 and 3–13, and summarized in Table 3–2.

$$\frac{1}{T_{\mathrm{e}}} = \frac{1}{\Delta}\left(\frac{2\delta}{T_{2,\mathrm{e}}} + \frac{\Delta - \delta}{T_{1,\mathrm{e}}} \right) \tag{3–12}$$

$$\frac{1}{T_{\mathrm{i}}} = \frac{1}{\Delta}\left(\frac{2\delta}{T_{2,\mathrm{i}}} + \frac{\Delta - \delta}{T_{1,\mathrm{i}}} \right) \tag{3–13}$$

Table 3–2. The spin-lattice (T_1) and the spin-spin (T_2) relaxation times of the tracer molecules depending on their locations; i: interiors, e: exteriors.

Diffuser	$T_{1,\mathrm{i}}$ (s)	$T_{1,\mathrm{e}}$ (s)	$T_{2,\mathrm{i}}$ (s)	$T_{2,\mathrm{e}}$ (s)
[EMIM]	1.9	0.8	10.1	1.2
1-Butylimidazole	2.5	0.3	3.3	0.5

Experimentally, the effective relaxation times (T_{i} and T_{e}) were obtained by the spin-lattice (T_1) and the spin-spin (T_2) relaxation times of tracer molecules, which also affect the attenuation profile and fitting result.[49] $T_{1,\mathrm{i}}$ and $T_{2,\mathrm{i}}$ are relaxations of observed protons in the interiors, and $T_{1,\mathrm{e}}$ and $T_{2,\mathrm{e}}$ are that in the medium. T_1 and T_2 were obtained

by the "protont1" and "Carr-Purcell-Meiboom-Gill (cpmg)" protocol, respectively, and the peaks from the interiors and exteriors were processed separately for T_e and T_i.

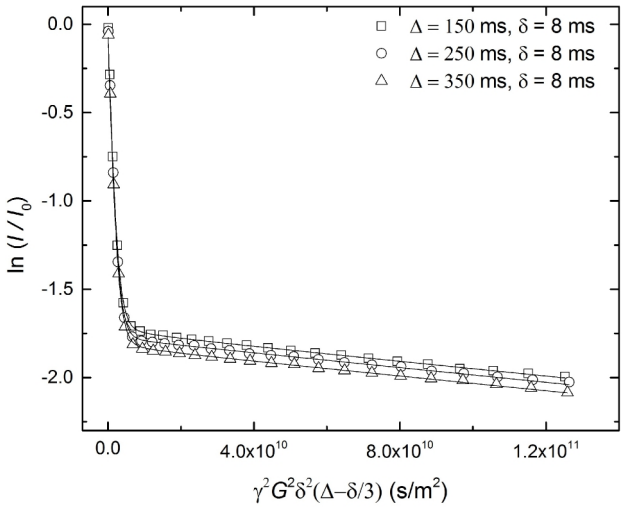

Figure 3–10. Experimental data and fitted echo curve of the proton from [EMIM] in the polymersome solution with various Δ. The data were fitted using eqn 3–4.

[EMIM] and 1-butylimidazole were employed as the tracer molecules for the PFG-NMR study. The gradient strength (G) was varied from 98% to 2% of the maximum gradient strength (0.47 T/m) for a duration δ = 8 ms. The NMR spectra of protons, H_b and H_c of [EMIM] and 1-butylimidazole (see Figure 3–5 for [EMIM] and Figure 3–11a for 1-butylimidazole), were recorded during three different diffusion times (Δ = 150 ms, 250 ms, and 350 ms). Since the exchange across the membranes occurs, both peaks from the interiors and the exteriors were integrated together through DOSY processing. The integrated results were fitted with the two-site model. Two apparent diffusion coefficients, D_i and D_e, were obtained from the initial and final slopes of the decay curves, and other parameters (Δ, δ, G, γ) were given. By the fitting, the residence time ($\tau_{i,e}$), and the mole fraction of the molecules in each site ($P_{i,e}$) can be obtained. Note that

because the two residence times and the two populations are related, there are only 2 parameters in the fits, given that the two *D*'s are set by the initial and final slopes. Also, the measurements were repeated several times to ensure the reliability of the fits. Finally, the values of ($P_{i,e}$) are also confirmed by the independent ^{1}H NMR spectra.

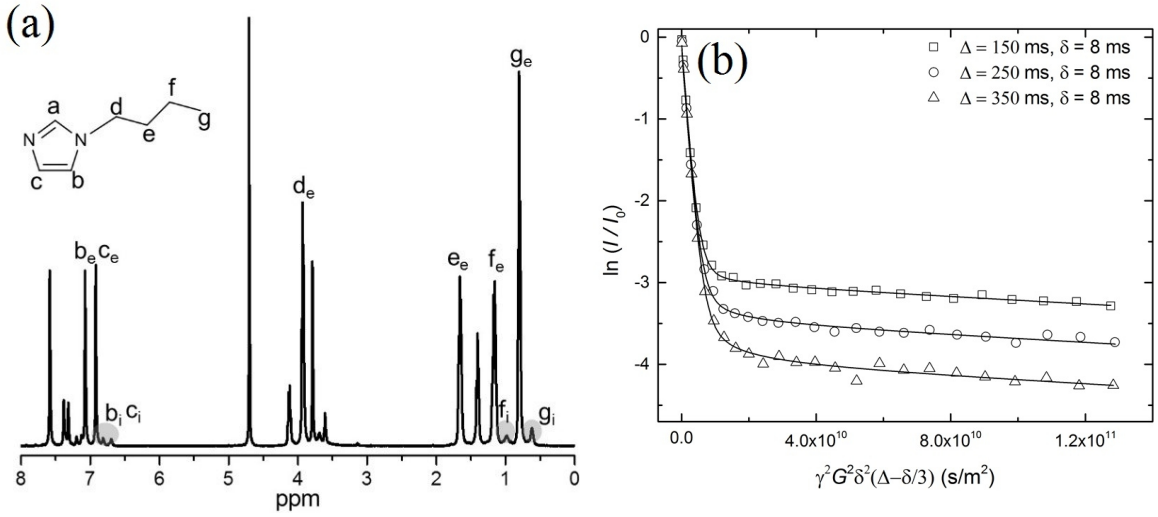

Figure 3–11. (a) ^{1}H NMR spectrum of 1-butylimidazole with PB–PEO(9–3) polymersomes, and (b) Experimental data and fitted echo curves of the protons from 1-butylimidazole with various *Δ*. The data were fitted using eqn 3–4.

Figure 3–10 shows the experimental data (□, ○, Δ) and fitted echo decay curve (solid line) of H_b and H_c on [EMIM]. The fitted results are summarized in Table 3–3. P_i of [EMIM] is 0.2, which is very close to the mole fraction of [EMIM] in the polymersomes from the 1-D spectrum (Figure 3–5). The mean residence time of molecules in the inside of polymersomes is $\tau_i \approx 5.8$ s, and that in the exterior is $\tau_e \approx 23$ s. In the case of 1-butylimidazole, due to the similar chemical structure with [EMIM], many peaks are not distinguishable from the [EMIM] peaks. Apparently distinguishable peaks are assigned in Figure 3–11a. For PFG-NMR, H_b and H_c of 1-butylimidazole were also used, and the data

(□, ○, Δ) and fit (solid line) are shown in Figure 3–11b. The parameters are also summarized in Table 3–3: $P_i \approx 0.07$, $\tau_i \approx 0.4$ s, and $\tau_e \approx 5.4$ s for 1-butylimidazole.

Table 3–3. Permeation rate with two-site exchange model.

Diffuser	D_e (m^2/s)	D_i (m^2/s)	P_i	P_e	$1/\tau_i$ (1/s)	$1/\tau_e$ (1/s)
[EMIM]	7.8×10^{-10}	2.1×10^{-12}	0.20	0.80	0.17	0.04
1-Butylimidazole	5.8×10^{-10}	2.2×10^{-12}	0.07	0.93	2.5	0.18

D_e and D_i represent the diffusion behavior of the molecules in the limit of short and long diffusion times, respectively. D_e values are similar to the free diffusion in D_2O, but the D_i values are somewhat lower than the diffusion coefficient of the vesicles from the DLS measurement, which was 3.0×10^{-12} m^2/s in D_2O. By using the Stokes-Einstein equation, R_h from NMR is 90 nm, which is bigger than that from the light scattering experiment (64 nm). This difference can be explained, at least in part, by the slower diffusion in a more concentrated solution. While the weight fraction of polymersomes was 0.01 wt % in the DLS measurement, the weight fraction in the NMR measurement was 0.5 wt%. The motion of the polymersomes in the concentrated solution can be retarded by the interaction between the vesicles.[48] Dispersity of vesicle size may also contribute to the small difference between NMR and DLS.

As the observation time (Δ) increases, the number of molecules that are initially observed in the confined interiors decreases, because there are more exchanges of tracer molecules during the longer Δ.[49] The difference of plateaus of 1-butylimidazole is much bigger than that of [EMIM] (see Figures 3–10 and 3–11b). Since longer residence time means that molecules prefer to be in the initial site, it can be concluded that the charged [EMIM] was slower to exchange through the hydrophobic PB membranes than the

neutral 1-butylimidazole. It is therefore apparent that the charged molecules are less exchangeable across the hydrophobic membranes. Permeability is defined as a product of solubility and diffusivity of a tracer molecule in a permeation medium.[50,51] For charged and neutral molecules of similar size, the diffusivity should not be very different.[52] But charged molecules experience a higher barrier to dissolve in hydrophobic membrane, reflected in a higher partitioning difference.[53] Hence, we speculate that the difference of permeation rate of the two tracer molecules arises primarily from the solubility difference in the PB membranes. Note that even if the charged molecule diffuses through the membrane as an ion pair, that would only reduce the diffusivity by a factor of about 2. The speed of escape ($1/\tau_i$) and entry ($1/\tau_e$) were also evaluated. The higher rate means higher permeation. Both $1/\tau_i$ and $1/\tau_e$ of 1-butylimidazole are an order of magnitude higher than that of [EMIM], as expected from the decay curve appearance.

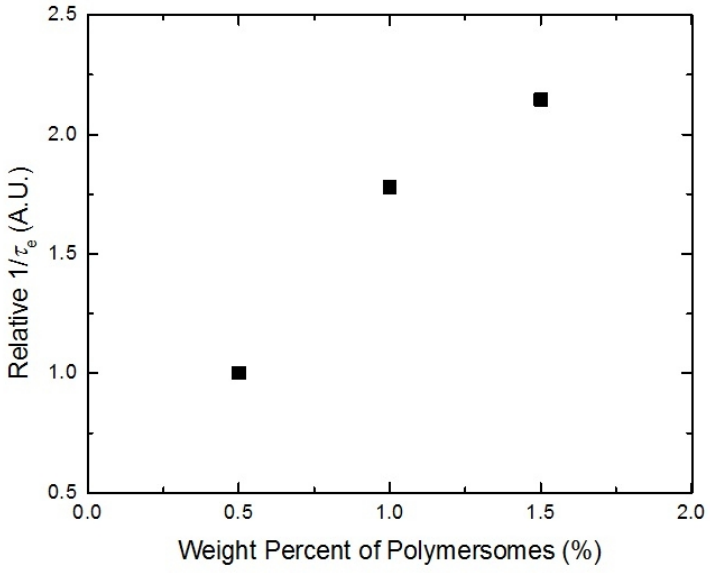

Figure 3–12. The relative rate of entry of 1-butylimidazole by changing the concentration of polymersome in the solution from 0.5 wt % to 1.5 wt %. As the number of polymersomes increases, the rate of entry also increases.

Furthermore, the effect of the polymersome concentration on the rate of entry ($1/\tau_e$) was studied. Three solutions having different concentrations were prepared, and PFG-NMR was conducted with same concentration of 1-butylimidazole (50mM). P and τ values were obtained by fitting with the two-site exchange model. As shown in Figure 3–12, as the polymersome content increases, $1/\tau_e$ increases. With increasing the number of polymersomes, the total surface area for permeation also increases. Higher number of polymersomes provided more surface area to the diffusing molecules, and they had more probability to penetrate through the membranes. This result coincides with the study of the vesicle size effect on the permeation rate. As the size of vesicle decreased, the molecular exchange rate increased because the membrane surface to the vesicle volume ratio increased with decreasing vesicle size.[54]

3.4 Conclusions

Polymersomes of PB–PEO(9–3) with [EMIM][TFSI] interiors dispersed in water were created by transferring the polymersomes in prepared [EMIM][TFSI] to water. The permeation of various tracer molecules through the membranes in this nanoemulsion solution was investigated by NMR techniques. Due to the magnetic susceptibility difference across the membrane, the permeation of [BMIM] and 1-butylimidazole was easily confirmed in 1-D ^{1}H NMR spectra. Moreover, the mole fraction of the tracer molecules in the interiors could be calculated by integrating of each set of peaks. PFG-NMR was also employed to investigate the speed of escape and entry of two similarly sized tracer molecules having different charges. The charged [EMIM] and the neutral 1-butylimidazole were permeable through the hydrophobic PB membranes with reasonable speed, but the rate of permeation of the neutral molecules was greater than the charged ones, in both directions. This permeation study by using NMR about the rate of

molecular transportation across the polymersome membrane will inform the design of a nanoreactor system based on the polymersomes with IL interiors in water.

3.5 References

1. Lee, J. C. M.; Bermudez, H.; Discher, B. M.; Sheehan, M. A.; Won, Y. Y.; Bates, F. S.; Discher, D. E. *Biotechnol. Bioeng.* **2001**, *73*, 135–145.
2. Meng, F.; Zhong, Z.; Feijen, J. *Biomacromolecules* **2009**, *10*, 197–209.
3. Watanabe, K.; Takizawa, S.-Y.; Murata, S. *Chem. Lett.* **2011**, *40*, 345–347.
4. Yow, H. N.; Routh, A. F. *Soft Matter* **2006**, *2*, 940–949.
5. Renggli, K.; Baumann, P.; Langowska, K.; Onaca, O.; Bruns, N.; Meier, W. *Adv. Funct. Mater.* **2011**, *21*, 1241–1259.
6. Discher, D. E.; Eisenberg, A. *Science* **2002**, *297*, 967–973.
7. Bai, Z.; Lodge, T. P. *J. Am. Chem. Soc.* **2010**, *132*, 16265–16270.
8. Yu, S.; Azzam, T.; Rouiller, I.; Eisenberg, A. *J. Am. Chem. Soc.* **2009**, *131*, 10557–10566.
9. Kim, K. T.; Meeuwissen, S. A.; Nolte, R. J. M.; van Hest, J. C. M. *Nanoscale* **2010**, *2*, 844–858.
10. Palivan, C. G.; Fischer-Onaca, O.; Delcea, M.; Itel, F.; Meier, W. *Chemical Society Reviews* **2012**, *41*, 2800–2823.
11. Bai, Z.; Lodge, T. P. *J. Phys. Chem. B* **2009**, *113*, 14151–14157.
12. Loverdo, C.; Benichou, O.; Moreau, M.; Voituriez, R. *Nat. Phys.* **2008**, *4*, 134–137.
13. Sato, T.; Kijima, M.; Shiga, Y.; Yonezawa, Y. *Langmuir* **1991**, *7*, 2330–2335.
14. Wu, J.; Eisenberg, A. *J. Am. Chem. Soc.* **2006**, *128*, 2880–2884.
15. Rodríguez-García, R.; Mell, M.; López-Montero, I.; Netzel, J.; Hellweg, T.; Monroy, F. *Soft Matter* **2011**, *7*, 1532–1542.
16. Paula, S.; Volkov, A. G.; Deamer, D. W. *Biophysical Journal* **1998**, *74*, 319–327.
17. Bolinger, P.; Stamou, D.; Vogel, H. *J. Am. Chem. Soc.* **2004**, *126*, 8594–8595.
18. Bai, Z.; Zhao, B.; Lodge, T. P. *J. Phys. Chem. B* **2012**, *116*, 8282–8289.

19. Battaglia, G.; Ryan, A. J.; Tomas, S. *Langmuir* **2006**, *22*, 4910–4913.
20. Choudhury, R. P.; Galvosas, P.; Schönhoff, M. *J. Phys. Chem. B* **2008**, *112*, 13245–13251.
21. Clarke, R. J.; Apell, H.-J. *Biophys. Chem.* **1989**, *34*, 225–237.
22. Price, W. S. *Concept. Magn. Reson.* **1997**, *9*, 299–336.
23. Rumplecker, A.; Föster, S.; Zähres, M.; Mayer, C. *J. Chem. Phys.* **2004**, *120*, 8740–8747.
24. Wong, B.; Boyer, C.; Steinbeck, C.; Peters, D.; Schmidt, J.; Zanten, R.; Chmelka, B.; Zasadzinski, J. *Adv. Mater.* **2011**, *23*, 2320–2325.
25. Meli, L.; Santiago, J. M.; Lodge, T. P. *Macromolecules* **2010**, *43*, 2018–2027.
26. Freire, M. G.; Carvalho, P. J.; Gardas, R. L.; Marrucho, I. M.; Santos, L. M. N. B. F.; Coutinho, J. A. P. *J. Phys. Chem. B* **2008**, *112*, 1604–1610.
27. Wu, D.; Chen, A.; Johnson, C. S. *J. Magn. Reson.* **1995**, *115*, 260–264.
28. Jakes, J. *Collect. Czech. Chem. Commun.* **1995**, *60*, 1781–1797.
29. He, Y.; Li, Z.; Simone, P. M.; Lodge, T. P. *J. Am. Chem. Soc.* **2006**, *128*, 2745–2750.
30. Simone, P. M.; Lodge, T. P. *Macromolecules* **2008**, *41*, 1753–1759.
31. Davis, K.; Lodge, T. P.; Bates, F. S. *Macromolecules* **2008**, *41*, 8289–8291.
32. Hesse-Ertelt, S.; Heinze, T.; Kosan, B.; Schwikal, K.; Meister, F. *Macromol. Symp.* **2010**, *294*, 75–89.
33. Kuchel, P.W.; Chapman, B.E.; Bubb, W.A.; Hansen, P.E.; Durrant, C.J.; Hertzberg, M.P. *Concepts Magn. Reson.* **2003**, *18A*, 56–71.
34. Skibsted, U.; Hansen, P. E. *NMR Biomed.* **1990**, *3*, 248–258.
35. Noda, A.; Hayamizu, K.; Watanabe, M. *J. Phys. Chem. B* **2001**, *105*, 4603–4610.
36. Tokuda, H.; Tsuzuki, S.; Susan, Md.; Hayamizu, K.; Watanabe, M. *J. Phys. Chem. B* **2006**, *110*, 19593–19600.

37. Sarraute, S.; Gomes, M.; Pádua, A. *J. Chem. Eng. Data* **2009**, *54*, 2389–2394.

38. McEwen, A. B.; Ngo, H. L.; LeCompte, K.; Goldman, J. L. *J. Electrochem. Soc.* **1999**, *146*, 1687–1695.

39. Geyer, U.; Johnson, W. L.; Schneider, S.; Qiu, Y.; Tombrello, T. A.; Macht, M.-P. *Appl. Phys. Lett*. **1996**, *69*, 2492–2494

40. Edward, J. T. *J. Chem. Educ.* **1970**, *47*, 261–270.

41. Sharman, M.; Yashonath, S. *Diffusion Fundamentals* **2007**, *7*, 11.1–11.15.

42. Bhattacharyya, S.; Bagchi, B. *J. Chem. Phys.* **1997**, *106*, 1757–1763.

43. Kaintz, A.; Baker, G.; Benesi, A.; Maroncelli, M. *J. Phys. Chem. B* **2013**, *117*, 11697–11708.

44. Gonfa, G.; Bustam, M. A.; Man, Z.; Abdul Mutalib, M. I. *Asian Transactions on Engineering* **2011**, *1*, 24–34.

45. Zhang, Q.; Wang, N.; Yu, Z. *J. Phys. Chem. B* **2010**, *114*, 4747–4754.

46. Ochab-Marcinek, A.; Hołyst, R. *Soft Matter* **2011**, *7*, 7366–7374.

47. Kärger, J. *Adv. Colloid Interfac.* **1985**, *23*, 129–148.

48. Adalsteinsson, T.; Dong, W.; Schönhoff, M. *J. Chem. Phys.*, **2004**, *108*, 20056–20063.

49. Linders, J.; Mayer, C.; Sekine, T.; Hoffmann, H. *J. Chem. Phys.* **2012**, *116*, 11459–11465.

50. Krevelen, D. W. *Properties of Polymers*, 4th ed.; Elsevier: Solvonia, 2009.

51. Wijmans, J. G.; Baker, R. W. *J. Membr. Sci.* **1995**, *107*, 1–21.

52. Kisak, E. T.; Coldren, B.; Evans, C. A.; Boyer, C.; Zasadzinski, J. A. *Curr. Med. Chem.* **2004**, *11*, 199–219.

53. Paula, S.; Volkov, A. G.; Deamer, D. W. *Biophys. J.* **1998**, *74*, 319–327.

54. Leson, A.; Hauschild, S.; Rank, A.; Neub, A.; Schubert, R.; Forster, S.; Mayer, C.

Small **2007**, *3*, 1074–1083.

Chapter 4

Interfacial Tension-Hindered Phase Transfer of Polystyrene-*b*-poly(ethylene oxide) Polymersomes from a Hydrophobic Ionic Liquid to Water*

4.1 Introduction

The phase transfer of molecules, nanoparticles, and supramolecular assemblies from one phase to the other in a biphasic system is desirable for various applications,[1] such as recycling or delivering of cargo and catalyst,[2,3] separations,[4–6] and delivery.[7–9] It has been demonstrated that the transfer between two immiscible phases can be controlled by employing a stimulus-responsive moiety on the surface.[10–15] For example, Wang and co-workers reported the pH-sensitive transfer of amine-functionalized silicate nanocomposites between an organic and an aqueous phase.[16] The phase transfer of silica nanocomposites was controlled by protonating and deprotonating the amine-functionalized surface under acidic and basic environment, respectively. Phase transfer can also be triggered by temperature;[17,18] for example, poly(ethylene oxide) (PEO) exhibits temperature-responsive transfer properties, in a biphasic system composed of a hydrophobic ionic liquid (IL) and water.[19–21] The solubility of PEO in water decreases with increasing temperature due to the approaching lower critical solution temperature (LCST). At room temperature, both PEO and PEO-coated colloidal aggregates prefer the

* This chapter is reproduced in part with permission from So, S.; Lodge, T. P. *Langmuir* **2015**, *31*, 594–601.

aqueous phase to the IL phase, but at elevated temperatures, closer to the LCST, transfer to the IL phase is possible. Block copolymers containing poly(2-ethyl-2-oxazoline) (PEtOx) also show similar behavior in a water/IL biphasic system, due to the LCST of PEtOx in water.[22]

One system of particular interest is the phase transfer of ionic liquid-filled vesicles, which has potential to combine the advantages of homogenous and heterogeneous catalysis.[23] We have recently reported on the phase transfer of 1,2-poly(butadiene)-*b*-poly(ethylene oxide) (PB–PEO) diblock copolymer vesicles (polymersomes) in the biphasic system of water/IL.[23–25] Ionic liquid-filled vesicles in the aqueous phase form a very stable kind of "nanoemulsion". ILs are of great interest as reaction media,[26–28] with the possibility of replacing organic solvents.[29] By confining a catalyst within an IL-filled nanoreactor, the mass transfer limitations of ILs can be mitigated, while also providing a facile route to quantitative catalyst recovery.

Both theoretical and experimental studies indicate that the primary driving force for the reversible and quantitative transfer of PB–PEO polymersomes is the affinity change of PEO towards the two solvents in the biphasic system upon heating.[30] Experimentally it has been shown that there is a linear relationship between the LCST of α- and ω-hydroxyl terminated PEO having various molecular weights, and the temperature of the phase transfer (T_t) from water to the IL, as shown in Figure 4–1.[31] The hydroxyl chain ends contribute more strongly to hydrogen bonding with water than ethylene oxide unit on the middle of PEO chains, whereby the higher molecular weight PEO shows lower LCST and T_t. However, the presence of a stimulus-sensitive moiety does not guarantee quantitative phase transfer. The molecular weight, the functionality of the terminal group, and the fraction of the stimulus-sensitive moiety can all affect the behavior of the transfer. The total free energy of transfer (G_{tot}) can be described by a summation of the free energy cost from the interface of the polymersomes ($G_{interface}$), any

conformation contribution from the membrane ($G_{membrane}$), and the solvation of the corona chains (G_{corona}).[32] During the phase transfer process, G_{tot} in the destination phase can be higher than the initial phase due to the penalty from $G_{interface}$.

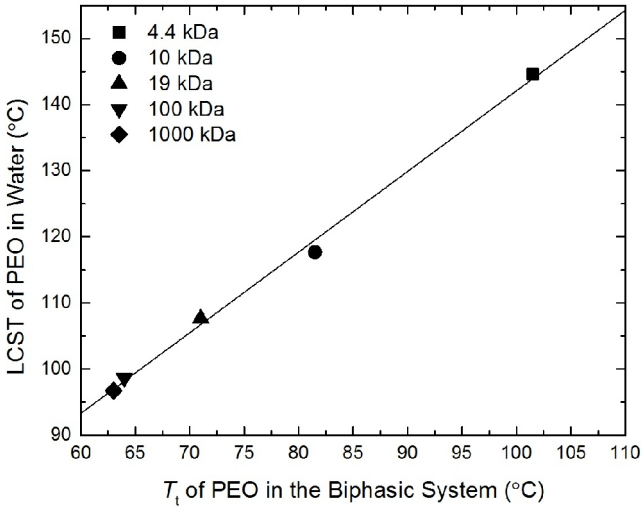

Figure 4–1. A relationship between the LCST of α- and ω-hydroxyl terminated PEO having various molecular weights, and the temperature of the phase transfer (T_t) from water to the IL. (Reproduced with permission from reference 31)

Herein, we described the phase transfer of polystyrene-*b*-poly(ethylene oxide) (PS–PEO) diblock copolymer polymersomes in a biphasic system of water and an IL, 1-ethyl-3-methylimidazolium bis(trifluoromethylsulfonyl) imide ([EMIM][TFSI]). Five different PS polymers were prepared, and PEO blocks were grown to yield 13 diblock copolymers with volume fractions of PEO (f_{PEO}) between 0.1 and 0.3. The phase transfer diagram of the polymersomes for different PEO volume fraction (f_{PEO}) versus PS molecular weight was explored by optical measurements. Furthermore, the effect of polymersome size on the transfer was studied, and rationalized in terms of the reduced tethering density of PEO (σ_{PEO}) on the polymersomes. To investigate the effect of interfacial tension between the PS and the solvent, the quality of the aqueous phase was

systemically changed by adding a water-selective good solvent, THF, and the size of polymersomes in each phase was measured by light scattering. The results indicate that the interfacial tension between the membrane and water can play an important role in the phase transfer, and the phase transfer can be controlled by either the solvent quality for the membrane, or the dimensions of the polymersomes.

4.2 Experimental section

4.2.1 Materials. A series of polystyrene-*b*-poly(ethylene oxide) (PS–PEO) diblock copolymers was synthesized by sequential anionic polymerization. First, five different ω-hydroxyl polystyrene homopolymers (PS-OH) were prepared. Styrene monomer was purified with di-*n*-butylmagnesium two times, and transferred to an oxygen- and moisture-free reactor. The monomers were initiated with *sec*-butyllithium, and propagated in anhydrous cyclohexane at 40 °C for 4 h, followed by the addition of ethylene oxide and stirring for 24 h. The PS-OH was then terminated with deoxygenated methanol. After precipitating and drying the homopolymers, PS-O^- macroinitiators were prepared by dissolving the PS-OH in anhydrous THF and adding potassium naphthalenide. The macroinitiators then reacted with weighed ethylene oxide at 45 °C for 24 h. The reaction was terminated in the same manner as PS-OH. The M_n and $Đ$ of the polymers were characterized by ^{1}H NMR spectroscopy and size exclusion chromatography (SEC), respectively. The characteristics of the synthesized PS–PEO polymers are listed in Table 4–1. Styrene, ethylene oxide monomers, di-*n*-butylmagnesium, *sec*-butyllithium, α- and ω-hydroxyl terminated poly(ethylene glycol) (PEG-200) (M_n = 200 g/mol), and triethylene glycol monomethyl ether (TGME) (M = 164 g/mol) were purchased from Sigma-Aldrich. The ionic liquid 1-ethyl-3-methyl-

imidazolium bis(trifluoromethylsulfonyl) imide ([EMIM][TFSI]) was synthesized as described previously.[33]

Table 4–1. Characteristics of PS–PEO diblock copolymers.

Polymer	M_{PS}[a] (kg/mol)	M_{PEO}[b] (kg/mol)	$Đ$[c]	f_{PEO}[d]
PS–PEO(10–1.6)	9.8	1.6	1.01	0.13
PS–PEO(10–1.8)	9.8	1.8	1.01	0.14
PS–PEO(10–2)	9.8	2.0	1.01	0.16
PS–PEO(10–3)	9.8	2.9	1.06	0.22
PS–PEO(14–2)	14.1	1.7	1.01	0.10
PS–PEO(14–2)	14.1	1.9	1.01	0.11
PS–PEO(14–2.5)	14.1	2.6	1.04	0.14
PS–PEO(14–3)	14.1	3.1	1.02	0.17
PS–PEO(18–2.5)	18.4	2.5	1.01	0.11
PS–PEO(18–3)	18.4	2.9	1.03	0.13
PS–PEO(18–3.6)	18.4	3.6	1.01	0.15
PS–PEO(20–5)	20.0	5.1	1.01	0.19
PS–PEO(27–4)	27.3	4.3	1.01	0.13

[a,b] Number average molecular weight of the ω-hydroxyl poly(styrene) homopolymer (PS-OH), and PEO block obtained from ^{1}H NMR spectroscopy, respectively. [c] Dispersity (M_w /M_n) of PS–PEO determined by SEC. [d] Volume fraction of PEO block in PS–PEO block copolymers calculated by using the bulk density of PS (ρ = 1.05 g/cm^3) and PEO (ρ = 1.13 g/cm^3).

4.2.2 Polymersome Solution Preparation. The polymersomes in [EMIM][TFSI] were prepared by a co-solvent protocol. PS–PEO polymers were first dissolved in dichloromethane, and then [EMIM][TFSI] was added to bring the volume ratio of dichloromethane:[EMIM][TFSI] to 60:40. The co-solvent dichloromethane was selectively removed under N_2 atmosphere, and then vacuum (~ 80 mTorr), to yield an 0.5 wt % polymersome solution in [EMIM][TFSI]. The solutions of PEG-200 and TGME were prepared by dissolving weighed amount of samples in [EMIM][TFSI] directly.

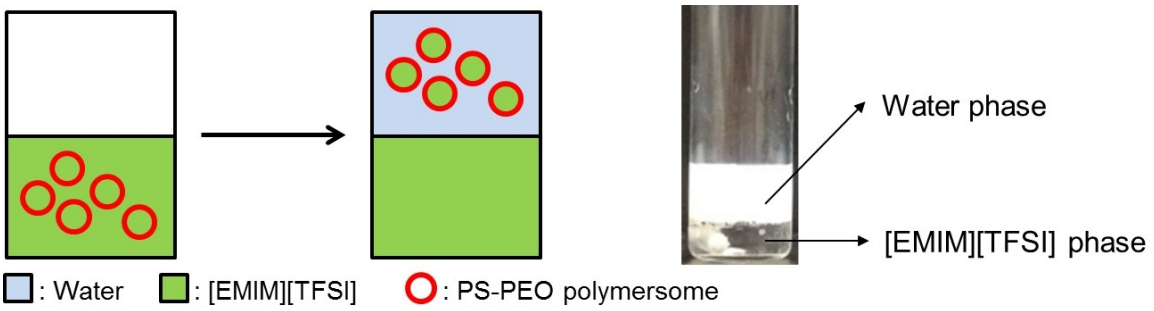

Figure 4–2. Schematic illustration of the transfer of PS–PEO polymersomes from [EMIM][TFSI] to the aqueous phase, and the image of PS–PEO(18–3.6) polymersome transfer after contacting the aqueous phase for 24 h.

4.2.3 Phase Transfer Measurement of the Polymersomes. An equal volume of deuterated water was added to an [EMIM][TFSI] solution of polymersomes, and the two immiscible phases were stirred (~ 100 rpm) for at least 24 h to allow the transfer of the polymersomes from the [EMIM][TFSI] to the aqueous phase. Visible cloudiness of the [EMIM][TFSI] phase was used to determine the complete transfer for the phase transfer diagram of PS–PEO. When complete transfer occurs, the [EMIM][TFSI] phase turns clear, whereas it is not completely transparent without full transfer. In a further series of experiments with variable interfacial tension between the aqueous phase and the polymersome membrane, the aqueous phase quality was systematically changed by

adding a volume fraction of tetrahydrofuran (THF) to the aqueous phase from 0 to 20 vol %. The mixed solvent of THF and water was added to the IL solution of the polymersomes, and the immiscible phases were contacted in the same manner as for the phase transfer from the IL to the aqueous phase without THF. THF is miscible with [EMIM][TFSI] and water, respectively, but THF is selectively dissolved in water in the biphasic system of [EMIM][TFSI] and water, with a partition coefficient (K_p = $C_{water}/C_{[EMIM][TFSI]}$ = 5.1) as measured by ^{1}H NMR spectroscopy.

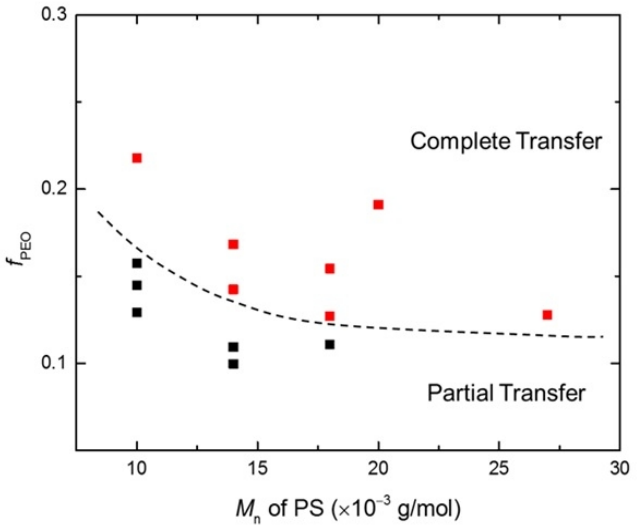

Figure 4–3. The phase transfer diagram of PS–PEO polymersomes and micelles from [EMIM][TFSI] to water for different PEO volume fraction (f_{PEO}) versus the number average molecular weight of PS (M_n). The red squares indicate that the polymers can be transferred, and the black squares indicate that the polymers cannot be transferred completely. The dashed line is the minimum f_{PEO} for the complete transfer ($f_{PEO,mim}$). All samples were prepared by the co-solvent method with a 60 vol % of dichloromethane initially.

4.2.4 Light Scattering and Transmittance. The average hydrodynamic radius <R_h> of the polymersomes were measured on a dynamic light scattering (DLS) instrument with a Brookhaven BI-200SM goniometer and a Brookhaven BI-9000AT correlator, with a

range of scattering angles from 60° to 120° at λ = 637 nm and at 25 °C or 30 °C. The scattering intensity from the polymersomes in the IL phase was obtained during the DLS measurement with laser intensity (λ = 637 nm) of 20 mW. The samples for the DLS and the light scattering measurements were prepared by diluting the solution to 0.001 wt % by adding filtered IL, and filtering through a syringe filter (Millex-SV 5.0 μm). The transmittance of the IL solution of the polymersomes was determined by using a polarized He-Ne laser (Uniphase 1105P) with wavelength 632.8 nm, and a laser power detector (SPEX). For the transmittance of the IL phase, the IL phase was diluted 10-fold with [EMIM][TFSI].

4.3 Results and discussion

Amphiphilic PS–PEO diblock copolymers with low volume fractions of the solvophilic block preferentially form vesicles in a selective solvent.[34–36] The polymersome solution is cloudy or bluish depending on their size,[37,38] a general optical feature that allows direct visualization of the partitioning of polymersomes in the biphasic water/[EMIM][TFSI] system, as shown in the experimental image of Figure 4–2. The IL phase is similarly cloudy before contacting water. However, when all of the polymersomes transfer to the aqueous phase after contacting water, the IL phase turns clear whereas the aqueous phase turns cloudy, as shown in Figure 4–2. Hydrophobic [EMIM][TFSI] with a higher density (ρ = 1.51 g/cm^3)[39] than water forms the bottom phase where the polymersomes initially are formed, as described in the schematic image in Figure 4–2. It has been demonstrated that the driving force for the phase transfer of self-assembled PB–PEO and PS–PEO micelles in the biphasic system is the higher affinity of PEO to water than [EMIM][TFSI] at room temperature.[19,20] However, we have found that the phase transfer of PS–PEO assemblies is also strongly dependent on the volume fraction of solvophilic PEO block

(f_{PEO}) in the block copolymers, as illustrated in Figure 4–3. Based on the phase transfer diagram (Figure 4–3), a minimum f_{PEO} ($f_{PEO,min}$) around 0.1 ~ 0.2 vol % is necessary to effect complete transfer, depending on the molecular weight of PS block. Below the dashed line, the polymersomes were not transferrable completely even after a month, but above the line, the polymersomes transferred completely within a day, as shown in the experimental images in Figure 4–4.

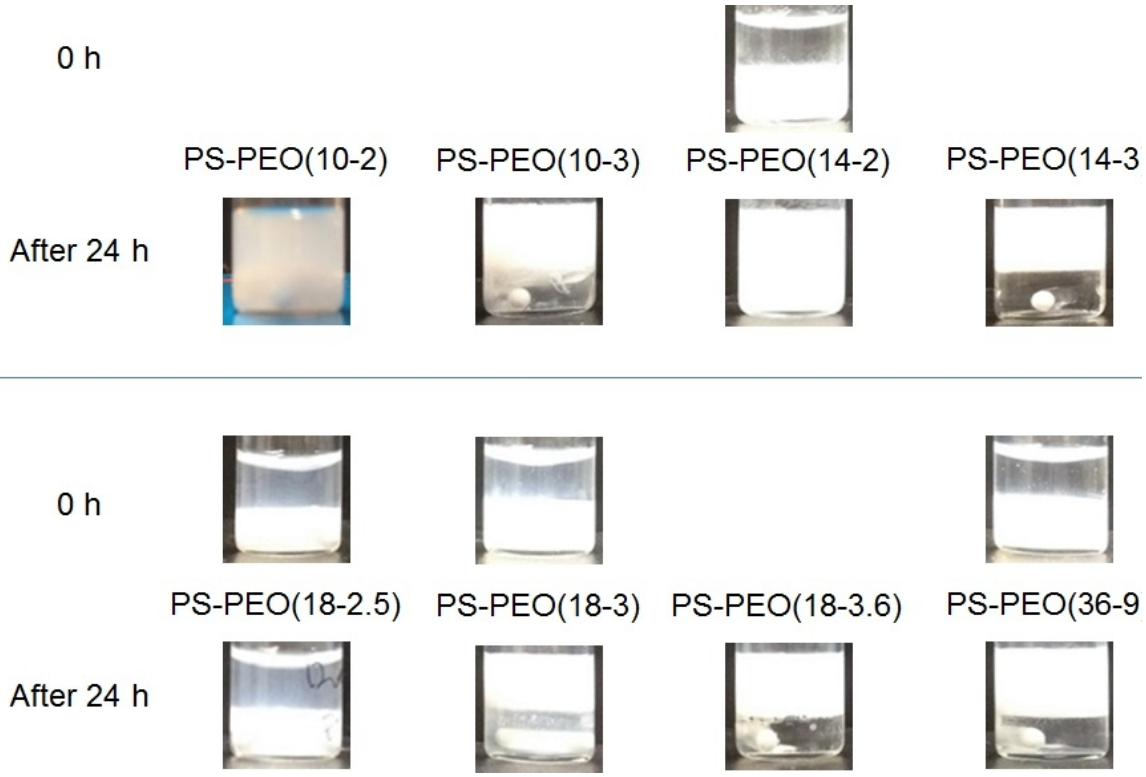

Figure 4–4. Experimental images of PS–PEO polymersome transfer in the biphasic water/[EMIM][TFSI] system. The images were taken just after adding water to polymersome solution, and after 24 h.

It was shown previously that the phase transfer of PEO homopolymers in the biphasic water/[EMIM][TFSI] system is not a function of the molecular weight of PEO, except that the transfer temperature decreases as M_{PEO} increases.[31] Doubly hydroxyl-terminated

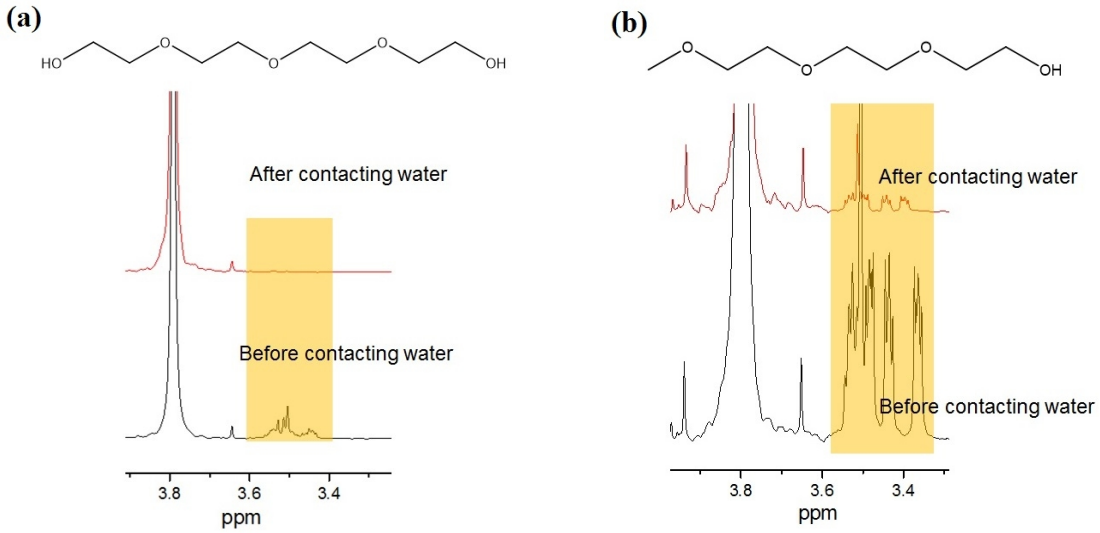

Figure 4–5. Chemical structure and ^{1}H NMR spectra of (a) poly(ethylene glycol) ($M_n \approx$ 200 g/mol), and (b) Triethylene glycol monomethyl ether (M = 164 g/mol) in [EMIM][TFSI] before and after contacting water.

PEO homopolymers showed complete transfer from [EMIM][TFSI] to water regardless of molecular weight from 200 g/mol to 1000 kg/mol. To test the effect of end group on phase transfer, we examined the transfer of TGME (M = 164 g/mol), which has a similar molecular weight and chemical structure with PEG-200 except for one methoxy end group. Under the same conditions for phase transfer, the proton peaks of PEG-200 in the IL phase disappeared, but there were some remaining peaks from TGME in the IL phase, with K_p = 9.1 as shown in the NMR spectra of Figure 4–5. Presumably, the hydroxyl end group of PEG interacts with water molecules more favorably than with the IL, and contributes to the phase transfer from the IL.[40] When one of the end groups is changed to a more hydrophobic group, the contribution of the hydroxyl end groups for the phase transfer is diminished. This result implies that the hydrophobic nature of a molecule or an assembly is important in the phase transfer from IL to water. Similarly, the interaction between the hydrophobic PS membrane and water can be a factor for the phase transfer of PS–PEO polymersomes, because the interfacial tension between PS and water is

significantly higher than that between PS and [EMIM][TFSI], as the solubility parameters (δ) imply: δ_{PS} = 18.6 MPa$^{1/2}$, $\delta_{[EMIM][TFSI]}$ = 27.6 MPa$^{1/2}$, and δ_{water} = 47.9 MPa$^{1/2}$.[41,42] To overcome the penalty from the hydrophobic PS interface with water for the phase transfer, the PEO corona should be long enough to reduce the tension on the hydrophobic interface with the aqueous phase. In the phase transfer diagram, however, $f_{PEO,min}$ for the phase transfer is dependent on the molecular weight of the PS block. As the PS block length increases, $f_{PEO,min}$ decreases. For example, although f_{PEO} of PS–PEO(10–2) is 0.16 higher than 0.13 of PS–PEO(18–3), PS–PEO(10–2) polymersomes do not show the complete transfer, whereas PS–PEO(18–3) do.

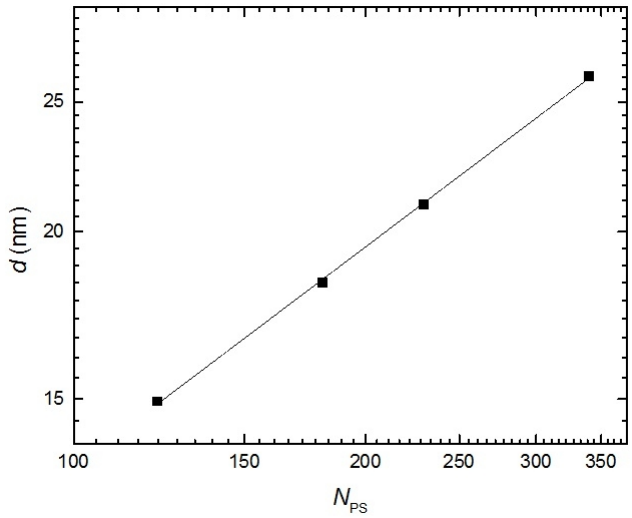

Figure 4–6. The membrane thickness (d) of PS–PEO polymersomes versus the degree of polymerization with respect to the reference volume, 118 Å^3. d was obtained from cryo-TEM images.

The hydrophobic nature of the polymersomes and the relation between $f_{PEO,min}$ and the PS molecular weight can be explained by computing the reduced tethering density (σ_{PEO}), which represents the ratio of the projected area of an unperturbed PEO corona chain

($\pi(R_{g,PEO})^2$) to the unit area per PS chain in the membrane ($8\pi(R_h–R_{g,PEO})^2/N_{agg}$).[43–45] For a polymersome, we define σ_{PEO} as

$$\sigma_{PEO} = \frac{N_{agg}\pi(R_{g,PEO})^2}{8\pi(R_h - R_{g,PEO})^2}, \quad (4–1)$$

where N_{agg} is the aggregation number, $R_{g,PEO}$ is the radius of gyration of the PEO single chain, and R_h is the hydrodynamic radius of a polymersome. N_{agg} can be simply calculated from the known membrane thickness d (Figure 4–6), the volume of the membrane (V_d), and the unit area of a polymer chain (a_0) using the equation,

$$N_{agg} = \frac{2\times V_d}{a_0 d} = \frac{8}{3}\pi \times \left(R_h^3 - \left(R_h - d\right)^3\right) \times \frac{\rho_{PS} N_A}{M_{n,PS}}, \quad (4–2)$$

assuming that the density of PS membrane is same as the bulk density of PS (ρ_{PS} = 1.05 g/cm^3),[46] and that the membrane is free of other components such as the PEO segments or solvent molecules. Here N_A is Avogadro's number, and $M_{n,PS}$ is the number average molecular weight of PS block. Polymersomes with higher σ_{PEO} have membranes more effectively covered by PEO chains. Chen and co-workers proposed that when $\sigma \leq 3.7 \sim 3.8$, corona chains are in the non-interacting regime, whereby the membrane surface is not densely covered with corona chains, but when $\sigma \geq 3.7 \sim 3.8$, the corona chains are in the crossover regime, and start to be stretched.[43] The phase transfer diagram with respect to f_{PEO} (Figure 4–3) can be re-plotted to a diagram with σ_{PEO} values, under the assumption that R_h of the polymersomes is around 100 nm, as shown in Figure 4–7. From the phase transfer diagram of σ_{PEO}, a constant line ($\sigma_{PEO} \sim 3.58$), corresponding to the onset of crossover regime, can be drawn between the transferable and non-transferable polymersomes. This constant boundary indicates that sufficient coverage of PEO on the polymersome membrane interface is necessary for the phase transfer from the IL phase to

water, and that the value of σ_{PEO} is an important parameter to design a block copolymer for the phase transfer of a polymersome in a biphasic system. The critical value of σ_{PEO} is also consistent with the first formation of a dense brush. The $f_{PEO,min}$ can be calculated for a plot of f_{PEO} versus $M_{n,PS}$ with a constant $\sigma_{PEO} \sim 3.58$, as shown in Figure 4–8. The log-log plot of $f_{PEO,min}$ and $M_{n,PS}$ falls on a straight line with a slope of –0.38, and the result provides the necessary PEO block length for the phase transfer at a specific $M_{n,PS}$. Furthermore, this relation explains the dependence of $f_{PEO,min}$ on $M_{n,PS}$ as depicted above in the phase transfer diagram with f_{PEO} (Figure 4–7).

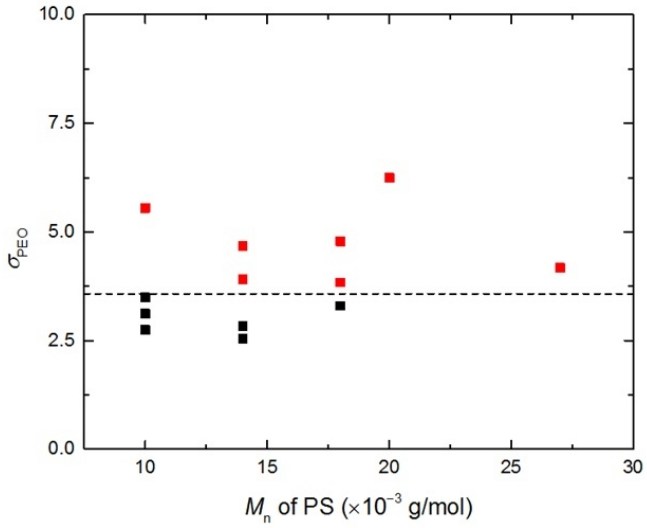

Figure 4–7. The phase transfer diagram with the reduced tethering density (σ_{PEO}) of PS–PEO series. The dashed line indicates the minimum σ_{PEO} to transfer the PS–PEO polymersomes completely from [EMIM][TFSI] phase to the aqueous phase.

We assumed that the R_h of the polymersomes are around 100 nm to calculate the parameter (σ_{PEO}). However, σ_{PEO} is also a function of R_h, as shown in eqn 4–1. In other words, the phase transfer should be controllable by simply varying the polymersome size. For PS–PEO(18–2.5), PS–PEO(18–3), and PS–PEO(18–3.6) polymersomes, σ_{PEO} was calculated as a function of polymersome size by eqns 4–1 and 4–2, and the results are

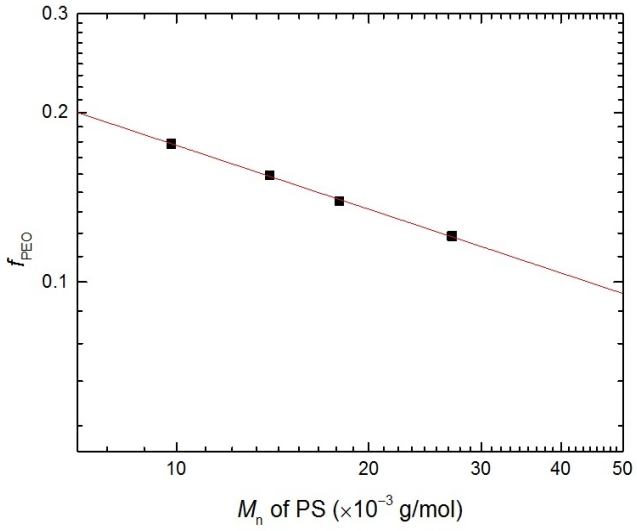

Figure 4–8. The volume fraction of PEO (f_{PEO}) needed to have σ_{PEO} = 3.58 as a function of M_n of PS with R_h = 100 nm of a polymersome.

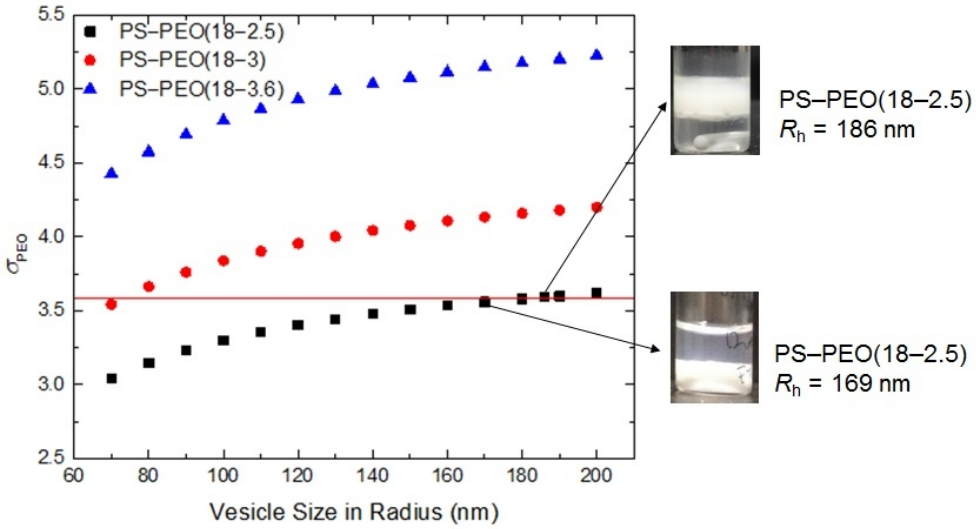

Figure 4–9. Estimated σ_{PEO} by varying the size of the PS–PEO polymersomes. Red line indicates the boundary of the phase transfer for the polymersomes. Above the line, the polymersomes can transfer to the aqueous phase, but below the line, the transfer is not possible. Images on the right are the biphasic systems having different R_h in [EMIM][TFSI] after contacting water for 24 h.

shown in Figure 4–9. As the polymersome size increases, σ_{PEO} also gradually increases. Most of the σ_{PEO} values for PS–PEO(18–3) and PS–PEO(18–3.6) polymersomes are above the critical $\sigma_{PEO} \sim 3.58$ over the range of R_h from 70 nm to 200 nm, but the values for PS–PEO(18–2.5) intersect the line with $\sigma_{PEO} \sim 3.58$. To test this result, two PS–PEO(18–2.5) polymersome samples with different R_h were prepared by varying the initial content of the co-solvent dichloromethane, to obtain different σ_{PEO} values. Two PS–PEO(18–2.5) polymersome samples were prepared with 60 and 30 vol % of dichloromethane, respectively, and designated as PS–PEO(18–2.5)-60 and PS–PEO(18–2.5)-30 based on the initial content of dichloromethane. After complete removal of co-solvent, the average R_h of PS–PEO(18–2.5)-60 was 169 nm (with dispersity, $\mu_2/\Gamma^2 = 0.22$), and that of PS–PEO(18–2.5)-30 was 186 nm ($\mu_2/\Gamma^2 = 0.49$) in [EMIM][TFSI]. With the mean R_h values of PS–PEO(18–2.5)-60 and PS–PEO(18–2.5)-30, σ_{PEO} was calculated as 3.55_6 for PS–PEO(18–2.5)-60, and 3.59_1 for PS–PEO(18–2.5)-30. These two values are on the opposite phase across the boundary line, $\sigma_{PEO} \sim 3.58$. Interestingly, whereas the smaller polymersomes (PS–PEO(18–2.5)-60) show incomplete transfer, the larger polymersomes (PS–PEO(18–2.5)-30) show complete transfer as shown in the experimental images in Figure 4–9. This significant difference in the phase transfer was also reproduced in the case of PS–PEO(10–2) polymersomes, as shown in Figure 4–10, when the size was increased by the decreasing the initial co-solvent content from 60 to 30 vol %. The dependence of phase transfer on the size of the polymersomes therefore supports the hypothesis that the phase transfer is strongly affected by the hydrophobic surface coverage by the hydrophilic moiety, represented by σ_{PEO}.

Experimentally, we have studied on other system with polybutadiene-*b*-poly(ethylene oxide) (PB–PEO) polymersomes.[23,25] Polymersomes were transferable from the IL phase to water, such as PB–PEO(14–4.5), PB–PEO(9–3) and PB–PEO(7–2). They have higher tethering density than 3.58. This result is consistent with the hypothesis, thus the value of

3.58 may be applicable to other systems as the critical value, because the tethering density generally gives the guideline to describe the degree of hydrophobic membrane coverage by corona chains.

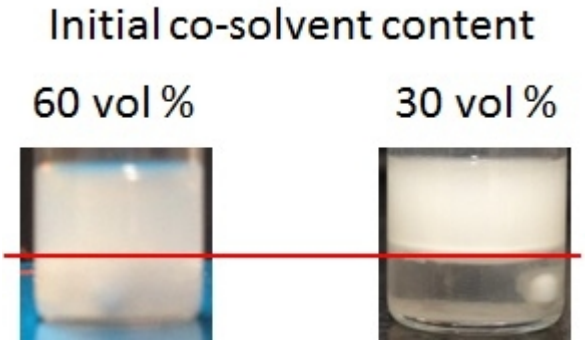

Figure 4–10. Experimental images of PS–PEO(10–2) polymersome transfer in the biphasic water/[EMIM][TFSI] system. The polymersomes in the IL were prepared by the co-solvent method with the initial dichloromethane content 60 vol % and 30 vol %, respectively. The images were taken after contacting water for 24 h.

The total free energy (G_{tot}) in one phase can be written as a summation of the free energy cost from the interface of the polymersomes ($G_{interface}$), the contribution of the membrane ($G_{membrane}$) and the corona chains (G_{corona}). During the phase transfer process, G_{tot} change can be described by

$$\Delta G_{tot} = G_{tot,water} - G_{tot,IL}, \quad (4–3)$$

where $G_{tot,water}$, and $G_{tot,IL}$ are the total free energy of a polymersome in the water and IL phases, respectively. In terms of $G_{membrane}$, $G_{interface}$, and G_{corona}, eqn 4–3 can be summarized as

$$\Delta G_{\text{tot}} = \Delta G_{\text{membrane}} + \Delta G_{\text{interface}} + \Delta G_{\text{corona}}. \quad (4\text{–}4)$$

When $\Delta G_{\text{tot}} < 0$, polymersomes are transferrable, but when $\Delta G_{\text{tot}} > 0$, polymersomes prefer the IL to the aqueous phase, and do not transfer. Since the dimensional change of the membrane is negligible during the phase transfer,[23] the sign of ΔG_{tot} is determined by the competition between interface ($\Delta G_{\text{interface}}$) and corona ($\Delta G_{\text{corona}}$) terms. $\Delta G_{\text{interface}}$ for a polymersome can be described as[47]

$$\Delta G_{\text{interface}} = \Delta\gamma_{\text{interface}} \times A = (\gamma_{\text{PS-water}} - \gamma_{\text{PS-IL}}) \times A, \quad (4\text{–}5)$$

where A is the outer surface area of a polymersome, and $\gamma_{\text{PS-water}}$ and $\gamma_{\text{PS-IL}}$ are the interfacial tensions between the PS membrane and water or IL, respectively. ΔG_{corona} for a mole of ethylene oxide (EO) units (ΔG_{EO}) was estimated to be about –0.61 kJ/mol based on the enthalpy (ΔH_{corona}) and entropy (ΔS_{corona}) for the phase transfer of PB–PEO micelles,[19] and for a polymersome, ΔG_{corona} can be evaluated by

$$\Delta G_{\text{corona}} = \frac{N_{\text{agg}} M_{\text{PEO}}}{2M_{\text{EO}}} \times \Delta G_{\text{EO}}, \quad (4\text{–}6)$$

where M_{PEO} and M_{EO} are the molecular weights of the PEO block and EO unit, respectively. Since the corona chains on the inside are always in contact with IL, only the contribution of the corona chains on the polymersome exterior was considered, as indicated by factor of 2 in denominator. To evaluate $\Delta\gamma_{\text{interface}}$, ΔG_{tot} for PS–PEO(18–2.5) polymersomes is assumed to be 0 at around R_{h} = 180 nm, where the boundary line meets the estimated σ_{PEO} of PS–PEO(18–2.5) as a function of R_{h}. The calculated $\Delta\gamma_{\text{interface}}$ is

around 17 mN/m, which is a reasonable value. The estimated ΔG_{tot} can therefore successfully explain the phase transfer behavior of PS–PEO polymersomes. As the M_n of PEO increases, ΔG_{tot} decreases linearly, and becomes negative at round 2700 g/mol (Figure 4–11a), which was estimated from the phase diagram with σ_{PEO} (Figure 4–8). Then, ΔG_{tot} decreases, as a function of R_h, and the sign changes from positive to negative at R_h = 180 nm (Figure 4–11b). The R_h dependent ΔG_{tot} also corresponds well with the experimental result and σ_{PEO} predictions in Figure 4–9. Through this thermodynamic analysis, the phase transfer can therefore be described as a competing process between the negative ΔG_{corona} and the positive $\Delta G_{interface}$.

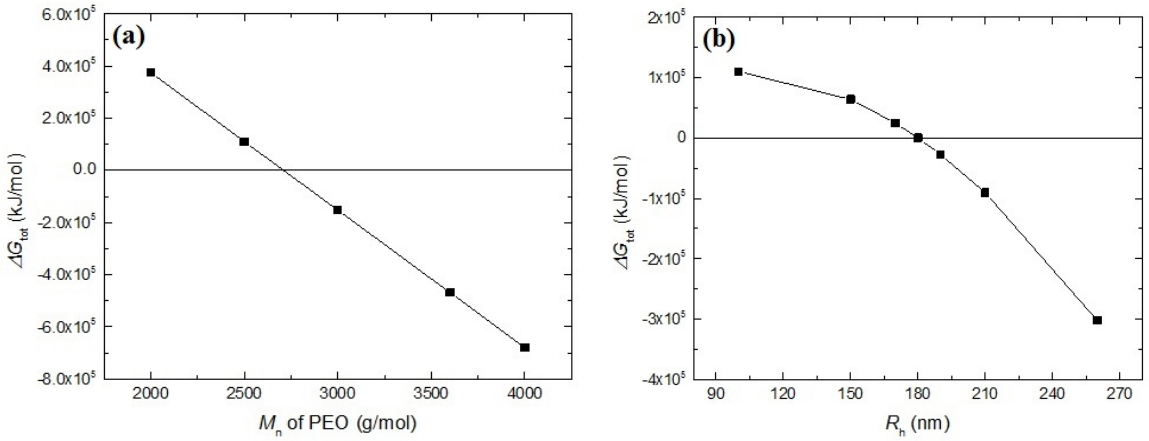

Figure 4–11. Total free energy difference (ΔG_{tot}) during the phase transfer of a mole of polymersomes from [EMIM][TFSI] to water as a function of (a) the molecular weight of PEO (M_n of PEO), and (b) the hydrodynamic radius of PS–PEO(18–2.5) polymersomes (R_h) at around 50 °C.

This analysis demonstrates that the interfacial tension between the hydrophobic membrane interface and the aqueous phase ($\gamma_{PS\text{-}water}$) plays an important role in the transfer from a hydrophobic ionic liquid to water. To test this further, and to vary $\gamma_{PS\text{-}water}$, the aqueous phase was selectively tuned by adding THF. Although THF is miscible with

both [EMIM][TFSI] and water, [EMIM][TFSI]/water/THF mixtures form a biphasic system. To visualize the two phases, the aqueous phase was selectively stained by fluorescein sodium salt as shown in Figure 4–12. The selectivity of THF was measured with ^{1}H NMR spectroscopy, by comparing the relative intensity of peaks from THF and [EMIM][TFSI] before and after contacting water, and the result confirmed that over 80% of the THF is in the aqueous phase. As shown in Figure 4–9, PS–PEO(18–2.5)-60 polymersomes cannot be transferred from the IL phase to the aqueous phase without the addition of THF. However, as the THF content increased, the IL phase became clear, while the aqueous phase turned cloudy (Figure 4–13). With 15 vol % THF, all of the polymersomes transferred to the aqueous phase. With 10 vol % THF in the aqueous phase, the bottom phase is still turbid with a transmittance of 0.28, but with 15 vol % THF, the transmittance is 0.99 as shown in Figure 4–14a, which is the same as the solid line from pure [EMIM][TFSI]. This step change also was confirmed by the scattered intensity change of the bottom phase, as shown in Figure 4–14b. The scattered intensity dropped by a factor of 50 with 15 vol % THF, and was comparable with the scattered intensity of pure IL. Since the scattered intensity is proportional to the number of scatterers in a solution if the polymersomes are identical in size, almost half of polymersomes (~ 40%) transferred to the aqueous phase in the transition from 10 to 15 vol % THF. The transmittance and scattered intensity measurements indicate that more than 10 vol % THF in the aqueous phase renders “non-transferable” polymersomes completely transferable.

According to the cryo-TEM images shown in Figure 4–15, even at 20 vol % THF, the polymersomes retain their vesicle morphology with the same membrane thickness (d = 22 ± 3 nm) as the polymersomes without THF addition (d = 22 ± 3 nm). The cryo-TEM results indicate that there was no significant conformational change after adding THF into the biphasic system, and that G_{membrane} and G_{corona} did not change significantly. However,

$G_{interface}$ is sensitive to the change of the interfacial tension between the PS membrane and the solvent quality because $G_{interface}$ is proportional to the interfacial tension (γ). THF is more compatible with PS than water, as the solubility parameters indicate δ_{PS} = 18.6 $MPa^{1/2}$, δ_{water} = 47.9 $MPa^{1/2}$, δ_{THF} = 18.7 $MPa^{1/2}$. Therefore, as the THF content increases, $\gamma_{PS\text{-}water}$ decreases, and G_{tot} becomes less in the water/THF phase than in the IL. Experimentally, the decrease of $\gamma_{PS\text{-}water}$ with increasing THF content in water has been studied by Seo and co-workers via the contact angle of water/THF mixture droplets on PS films.[48] In Figure 4–16, an estimate of $\gamma_{PS\text{-}water}$ based on the harmonic-mean equation was plotted as a function of THF content in the aqueous phase.

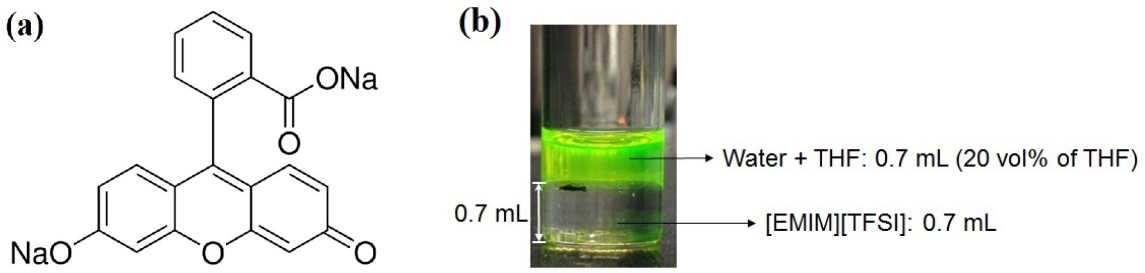

Figure 4–12. (a) Chemical structure of fluorescein sodium salt, and (b) Image of the biphasic system of [EMIM][TFSI] (0.7 mL) and water/THF (0.7 mL, 80/20 in volume). The upper phase was stained by fluorescein salt selectively.

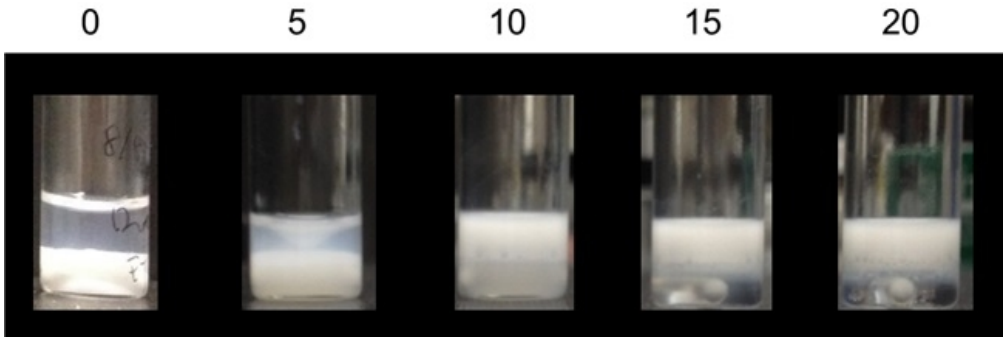

Figure 4–13. Images of PS–PEO(18–2.5) polymersomes in the biphasic [EMIM][TFSI] (bottom phase) and water/THF (upper phase) system. The composition of the upper phase was varied from 0 to 20 vol % THF.

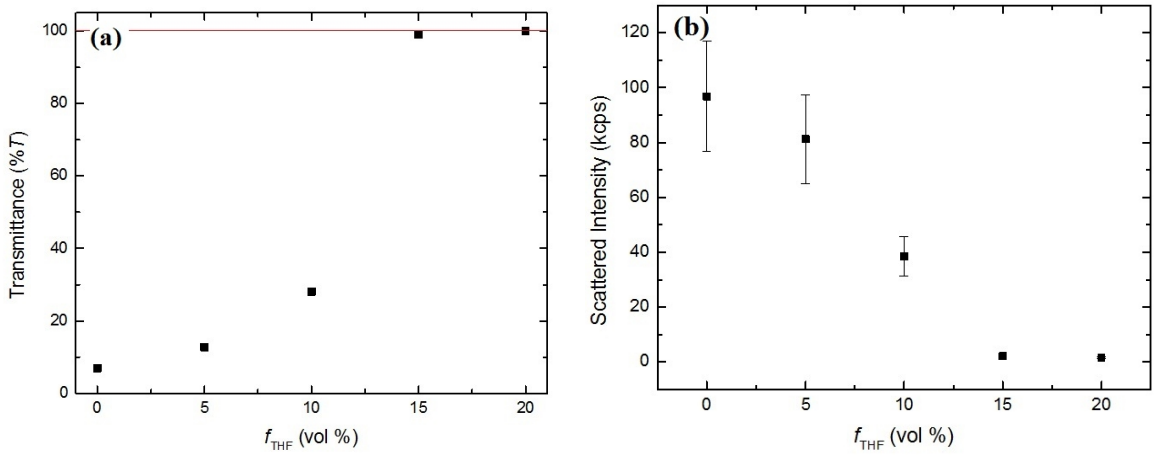

Figure 4–14. THF volume fraction dependence of (a) transmittance, and (b) scattering intensity of the IL phase of the biphasic [EMIM][TFSI]/(water/THF) system containing PS–PEO(18–2.5) polymersomes.

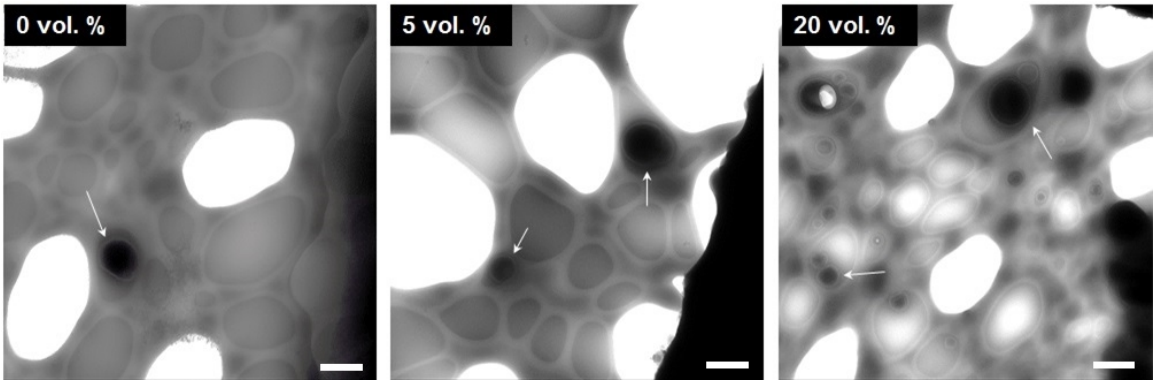

Figure 4–15. Cryo-TEM images of PS–PEO(18-2.5) polymersomes in the aqueous phase at 0 vol. %, 5 vol. %, and 20 vol. % of THF addition. Scale bar is 500 nm, and the white arrows point the polymersomes. (scale bars: 500 nm)

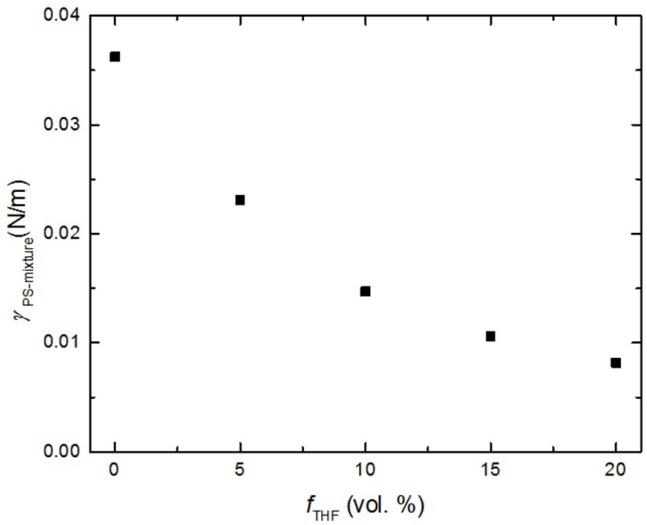

Figure 4–16. Interfacial tension (γ) between the bulk polystyrene and the mixed water/THF mixture dependence on the volume fraction of THF.

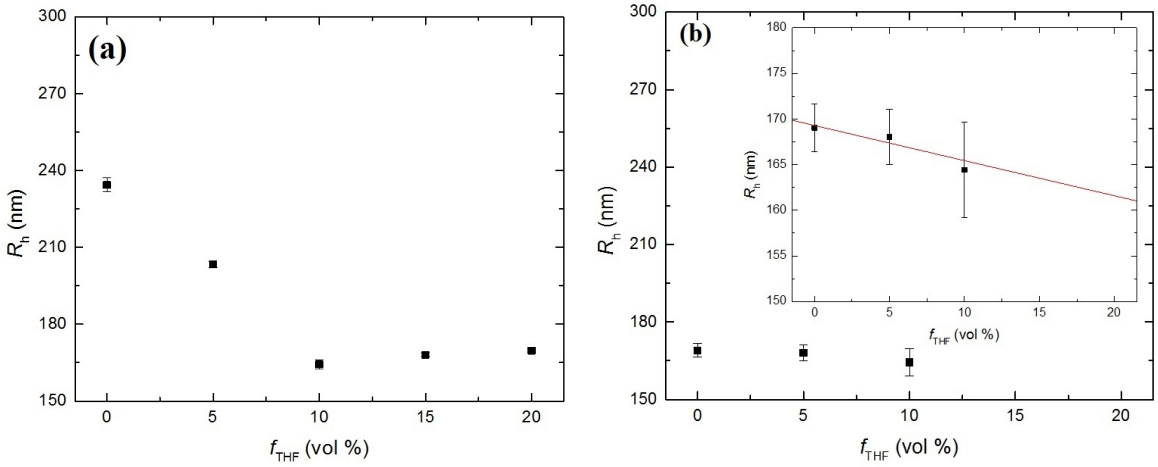

Figure 4–17. Effect of THF volume fraction on the average hydrodynamic radius (R_h) of PS–PEO(18–2.5) polymersomes in (a) water/THF phase, and (b) [EMIM][TFSI] phase.

As some cloudiness in the upper phase is evident in Figure 4–13 even with less than 15 vol % THF, some of the polymersomes in the IL phase transferred to the aqueous phase. The upper phase and the bottom phase were sampled, and DLS measurements were conducted to analyze the size of polymersomes in each phase. The average R_h in the aqueous phase decreases from around 240 nm to a constant R_h around 170 nm (Figure

4–17a), whereas the mean R_h of the polymersomes in the bottom phase also decreases slightly, as shown in the inset of Figure 4–17b. These results indicate that only the larger polymersomes are selectively transferrable at low THF content, while smaller polymersomes cannot transfer due to the higher barrier from $\gamma_{PS\text{-}water}$. The selective phase transfer in polymersome size is consistent in terms of σ_{PEO}. According to eqn 4–1 and Figure 4–9, σ_{PEO} is larger for the bigger polymersomes than the smaller ones. With high content of THF, PEO corona does not need to protect the PS membrane as much for the phase transfer due to the reduced interfacial tension. In the polydisperse vesicle solution (the dispersity from DLS was 0.22), the larger polymersomes can move to the aqueous phase at low THF content, but the smaller ones cannot.

4.4 Conclusions

Interfacial tension-hindered phase transfer of PS–PEO polymersomes from an ionic liquid to water was demonstrated, by varying the block lengths of PS–PEO, the polymersome size, and the organic solvent content in the aqueous phase. It was found that the hydrophobic PS membranes were more shielded by the PEO corona chains when the polymersome size was larger. The fraction f_{PEO} necessary for phase transfer was also examined, with the proposed reduced tethering parameter σ_{PEO} indicating the extent of the PS membrane protection from the aqueous medium. Furthermore, we found that the phase transfer can be controlled by tuning the interfacial tension between the membrane and the aqueous phase. The phase transfer driven by the organic solvent addition was explained by the decrease of the interfacial tension between PS and water/THF as the THF content increased. The results demonstrate that the phase transfer of polymersomes with PEO coronas can be hindered by the interfacial tension between the hydrophobic membrane and the aqueous phase, and also indicate that the phase transfer of

self-assembled polymersomes can be controlled by tuning the block copolymers, changing the dimension of the polymersomes, or the quality of the aqueous medium toward hydrophobic membrane. Furthermore, the phase transfer behavior was analyzed thermodynamically with the free energy difference of the polymersomes in [EMIM][TFSI] and water, and was shown to be a competition between the free energy of the corona and the interface. The interfacial tension-hindered phase transfer of polymersomes in the water/[EMIM][TFSI] system provides useful information to design temperature sensitive and reversible nanoreactors, as well as extraction and separation processes, in biphasic systems.

4.5 References

1. Yang, J.; Lee, J. Y.; Ying, J. Y. *Chem. Soc. Rev.* **2011**, *40*, 1672–1696.
2. Luthra, S. S.; Yang, X.; Livingston, A. G.; Freitas dos Santos, L. M.; White, L. S. *Chem. Commun.* **2001**, 1468–1469.
3. Peng, L.; You, M.; Wu, C.; Han, D. Öçsoy, I.; Chen, T.; Chen, Z.; Tan, W. *ACS Nano* **2014**, 8, 2555–2561.
4. Spitzer, M.; Sabadini, E.; Loh, W. *J. Braz. Chem. Soc.* **2002**, *13*, 7–9.
5. Jiang, Y.; Xu, S.; Wang, C.; Shao, H.; Wang, Z.; Cui, Y. *J. Mater. Chem.* **2012**, *22*, 13469–13472.
6. Dorokhin, D.; Tomczak, N.; Han, M.; Reinhoudt, Ḱ. D. N.; Velders, A. H.; Vancso, G. J. *ACS Nano* **2009**, *3*, 661–667.
7. Holowka, E. P.; Sun, V. Z.; Kamei, D. T.; Deming, T. J. *Nat. Mater.* **2007**, *6*, 52–57.
8. Cheng, Y.; Samia, A. C.; Meyers, J. D.; Panagopoulos, I.; Fei, B.; Burda, C. *J. Am. Chem. Soc.* **2008**, *130*, 10643–10647.
9. Tian, H.; Chen, X.; Lin, H.; Deng, C.; Zhang, P.; Wei, Y.; Jing, X. *Chemistry* **2006**, *12*, 4305–4312.
10. Chechik, V.; Zhao, M.; Crooks, R. M. *J. Am. Chem. Soc.* **1999**, *121*, 4910–4911.
11. He, Y.; Lodge, T. P. *J. Am. Chem. Soc.* **2006**, *128*, 12666–12667.
12. Wu, Y.; Zhang, C.; Qu, X.; Liu, Z.; Yang, Z. *Langmuir* **2010**, *26*, 9442–9448.
13. Ueki, T.; Sawamura, S.; Nakamura, Y.; Kitazawa, Y.; Kokubo, H.; Watanabe, M. *Langmuir* **2013**, *29*, 13661–13665.
14. Li, D.; Zhao, B. *Langmuir* **2007**, *23*, 2208–2217.
15. Li, D.; Dunlap, J. R.; Zhao, B. *Langmuir* **2008**, *24*, 5911–5918.
16. Wang, H.; Yang, H.; Liu, H.; Yu, Y.; Xin, H. A *Langmuir* **2013**, *29*, 6687–6696.
17. Bai, Z.; He, Y.; Young, N. P.; Lodge, T. P. *Macromolecules* **2008**, *41*, 6615–6617.

18. Wang, Y.; Leng, W.; Gao, Y.; Guo, J. *ACS Appl. Mater. Interfaces* **2014**, *6*, 4143–4148.
19. Bai, Z.; Lodge, T. P. *J. Phys. Chem. B* **2009**, *113*, 14151–14157.
20. Bai, Z.; He, Y.; Lodge, T. P. *Langmuir* **2008**, *24*, 5284–5290.
21. Horton, J. M.; Bai, Z.; Jiang, X.; Li, D.; Lodge, T. P.; Zhao, B. *Langmuir* **2011**, *27*, 2019–2027.
22. Guerrero-Sanchez, C.; Wouters, D.; Hoeppener, S.; Hoogenboom, R.; Schubert, U. S. *Soft Matter* **2011**, *7*, 3827–3831.
23. Bai, Z.; Lodge, T. P. *J. Am. Chem. Soc.* **2010**, *132*, 16265–16270.
24. Bai, Z.; Zhao, B.; Lodge, T. P. *J. Phys. Chem. B* **2012**, *116*, 8282–8289.
25. So, S.; Lodge, T. P. *J. Phys. Chem. C* **2014**, *118*, 21140–21147.
26. Wei, D.; Ivaska, A. *Analytica Chimica Acta* **2008**, *607*, 126–135.
27. Oliver-Bourbigou, H.; Magna, L.; Morvan, D. *Applied Catalysis A* **2010**, *373*, 1–56.
28. Stoimenovski, J.; MacFarlane, D. R. *Chem. Commun.* **2011**, *47*, 11429–11431.
29. Welton, T. *Chem. Rev*. **1999**, *99*, 2071–2083.
30. Soto-Figueroa, C.; Rodríguez-Hidalgo, M.-R.; Vicente, L. *Chem. Phys. Lett.* **2012**, *531*, 155–159.
31. Bai, Z.; Nagy, M. W.; Zhao, B.; Lodge, T. P. *Langmuir* **2014**, *30*, 8201–8208.
32. Mai, Y.; Eisenberg, A. *Chem. Soc. Rev.* **2012**, *41*, 5969–5985.
33. Meli, L.; Santiago, J. M.; Lodge, T. P. *Macromolecules* **2010**, *43*, 2018–2027.
34. Meeuwissen, S. A.; Kim, K. T.; Chen, Y.; Pochan, D. J.; van Hest, J. C. M. *Angew. Chemie* **2011**, *123*, 7208–7211.
35. Wilson, D. A; Nolte, R. J. M.; van Hest, J. C. M. *Nat. Chem.* **2012**, *4*, 268–274.
36. Mok, M. M.; Lodge, T. P. *J. Polym. Sci. Part B Polym. Phys.* **2012**, *50*, 500–515.
37. Liu, T.; Diemann, E.; Li, H.; Dress, A. W. M. *Nature* **2003**, *426*, 59–62.

38. Tung, S.-H.; Lee, H.-Y.; Raghavan, S. R. *J. Am. Chem. Soc.* **2008**, *130*, 8813–8817.

39. Tokuda, H.; Tsuzuki, S.; Bin, A.; Susan, H.; Hayamizu, K. *J. Phys. Chem. B* **2006**, *110*, 19593–19600.

40. Spitzer, M.; Sabadini, E.; Loh, W. *J. Phys. Chem. B* **2002**, *106*, 12448– 12452.

41. Choucair, A.; Lavigueur, C.; Eisenberg, A. *Langmuir* **2004**, *20*, 3894–3900.

42. Lee, S. H.; Lee, S. B. *Chem. Commun.* **2005**, 3469–3471.

43. Chen, W.; Zheng, J.; Cheng, S.; Li, C.; Huang, P.; Zhu, L.; Xiong, H.; Ge, Q.; Guo, Y.; Quirk, R.; Lotz, B; Deng, L.; Wu, C.; Thomas, E. L. *Phys. Rev. Lett.* **2004**, *93*, 028301.

44. Svaneborg, C.; Pedersen, J. S. *Macromolecules* **2002**, *35*, 1028–1037.

45. Sanada, Y.; Akiba, I.; Sakurai, K.; Shiraishi, K.; Yokoyama, M.; Mylonas, E.; Ohta, N.; Yagi, N.; Shinohara, Y.; Amemiya, Y. *J. Am. Chem. Soc.* **2013**, *135*, 2574–2582.

46. Simone, P. M.; Lodge, T. P. *Macromol. Chem. Phys.* **2007**, *208*, 339–348.

47. Bhargava, P.; Zheng, J. X.; Li, P.; Quirk, R. P.; Harris, F. W.; Cheng, S. Z. D. *Macromolecules* **2006**, *39*, 4880–4888.

48. Seo, Y. S.; Kim, M. W.; Ou-yang, D. H.; Peiffer, D. G. *Polymer* **2002**, *43*, 5629–5638.

Chapter 5

Fractionation of Vesicles from Mixtures of Vesicles and Worm-like Micelles by Interfacial Tension-Controlled Phase Transfer

5.1 Introduction

Amphiphilic diblock copolymers in selective solvents have been reported to self-assemble into more than 20 morphologies, including spherical micelles, worm-like micelles, vesicles, and large compound micelles.[1–6] Multimorphological self-assembly of polymers in water, organic solvents, and ionic liquids (ILs) offers considerable potential to adapt copolymers for a range of applications in the areas of biotechnology, catalysis, and separations.[7–12] In many applications, however, not only the type of morphology, but also the average size and size distribution affects performance.[13–15] For example, the encapsulation efficiency of a hydrophobic drug is greater in worm-like micelles relative to spherical micelles of poly(styrene oxide)-*b*-poly(ethylene oxide) diblock copolymers.[16] In the systems with vesicles or polymersomes, the reaction rate of chemical reactions and the blood circulation time for drug delivery are significantly influenced by the size.[17–19] Therefore, strategies to control the morphology and the size are highly desirable.

To achieve specific self-assembled morphology and size, many approaches have been studied and proposed. The morphology can be controlled by varying the volume fraction of hydrophilic block, the quality of selective solvents, polymer concentration, preparation protocol and by an external stimulus.[20–24] These factors also affect the size.[25–28] Eisenberg group studied the size changes by varying co-solvent content,[25] and also morphology

changes from micelles to vesicles by varying co-solvent content,[29] and block ratio.[12] Davies et al. demonstrated an interesting morphology transform between vesicles and wormlike micelles depending on temperature.[21] They employed an acid additive in a lipid solution. Since the interaction between the additive and lipid molecule is stronger at higher temperature, the packing was loosened between the hydrophobic tails of the lipid, and the spontaneous morphology changes was observed. Moreover, using separation techniques, such as chromatography, extrusion, centrifugation, and field-flow fractionation techniques, the aggregates can be separated based on their size.[30–33]

Table 5–1. Characteristics of PS–PEO diblock copolymers.

Polymer	M_{PS}[a] (kg/mol)	M_{PEO}[b] (kg/mol)	$Đ$[c]	f_{PEO}[d]
PS–PEO(10–3)	9.8	2.9	1.06	0.24
PS–PEO(18–3.6)	18.4	3.6	1.01	0.17

[a,b] Number average molecular weight of the ω-hydroxyl polystyrene homopolymer (PS-OH), and PEO block obtained from ^{1}H NMR spectroscopy, respectively. [c] Dispersity (M_w /M_n) of PS–PEO determined by SEC. [d] Volume fraction of PEO block in PS–PEO block copolymers calculated by using the bulk density of PS (ρ = 1.05 g/cm^3) and PEO (ρ = 1.13 g/cm^3).

Our group has studied the phase transfer behavior of polymer vesicles (polymersomes) and micelles having poly(ethylene oxide) (PEO) moieties in the biphasic systems of water and water immiscible ILs.[34–36] The low critical solution temperature (LCST) behavior of PEO in water makes the system thermally responsive and reversible.[37] Above the phase transfer temperature (T_t), the self-assemblies transfer to the IL phase, but below T_t, they prefer the aqueous phase. During the transfer process between two immiscible phases, the morphology of the polymersomes and micelles is unperturbed; similarly, the polymersomes retain the IL interiors without any loss.[38,39]

These characteristics of the phase transfer could have potential application in separations, delivery of hydrophobic materials, and reversible nanoreactors. However, the phase transfer in the biphasic system is not always feasible, and is influenced by the interfacial tension between the aqueous solvent and the polymersome membrane block.[40]

The phase transfer behavior of various polystyrene-*b*-poly(ethylene oxide) (PS– PEO) polymersomes between water and IL, 1-ethyl-3-methylimidazolium bis(trifluoro-methylsulfonyl) imide ([EMIM][TFSI]) has been presented as a competition between the free energy of the PEO corona and the free energy of the outer interface of the PS membrane. In this chapter, by using the interfacial tension-hindered phase transfer behavior, we propose a simple fractionation method to extract a specific morphology and size of self-assemblies of PS–PEO. Broadly dispersed polymersomes were fractionated based on their size, and polymersomes were selectively separated from a mixture of worm-like micelles and polymersomes.

5.2 Experimental Section

5.2.1 Materials. Two different PS–PEO diblock copolymers, PS–PEO(10–3) and PS–PEO(18–3.6), were synthesized via sequential anionic polymerization, corresponding to number-average molecular weights (M_n) of PS $M_{n,PS}$ = 9.8 or 18.4 kg/mol, and PEO $M_{n,PEO}$ = 2.9 or 3.6 kg/mol, as shown in Table 5–1. The ionic liquid, [EMIM][TFSI] was synthesized in water as described previously.[41] Sodium chloride (NaCl) was purchased from Sigma Aldrich, and dichloromethane (CH_2Cl_2) was purchased from Fisher Scientific, and they were used as received.

5.2.2 Phase Transfer of PS–PEO Assemblies at Different NaCl Concentration. A solution of PS–PEO was prepared by a co-solvent protocol. Weighed polymers were dissolved in CH_2Cl_2 followed by addition of [EMIM][TFSI], and vacuum to yield 0.5 wt % in the IL after the co-solvent is removed. Phase transfer of PS–PEO assemblies was

conducted by adding an equal volume of water or NaCl solution to an [EMIM][TFSI] solution of PS–PEO. NaCl has poor solubility in [EMIM][TFSI],[42,43] but is highly soluble in water. The NaCl concentration in water was varied from 0 to 0.2 M to control the surface tension of the aqueous phase. It is well known that the surface tension (γ) of an aqueous solution rises linearly,[44] and the solvent quality for PEO becomes poorer with the concentration of NaCl; for example, the LCST of PEO in water decreases in salted water.[45] Two immiscible phases were contacted for at least 24 h with gentle stirring (~ 100 rpm).

5.2.3 Light Scattering. The aqueous phase after the phase transfer was separated and diluted over 150-fold and filtered through a syringe filter (Millex-SV 5.0 μm) for scattering intensity and dynamic light scattering (DLS) experiments. The measurements were conducted using a light scattering system with a Brookhaven BI-200SM goniometer, a Brookhaven BI-9000AT correlator, and a polarized He-Ne laser (λ = 637 nm) at 25 °C. The scattering intensity was recorded in units of kcps (kilo counts of scattered photons per second). The hydrodynamic radius (R_h) and the dispersity (μ_2/Γ^2, μ_2: second cumulant, Γ: mean decay rate) of polymersomes were obtained using cumulant analysis with the normalized intensity correlation function. The size distribution of the polymersomes was obtained using a Laplace inversion program, GENDIST for the REPES (Regularized Positive Exponential Sum) algorithm.[46,47]

5.2.4 Cryogenic Transmission Electron Microscopy (cryo-TEM). The morphology and the size of PS–PEO assemblies in each phase were directly investigated with cryo-TEM. The cryogenic samples were prepared in a FEI Vitrobot Mark III vitrification robot with 0.3 μL of solution. Samples placed on a carbon-coated and lacey film-supported copper TEM grid were plotted once during 1.5 s with –1 mm of blot offset, and 3 s drain time. For viscous samples, such as IL solution of polymersomes, the manual blotting was applied before blotting with the vitrification robot. After blotting, the samples were

vitrified in liquid ethane (~ –180 °C), then quickly moved and stored in liquid N_2. The images were taken using a FEI Tecnai G2 Spirit BioTWIN, operating at 120 kV under liquid N_2 cryo conditions with an Eagle 4 mega pixel CCD camera. The size of the assemblies were analyzed using ImageJ software without any background substractions.

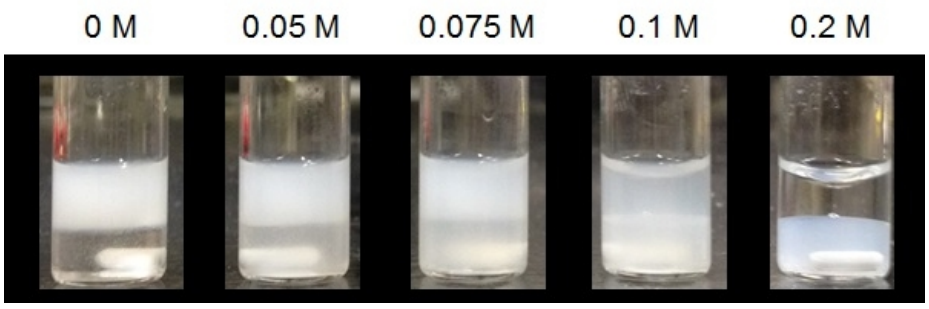

Figure 5–1. Images of [EMIM][TFSI] (bottom phase) and aqueous NaCl solution (upper phase) biphasic system with PS–PEO(18–3.6) polymersomes. The concentration of NaCl in the upper phase was varied from 0 M to 0.2 M. The images were taken after contacting the two phases for at least 24 hr. Initially, all of the polymersomes were in the IL phase, as in the image at 0.2 M NaCl.

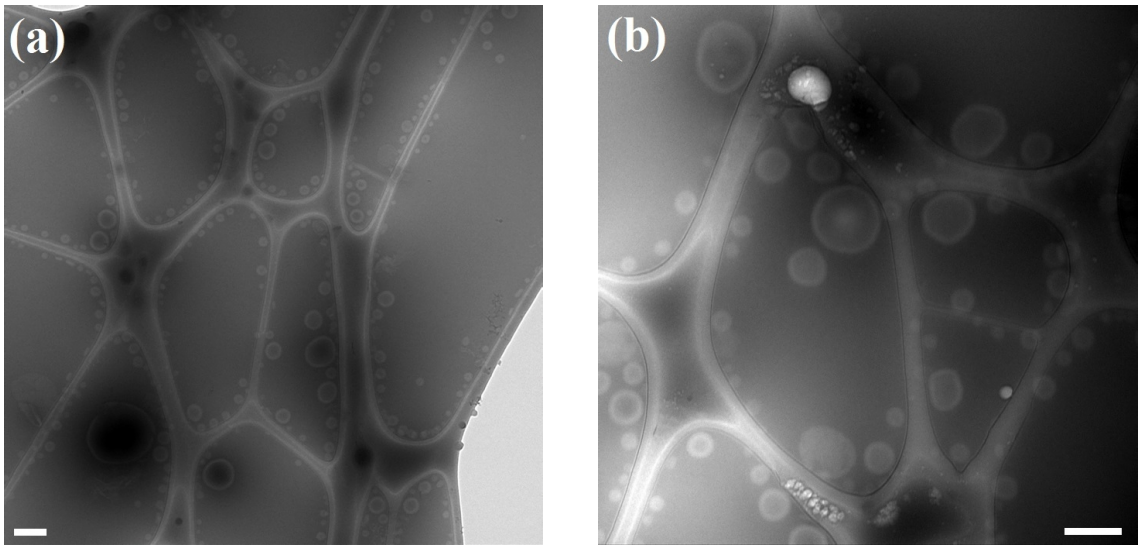

Figure 5–2. Cryo-TEM images of PS–PEO(18–3.6) polymersomes in [EMIM][TFSI] before contacting the aqueous phase. Scale bars, 200 nm.

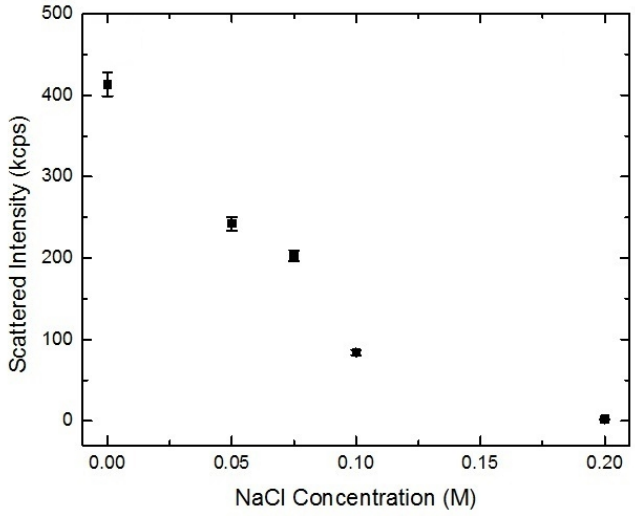

Figure 5–3. Scattered intensity of the upper phase after diluting to 0.01 wt. % at different NaCl concentration with 637 nm He-Ne laser at 90° under 20 mW.

5.3 Results and Discussion

Previously, we have shown that non-transferrable PS–PEO polymersomes could transfer to the aqueous phase, if the interfacial tension between PS and the aqueous phase ($\gamma_{PS\text{-}water}$) was reduced by introducing tetrahydrofuran (THF) to the aqueous phase.[41] Here, in contrast, $\gamma_{PS\text{-}water}$ was increased by adding NaCl, and larger polymersomes were preferentially transfered. As shown in the cryo-TEM image of Figure 5–2, with PS–PEO(18–3.6), polymersomes are preferentially formed in [EMIM][TFSI], though there are some spherical micelles. Bright regions represent the PS membrane and core, but the well-solubilized PEO corona in the IL is not visible. The broadly dispersed polymersomes in the IL were contacted with aqueous phases with various NaCl concentrations from 0 M to 0.2 M for the phase transfer. After at least 24 h, the phase transfer of the assemblies reached a steady state under equilibrium as shown in Figure 5–1. Figure 5–1 clearly shows the cloudiness changes of the aqueous phase and the IL phase as a function of the salt concentration. Without NaCl, all of the polymersomes were transferred to the top water phase from the IL phase, and the bottom IL phase turned clear. As the salt concentration was increased, the cloudiness of the aqueous phase

decreased and the aqueous phase became clear at 0.2 M NaCl, whereas the cloudiness of the IL phase increased. Figure 5–3 shows the scattered intensity of the diluted aqueous phase. The scattered intensity diminishes with the salt concentration and becomes the same as that without polymers (~ 2 kcps). The visible cloudiness trend (Figure 5–1) and the scattered intensity of the aqueous phase (Figure 5–3) clearly indicate that the increased surface tension influenced in the phase transfer of PS–PEO(18–3.6) polymersomes. The self-assembled structures and their dimensions are not changed during phase transfer even with the aqueous solution of NaCl, isomaltotriose, and THF as shown in the literature,[40,48] because they are "frozen", and not able to equilibrate during transfer. The following DLS results with PS–PEO(18–3.6) at different NaCl concentrations also support that the size was not changed by the salt concentration. An aliquot of a 0.5 wt. % aqueous solution of PS–PEO(18–3.6) polymersomes was diluted to 0.01 wt. % with pure water, 0.05 M NaCl, and 0.1 M NaCl solution, respectively, to see the effect of added NaCl on the size of the PS–PEO polymersomes. R_h and μ_2/Γ^2 were not changed with salt concentration as R_h = 114 nm (± 0.9 nm), μ_2/Γ^2 = 0.19 (± 0.01) in pure water, R_h = 116 nm (± 0.9 nm), μ_2/Γ^2 = 0.19 (± 0.01) at 0.05 M NaCl, and R_h = 114 nm (± 0.5 nm), μ_2/Γ^2 = 0.18 (± 0.02) at 0.1 M NaCl. Moreover, since the samples were diluted over 150 times in pure water to analyze the size of the upper phase with the DLS measurement, the effect of NaCl on the size of polymersomes is negligible when comparing the size of the polymersomes.

As shown in Figure 5–4, the average R_h of the polymersomes in the aqueous phase increases from 97 nm to 130 nm (Figure 5–4a), but μ_2/Γ^2 decreases from 0.2 to 0.1 (Figure 5–4b), when the concentration of NaCl changed from 0 M to 0.1 M. By controlling the surface tension of the aqueous phase in the biphasic system, more narrowly dispersed and larger polymersomes were selectively separated. This fractionation was also quantified by using cryo-TEM images (some are in Figure 5–5)

used to determine the distribution of polymersome size (Figure 5–6) from measurements of more than 550 polymersomes with the aqueous solutions at 0 M and 0.1 M NaCl. The mean of the distribution moves to larger polymersome radius (R) and the polymersomes below R = 50 nm disappear. The size distribution was fitted with a lognormal distribution function,[49] and the fitting parameters, average radius ($\langle R \rangle$) and standard deviation (w) were obtained. The absolute values of $\langle R \rangle$ are different than R_h because the number averaged value $\langle R \rangle$ is always smaller than the scattered intensity weighted R_h for polydispersed sample, but it is clear that relatively larger polymersomes could be found at higher NaCl concentration, as shown in the distributions. $\langle R \rangle$ increased from 65 nm (w = 32 nm) to 87 nm (w = 28 nm), and the dispersity value ($w/\langle R \rangle$) analogous to μ_2/Γ^2 in DLS, decreased from 0.24 to 0.10.

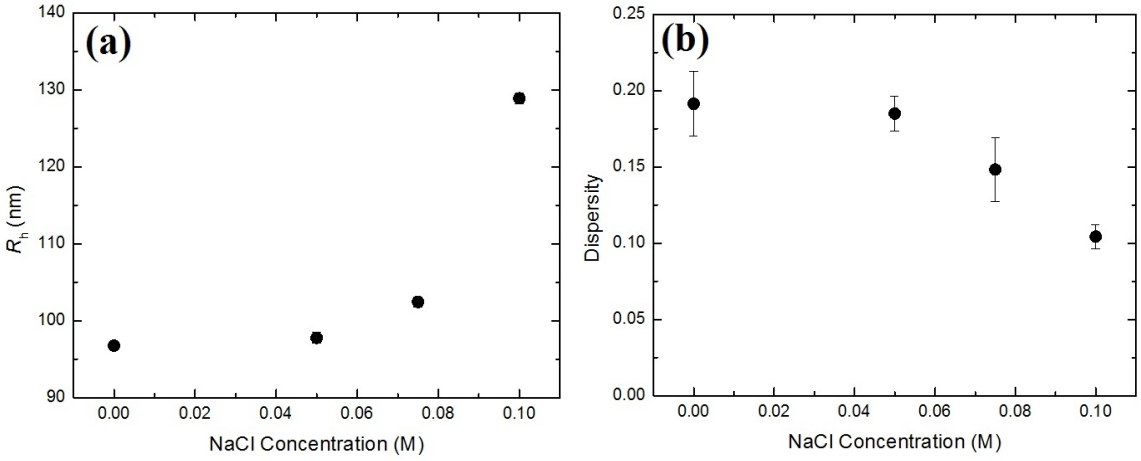

Figure 5–4. The variation of (a) Mean hydrodynamic radius (R_h) of the polymersomes in the upper phase, and (b) their size dispersity (μ_2/Γ^2) at different NaCl concentration from the DLS measurement.

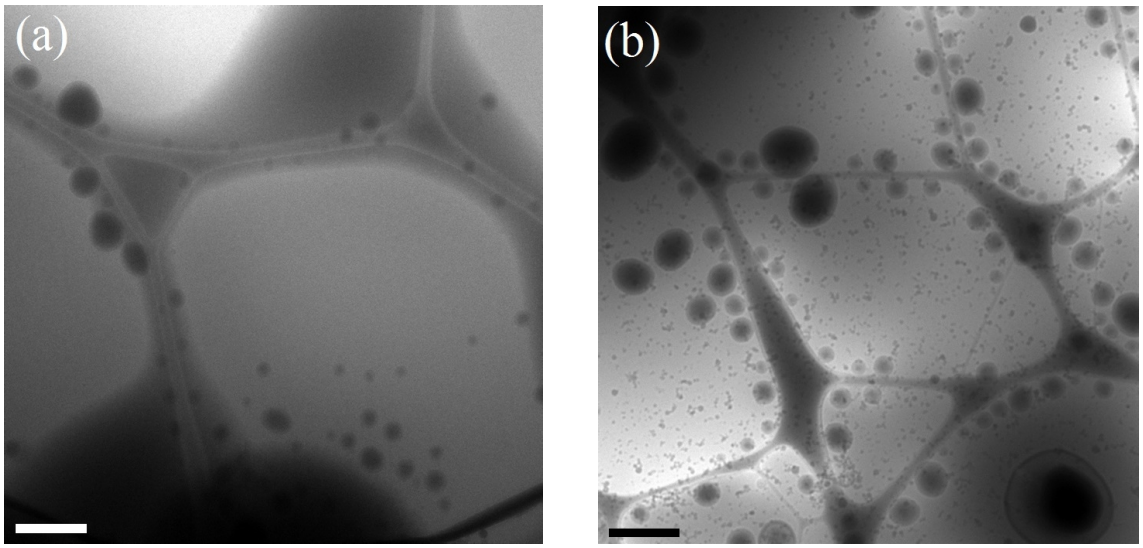

Figure 5–5. Cryo-TEM images of PS–PEO(18–3.6) polymersomes in the aqueous phase of (a) 0 M NaCl, and (b) 0.1 M NaCl, respectively, from the IL phase by the transfer. Dark dots in (b) are from ethane contamination. Scale bars, 500 nm.

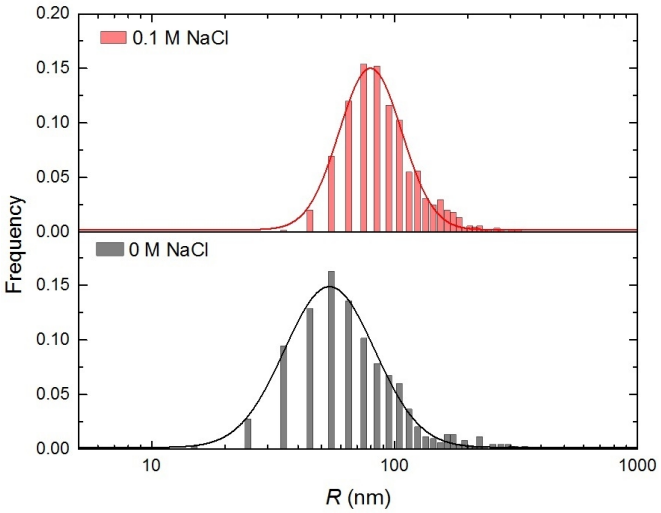

Figure 5–6. Size distribution of PS–PEO(18–3.6) assemblies from cryo-TEM images. The cryo samples were prepared with the aqueous solution of the biphasic system without NaCl and with 0.1 M NaCl.

The fractionation based on the size can be explained by the total free energy change (ΔG_{tot}) of the self-assemblies. ΔG_{tot} can be written as a summation of three contributions from the membrane interface ($\Delta G_{interface}$), the membrane or micelle core (ΔG_{core}), and the corona (ΔG_{corona}) as[50]

$$\Delta G_{tot} = \Delta G_{core} + \Delta G_{interface} + \Delta G_{corona}. \quad (5\text{–}1)$$

Depending on the sign of ΔG_{tot}, the phase transfer behavior can be estimated. When it is negative, the self-assemblies can transfer to the aqueous phase, but when it is positive, complete phase transfer does not happen. Here ΔG_{tot} can be simplified to two competing terms, positive $\Delta G_{interface}$ and negative ΔG_{corona}, due to negligible dimensional changes of the assemblies as[51]

$$\Delta G_{tot} = \Delta G_{interface} + \Delta G_{corona} = (\gamma_{PS\text{-}water} - \gamma_{PS\text{-}IL}) \times A + \Delta G_{corona}, \quad (5\text{–}2)$$

where A is the outer surface area of an assembly, and $\gamma_{PS\text{-}water}$ and $\gamma_{PS\text{-}IL}$ are the interfacial tension between PS core membrane and water or the IL, respectively. As NaCl concentration increases, $\gamma_{PS\text{-}water}$ increases, and therefore the interfacial tension penalty, $\Delta\gamma_{Interface} = \gamma_{PS\text{-}water} - \gamma_{PS\text{-}IL}$ increases, and ΔG_{corona} also increases due to increased hydrophobicity of PEO in the aqueous phase.[45] To have phase transfer at high salt concentration, the increased interfacial tension penalty should be mitigated by covering the hydrophobic core more by corona chains. The degree of the coverage can be quantified by the reduced tethering density (σ_{PEO}) which is defined as[52,53]

$$\sigma_{PEO} = \pi R_{g,PEO}^{\ 2}/S, \quad (5\text{–}3)$$

where $R_{g,PEO}$ is the radius of gyration of the PEO single chain, and S is the unit area per PS chain on the PS core or membrane, calculated by

$$S = A/N_{agg} \tag{5–4}$$

where A is the total surface area of PS core or membrane and N_{agg} is the aggregation number. Depending on geometry, A can be determined and described by following equations

$$A_{spherical} = 4\pi R_c^2, \tag{5–5a}$$

$$A_{worm\text{-}like} = 2\pi R_c L, \tag{5–5b}$$

and

$$A_{polymersome} = 8\pi R^2, \tag{5–5c}$$

where R_c is the core dimension radius for worm-like and spherical micelles, R in eqn 5–5c is the radius of polymersomes excluding outer corona length. L in eqn 5–5b is the length of worm-like micelles. N_{agg} can be calculated from the equation,[54]

$$N_{agg} = \frac{V_c \rho_{PS} N_A}{M_{n,PS}}, \tag{5–6}$$

where V_c is volume of polymersome membrane or micelle core, N_A is Avogadro's number, and $M_{n,PS}$ is the number averaged molecular weight of PS block. The density of PS membrane is assumed to be $\rho_{PS} = 1.05$ g/cm^3, the same as the bulk density of PS.[55]

We showed that σ_{PEO} has a critical value to determine the phase transfer of PS–PEO polymersomes, $\sigma_{PEO,c}$. The polymersomes can transfer above $\sigma_{PEO,c}$, but not below. As the salt concentration increases $\sigma_{PEO,c}$ is expected to shift to a higher value due to the

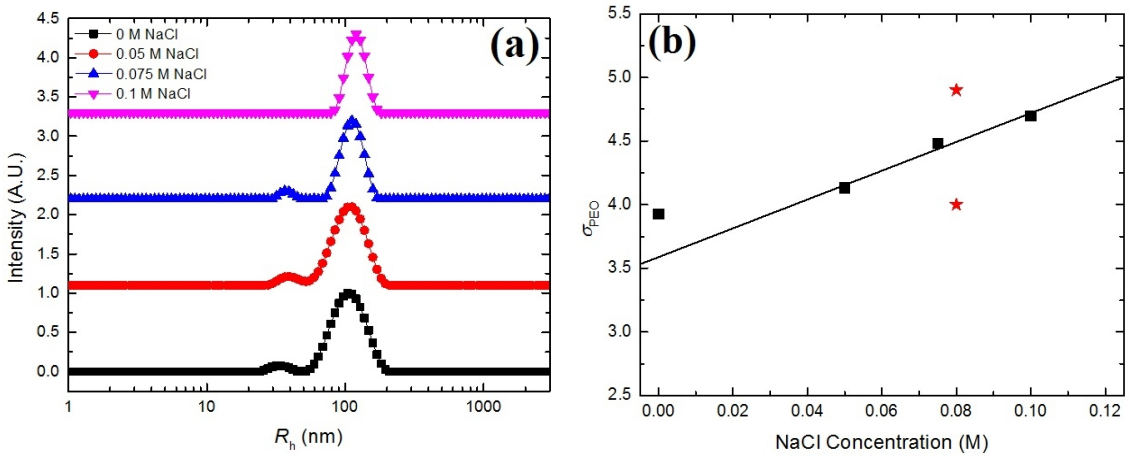

Figure 5–7. (a) Size distribution of PS–PEO(18–3.6) assemblies in the aqueous phase measured by DLS, and (b) Reduced tethering density (σ_{PEO}) with the cut-off size at various NaCl concentration from 0 M to 0.1 M. The line is a proposed boundary line for the phase transfer, and the values (★) represents σ_{PEO} of the polymersomes (4.9) and the worm-like micelles (4.0) of PS–PEO(10–3).

increased interfacial tension penalty. As a result polymersomes having σ_{PEO} less than a new $\sigma_{PEO,c}$ would not undergo phase transfer. New $\sigma_{PEO,c}$ values at different salt concentrations were estimated based on the size distribution from the DLS measurements (Figure 5–7(a)). The minimum size from the main peaks, which can be considered as a cut-off size of the polymersomes, was selected at each concentration in Figure 5–7(a), and the corresponding σ_{PEO} values were calculated using eqn 5–3. As expected from the thermodynamic analysis, the calculated σ_{PEO} (■) at the minimum size increased with the concentration of NaCl from 3.9 to 4.7. Especially, the values within the range from 0.05 M to 0.1 M NaCl fall on a single straight line as shown in Figure 5–7(b), but the value at 0 M NaCl is off from the straight line. This trend is reasonable because only $\sigma_{PEO,c}$ in pure water is well below the σ_{PEO} values of all polymersomes, whereas others at higher NaCl content are in the range of the polymersomes' σ_{PEO} values. Therefore, σ_{PEO} values above 0.05 M NaCl with the minimum size of the polymersomes can be considered as new $\sigma_{PEO,c}$ values, and the straight line can be considered as a phase transfer boundary as a

function of the concentration of NaCl. Interestingly, the intercept of the boundary line is around 3.6 corresponding to the universal value reported before in pure water,[40,52] so it is a plausible method to estimate $\sigma_{PEO,c}$.

Using the relation between $\sigma_{PEO,c}$ and the NaCl concentration (Figure 5–7b), PS–PEO(10–3) polymersomes and worm-like micelles could be separated. PS–PEO(10–3) polymers in [EMIM][TFSI] self-assembled into two different morphologies, polymersomes and worm-like micelles, as shown in Figure 5–8. Cloudiness was also used to determine the phase transfer of two kinds of assemblies, because a solution is cloudy in the presence of large assemblies.[56] As shown in the experimental images (Figure 5–9), at 0 M NaCl, all of the assemblies transferred to the top water phase from the IL phase, and the bottom IL phase turned clear. After the phase transfer, PS–PEO(10–3) assemblies also maintained their polymersome and worm-like micelle structures, as shown in Figure 5–10a. Considering the medium of the polymersome solution changes from the IL to water, the phase contrast in the image is changed due to the electron density difference; the dark interiors represent the encapsulated IL phase, the gray domains represent the PS membrane and micelle core, and the aqueous medium is lighter than the IL and PS cores. With the dimensional information from the TEM images (Figure 5–10a), σ_{PEO} values could be calculated that σ_{PEO} of the polymersomes ($<R> \approx 51$ nm) is around 4.9, whereas the calculated σ_{PEO} of the worm-like micelles is around 4.0. To have selective phase transfer of the polymersomes, $\sigma_{PEO,c}$ was set around 4.5, which is between the σ_{PEO} values of the polymersomes and the worm-like micelles, by varying the NaCl content to 0.08 M NaCl (see the values (★) of worm-like micelle and polymersomes in Figure 5–7b). As the salt content increased, the aqueous phase became less cloudy, whereas the IL phase turned cloudy (Figure 5–9). This visible cloudiness change in each phase clearly show that the controlled $\sigma_{PEO,c}$ was effective on the phase transfer of PS–PEO(10–3) assemblies. To

investigate the morphology of self-assemblies in the aqueous and IL phase after controlling $\sigma_{PEO,c}$, the vitrified samples were prepared and imaged by the cryo-TEM. When the concentration of NaCl was increased to 0.08 M, only polymersomes could be seen in the aqueous phase, but worm-like micelles were not observed, as shown in Figure 5–10b. Interestingly, as shown in Figure 5–10c, the non-transferred worm-like micelles were mainly found in the cryo-TEM image of the IL phase at 0.08 M NaCl. Some polymersomes can also be found, but they have relatively smaller size ($<R>$ = 38 nm, σ_{PEO} ~ 4.5), which were rejected by the shifted $\sigma_{PEO,c}$, compared to the transferred polymersomes ($<R>$ = 57 nm, σ_{PEO} ~ 5.1). Thus, the worm-like micelles could not transfer to the aqueous phase and remained in the IL phase due to the shifted $\sigma_{PEO,c,}$ while polymersomes having higher σ_{PEO} than the new $\sigma_{PEO,c}$ ~ 4.5 could transfer to the aqueous phase. Therefore, the phase transfer boundary obtained from PS–PEO(18–3.6) polymersome case was successfully applied to a different system having different molecular weight and morphologies.

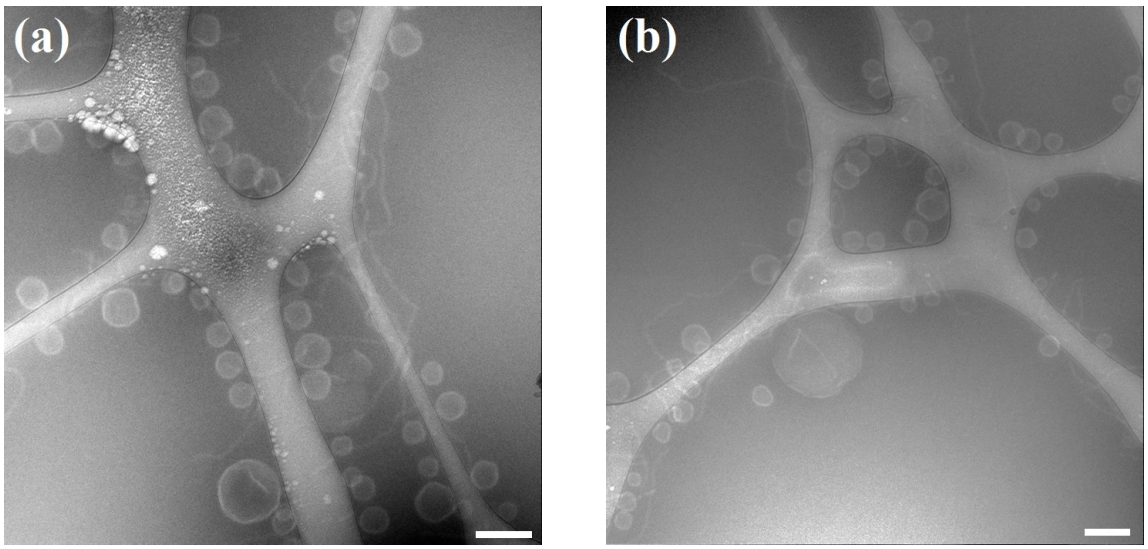

Figure 5–8. Cryo-TEM images of PS–PEO(10–3) polymersomes and worm-like micelles in [EMIM][TFSI] before contacting the aqueous phase. Scale bar is 200 nm.

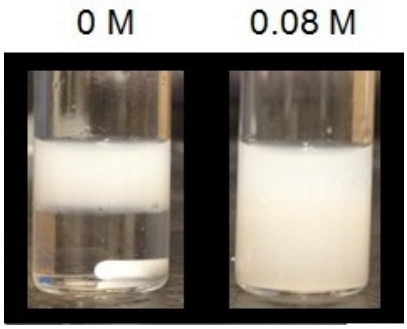

Figure 5–9. Images of PS–PEO(10–3) polymersome in [EMIM][TFSI] (bottom phase) and aqueous NaCl solution (upper phase) biphasic system. The concentration of NaCl in the upper phase were varied from 0 M to 0.08 M.

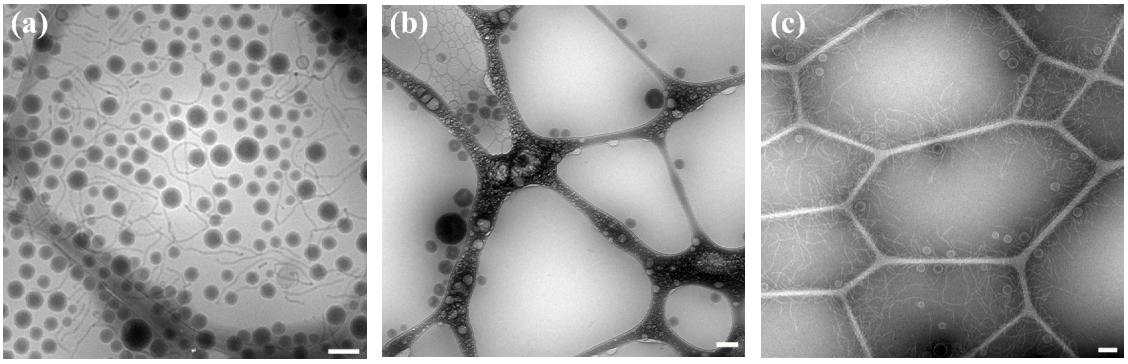

Figure 5–10. Cryo-TEM images of PS–PEO(10–3) assemblies in (a) the aqueous phase at 0 M NaCl, (b) the aqueous phase and (c) the IL phase at 0.08 M NaCl after contacting the IL solution of PS–PEO(10–3) assemblies with the aqueous solution at least 24 hr. Scale bars, 200 nm.

In addition to the fractionation, this interfacial tension-controlled phase transfer can also be used to have the assemblies transfer back to the IL phase at room temperature. When NaCl was added (the target concentration in the aqueous phase was 0.5 M NaCl) to the biphasic system after the complete phase transfer, all of the PS–PEO assemblies reversely transferred to the IL phase from the aqueous phase, as shown in Figure 5–11. With the combination of the phase transfer "from the IL to water" and "from water to the IL", the finely selected assemblies in size possibly can be obtained.

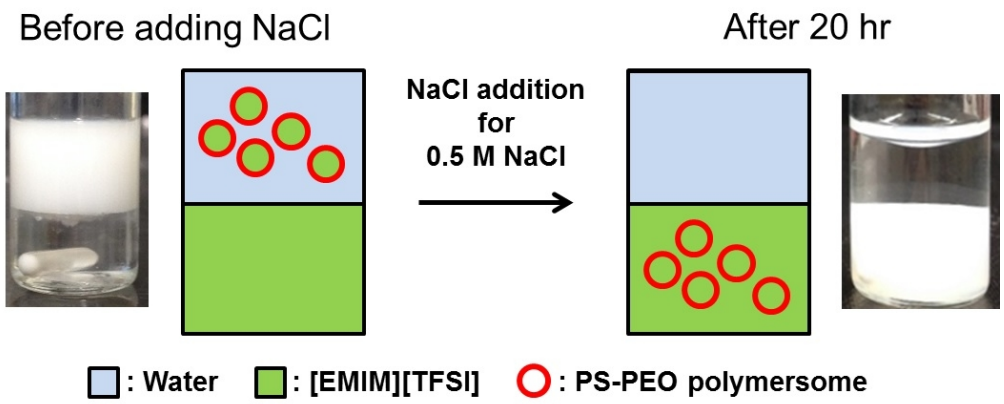

Figure 5–11. Experimental images and schemes of reverse-phase transfer of PS–PEO(18–3.6) / PS–PEO(18–2.5) polymersomes by adding NaCl to the biphasic system of the IL and water. The polymersomes solution was prepared by using 4:7 mixture of PS–PEO(18–3.6) and PS–PEO(18–2.5) in weight ratio. At room temperature, with gentle stirring which keep two immiscible phases, all of the polymersomes could be recovered to the IL phase.

5.4 Conclusions

In summary, we have applied the phase transfer behavior of PS–PEO in the biphasic system to a new simple fractionation process depending on the size and morphology of the assemblies. The increased surface tension of the aqueous phase could increase the interfacial penalty for the phase transfer, and shift the necessary value of $\sigma_{PEO,c}$ to a higher value. The shifted boundary was proposed on the basis of the result of the polymersome size-fractionation, and successfully applied to the separation of the polymersomes from a mixture of polymersomes and worm-like micelles. This fractionation method is a new approach to achieve a desired morphology and size of assembly by simply controlling the salt content in the aqueous phase. This new fractionation technique has potential to be applied to the fields of biotechnology and reversible nanoreactors system.

5.5 References

1. Jain, S.; Bates, F. S. *Science* **2003**, *300*, 460–464.
2. Yu, K.; Zhang, L.; Eisenberg, A. *Langmuir* **1996**, *12*, 5980–5984.
3. Zhou, Z.; Li, Z.; Ren, Y.; Hillmyer, M. A.; Lodge, T. P. *J. Am. Chem. Soc.* **2003**, *125*, 10182–10183.
4. Du, J.; O'Reilly, R. K. *Chem. Soc. Rev.* **2011**, *40*, 2402–2416.
5. Meeuwissen, S. A.; Kim, K. T.; Chen, Y.; Pochan, D. J.; Van Hest, J. C. M. *Angew. Chemie - Int. Ed.* **2011**, *50*, 7070–7073.
6. Zhang, L. F.; Eisenberg, A. *Polym. Adv. Technol.* **1998**, *9*, 677–699.
7. He, Y.; Li, Z.; Simone, P.; Lodge, T. P. *J. Am. Chem. Soc.* **2006**, *128*, 2745–2750.
8. Napoli, A.; Valentini, M.; Tirelli, N.; Müller, M.; Hubbell, J. A. *Nat. Mater.* **2004**, *3*, 183–189.
9. Rodríguez-Hernández, J.; Lecommandoux, S. *J. Am. Chem. Soc.* **2005**, *127*, 2026–2027.
10. Bang, J.; Jain, S.; Li, Z.; Lodge, T. P.; Pedersen, J. S.; Kesselman, E.; Talmon, Y. *Macromolecules* **2006**, *39*, 1199–1208.
11. Blanazs, A.; Armes, S. P.; Ryan, A. J. *Macromol. Rapid Commun.* **2009**, *30*, 267–277.
12. Azzam, T.; Eisenberg, A. *Angew. Chemie - Int. Ed.* **2006**, *45*, 7443–7447.
13. Geng, Y.; Dalhaimer, P.; Cai, S.; Tsai, R.; Tewari, M.; Minko, T.; Discher, D. E. *Nat. Nanotechnol.* **2007**, *2*, 249–255.
14. Leson, A.; Leson, A.; Hauschild, S.; Rank, A.; Neub, A.; Schubert, R.; Forster, S.; Mayer, C. *Small* **2007**, *3*, 1074–1083.
15. Nagayasu, A.; Uchiyama, K.; Kiwada, H. *Adv. Drug Deliv. Rev.* **1999**, *40*, 75–87.

16. Crothers, M.; Zhou, Z.; Ricardo, N. M. P. S.; Yang, Z.; Taboada, P.; Chaibundit, C.; Attwood, D.; Booth, C. *Int. J. Pharm.* **2005**, *293*, 91–100.
17. Antonietti, M.; Förster, S. *Adv. Mater.* **2003**, *15*, 1323–1333.
18. Chen, Q.; Schonherr, H.; Vancso, G. J. *Small* **2009**, *5*, 1436–1445.
19. Wong, B.; Boyer, C.; Steinbeck, C.; Peters, D.; Schmidt, J.; van Zanten, R.; Chmelka, B.; Zasadzinski, J. A. *Adv. Mater.* **2011**, *23*, 2320–2325.
20. Shen, H.; Eisenberg, A. *J. Phys. Chem. B* **1999**, *103*, 9473–9487.
21. Davies, T. S.; Ketner, A. M.; Raghavan, S. R. *J. Am. Chem. Soc.* **2006**, *128*, 6669–6675.
22. Geng, Y.; Ahmed, F.; Bhasin, N.; Discher, D. E. *J. Phys. Chem. B* **2005**, *109*, 3772–3779.
23. Mendes, E.; Narayanan, J.; Oda, R.; Kern, F.; Candau, S. J.; Pascal, B.; Manohar, C. *J. Phys. Chem. B* **1997**, *101*, 2256–2258.
24. Discher, D. E.; Eisenberg, A. *Science* **2002**, *297*, 967–973.
25. Luo, L.; Eisenberg, A. *Langmuir* **2001**, *17*, 6804–6811.
26. Sanson, C.; Schatz, C.; Le Meins, J.-F.; Brûlet, A.; Soum, A.; Lecommandoux, S. *Langmuir* **2010**, *26*, 2751–2760.
27. Meli, L.; Santiago, J. M.; Lodge, T. P. *Macromolecules* **2010**, *43*, 2018–2027.
28. Battaglia, G.; Ryan, A. J. *Macromolecules* **2006**, *39*, 798–805.
29. Yu, Y.; Zhang, L.; Eisenberg, A. *Macromolecules* **1998**, *31*, 1144–1154.
30. Brunner, G.; Ferber, E.; Resch, K. *Anal. Biochem.* **1977**, *80*, 420–429.
31. Kang, Y.; Li, D.; Kalams, S. A.; Eid, J. E. *Biomed. Microdevices* **2008**, *10*, 243–249.
32. Yao, L.; Heubi, J. E.; Buckley, D. D.; Fierra, H.; Setchell, K. D. R.; Granholm, N. A; Tso, P.; Hui, D. Y.; Woollett, L. A. *J. Lipid Res.* **2002**, *43*, 654–660.

33. Lecuyer, S.; Ristenpart, W. D.; Vincent, O.; Stone, H. A. *Appl. Phys. Lett.* **2008**, *92*, 92–94.
34. He, Y.; Lodge, T. P. *J. Am. Chem. Soc.* **2006**, *128*, 12666–12667.
35. Bai, Z.; He, Y.; Young, N. P.; Lodge, T. P. *Macromolecules* **2008**, *41*, 6615–6617.
36. Bai, Z.; Lodge, T. P. *J. Phys. Chem. B* **2009**, *113*, 14151–14157.
37. Bai, Z.; Nagy, M. W.; Zhao, B.; Lodge, T. P. *Langmuir* **2014**, *30*, 8201–8208.
38. Bai, Z.; Lodge, T. P. *J. Am. Chem. Soc.* **2010**, *132*, 16265–16270.
39. So, S.; Lodge, T. P. *J. Phys. Chem. C* **2014**, *118*, 21140–21147.
40. So, S.; Lodge, T. P. *Langmuir* **2015**, *31*, 594–601.
41. Meli, L.; Santiago, J. M.; Lodge, T. P. *Macromolecules* **2010**, *43*, 2018–2027.
42. Ghareh Bagh, F. S.; Mjalli, F. S.; Hashim, M. A.; Hadj-Kali, M. K. O.; Alnashef, I. M. *Ind. Eng. Chem. Res.* **2013**, *52*, 11488–11493.
43. Pereiro, A. B.; Araújo, J. M. M.; Oliveira, F. S.; Esperança, J. M. S. S.; Canongia Lopes, J. N.; Marrucho, I. M.; Rebelo, L. P. N. *J. Chem. Thermodyn.* **2012**, *55*, 29–36.
44. Liao, C.; Chao, K.; Tsai, J. *IEEE J. Quantum Electron.* **2010**, *46*, 1268–1274.
45. Florin, E.; Kjellander, R.; Eriksson, J. C. *J. Chem. Soc. Faraday Trans. 1* **1984**, *80*, 2889.
46. Schillen, K.; Brown, W.; Johnsen, R. M. *Macromolecules* **1994**, *27*, 4825–4832.
47. Jakes, J. *Collect. Czech. Chem. Commun.* **1995**, *60*, 1781–1797.
48. Bai, Z.; He, Y.; Lodge, T. P. *Langmuir* **2008**, *24*, 5284–5290.
49. Siano, D. B. *J. Chem. Educ.* **1972**, *49*, 755–757.
50. Mai, Y.; Eisenberg, A. *Chem. Soc. Rev.* **2012**, *41*, 5969–5985.
51. Seo, Y. S.; Kim, M. W.; Ou-yang, D. H.; Peiffer, D. G. *Polymer* **2002**, *43*, 5629–5638.

52. Chen, W. Y.; Zheng, J. X.; Cheng, S. Z. D.; Li, C. Y.; Huang, P.; Zhu, L.; Xiong, H.; Ge, Q.; Guo, Y.; Quirk, R. P.; Lotz. B.; Deng, L.; Wu, C.; Thomas, E. L. *Phys. Rev. Lett.* **2004**, *93*, 028301.

53. Sanada, Y.; Akiba, I.; Sakurai, K.; Shiraishi, K.; Yokoyama, M.; Mylonas, E.; Ohta, N.; Yagi, N.; Shinohara, Y.; Amemiya, Y. *J. Am. Chem. Soc.* **2013**, *135*, 2574–2582.

54. He, Y.; Li, Z.; Simone, P.; Lodge, T. P. *J. Am. Chem. Soc.* **2006**, *128*, 2745–2750.

55. Simone, P. M.; Lodge, T. P. *Macromol. Chem. Phys.* **2007**, *208*, 339–348.

56. Zhang, M.; Wang, M.; He, S.; Qian, J.; Saffari, A.; Lee, A.; Kumar, S.; Hassan, Y.; Guenther, A.; Scholes, G.; Winnik, M. A. *Macromolecules* **2010**, *43*, 5066–5074.

Chapter 6

Concluding Remarks

6.1 Summary

The objective of this thesis is to understand transportation phenomena with the nanoemulsion-like polymersomes for a biphasic system of water and ionic liquids, and to provide grounding information in "nanoreactor" applications. Block copolymer vesicles possessing poly(ethylene oxide) coronas, such as from 1,2-polybutadiene-*b*-poly(ethylene oxide) (PB–PEO) and polystyrene-*b*-poly(ethylene oxide) (PS–PEO) block copolymer, show reversible phase transfer between a hydrophobic ionic liquid and water, depending on temperature. The polymersome shuttle system with ionic liquids has several advantages for reactions in terms of process and efficiency. First, catalysts and ionic liquids can be recovered after the reactions. Second, additional separation processes for the products are not necessary since they can be obtained simultaneously with recovering the nanoreactors. Third, the proposed reaction process is environmentally benign and cost effective because volatile organic solvents are not used during the reaction process, and the amount of the encapsulated ionic liquid as a solvent for the reaction is only a few percent of the aqueous medium. Fourth, the confined ionic liquid interior can enhance the catalyst activity, stability, and reaction selectivity.

Two different kinds of transport behaviors are involved to realize various reactions using the nanoemulsion-like polymersomes; one is permeability of molecules through the polymersome membrane, and the other is phase transfer of the ionic liquid-filled polymersomes between two immiscible phases. Polymersome size is an important

parameter for the transportation studies, since both molecular permeation and polymersome transfer are affected by size.

Two general approaches, mechanical and kinetic, to control the size were proposed for polymersomes having rubbery (PB) or glassy (PS) hydrophobic blocks. For the mechanical process, extrusion through a membrane was employed with the polymersome solution formed from the "thin film hydration" protocol. As the solution was pushed through the membrane, relatively large polymersomes were broken up and reorganized into vesicles with mean size comparable to the membrane pore (100 nm radius); the width of the size distribution also decreased significantly with subsequent passes. Kinetic processes were studied using the co-solvent method, whereby the initial content of the co-solvent and the PEO block length of PS–PEO were systemically changed. The dichloromethane co-solvent was selectively evaporated from the ionic liquid/ dichloromethane/polymer solution under vacuum. The non-volatility of the ionic liquid directly led to the desired concentration of polymersomes in the ionic liquid using a single step, without the dialysis conventionally used in aqueous systems. With increased amounts of dichloromethane or a longer PEO block, the diameter and size dispersity decreased.

With the size-controlled polymersomes, permeability of probing molecules was studied depending on the charge status of molecule. The molecular permeation was explored with a combination of ^{1}H NMR spectroscopy and pulsed-field-gradient NMR (PFG-NMR) experiments. Similarly size tracer molecules, but having different properties, including 1-ethyl-3-methylimidazolium ([EMIM]), 1-buthyl-3-methylimidazolium ([BMIM]), and 1-butylimidazole were employed. Generally, molecular permeation in the nanoemulsion-like polymersome solution showed similar features as permeability through bulk polymer films, and through conventional vesicle membranes having same fluids inside and outside. The charged molecule ([EMIM]) were

approximately 10 times slower than the neutral molecule (1-butylimidazole). However, the molecules could permeate through the hydrophobic PB membranes on a time scale of seconds, and these results confirm that this system has the potential to serve as a nanoreactor, facilitating reactions with various kinds of molecules including both charged and neutral molecules.

The other transportation phenomenon is phase transfer of polymersomes from the ionic liquid phase to water, enabling nanoemulsion formation. The phase transfer is a thermodynamic compatible between two Gibbs free energy; a positive interfacial tension penalty ($\Delta G_{\text{interface}}$), and a negative free energy change of PEO corona (ΔG_{corona}). This thermodynamic phase transfer featured by a general boundary for the phase transfer in terms of a reduced tethering density for PEO (σ_{PEO}), which is independent of the molecular weight of the hydrophobic PS. The reduced PEO tethering density was controlled by changing the polymersome size (i.e., increased polymersome sizes increase σ_{PEO}) confirming that it is the driving force in the transfer of PS–PEO polymersomes at room temperature.

Given the phase transfer study, σ_{PEO} was also tuned by controlling the surface tension of water with tetrahydrofuran and NaCl, which can alter the interfacial tension penalty, then the phase transfer of polymersomes could be controlled with the concentration of additives. Applications in fractionation and separation based on polymersome size and morphology was also shown with the phase transfer phenomenon of PS–PEO in the biphasic system.

6.2 Proposed Future Directions

Recently Bai and Lodge studied the molecular permeability of a PB bilayer membrane of the ionic liquid-filled PB–PEO polymersomes in water by a fluorescence quenching experiment.[1] The quenching process of a hydrophobic fluorescent dye, Nile Red, by a

quencher, dichloroacetamide, resemble bimolecular reaction,[2] since the collision between Nile Red and dichloroacetamide is involved for the quenching. This study clearly shows the possible application of the nanoemulsion-like polymersomes as nanoreactors.

It would be of interest to run chemical reactions in the nanoremulsion-like solutions by loading appropriate catalyst into the membranes and polymersome interiors. Especially, since there are three different phases in the nanoemulsion-like polymersome solution, the ionic liquid, polymersome membrane, and water,[3] a multi-step cascade reaction would be possible.[4,5]

Polymersomes in ionic liquids and water have some other practical difficulties to be resolved, *e.g.*, the affinity of the species to the ionic liquid and water is related to the rate of transport of reactants and products and the stability of the catalysts. These limitations can be lessened by introducing a carefully selected bulk component. Water-in-ionic liquid type (W/I) nanoemulsion would be one of the solutions for the reactions with catalyst, which is not active in ionic liquids. For example, hydrolysis of *p*-nitrophenyl butyrate catalyzed by Burkholderia cepacia lipase showed higher conversion in the ionic liquid saturated water, but there was no conversion in the water saturated ionic liquid.[6] W/I nanoemulsion, which also has advantages of biphasic system, can be prepared by phase transfer of water-filled polymersomes to ionic liquids.

Furthermore, to cover the various kinds of reactions by the proposed process (Scheme 1–1), the model system can be modified by employing a third phase. An organic phase as a third phase can be employed to form an organic/aqueous biphasic system after the transfer of the nanoreactors to the aqueous phase (see Scheme 6–1). For example, Lan *et al.* conducted the hydrogenation of olefins (cinnamic alcohol, styrene, butyl acrylate, and etc.) by using Pd-catalysts in polymeric microreactors composed of polyacrylamide corona and polystryrene-*b*-poly(2-acetoacetoxy-ethylmethacrylate) under the organic/ aqueous biphasic system.[7] The olefins in the organic phase diffused into the

polymersome reactors in the aqueous phase and were hydrogenated by the Pd catalyst. After the reaction, the hydrogenated olefins diffused back to the organic phase for easy separation. This example demonstrates that the partition problem of the model system can be resolved by the judicious choice of bulk component, while still keeping the advantages of the ionic liquid-filled polymersome nanoreactors dispersed in water, e.g. the aqueous medium of the nanoreactors can be recycled by loading new organic phase for the reactions.

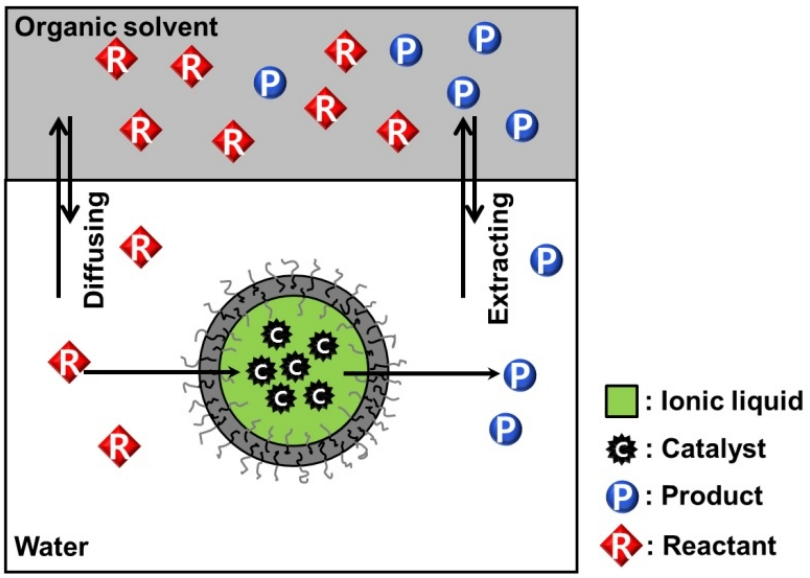

Scheme 6–1. General reaction system of polymersome nanoreactors with ionic liquid interiors in an organic/aqueous biphasic system.

Emulsion-like vesicles are beneficial because they can expand the selection of components for a reaction by delivering them to the other phase, which is not compatible with the loaded components. As the example of polymersome colloidosomes, which is similar to Pickering emulsion,[8] emulsion-like vesicles would provide the stabilized inner phase, which is well compartmentalized from the medium, and be expected to have better performance in catalysis. However, there is still issue of contaminating the aqueous phase by catalyst in the ionic liquid phase, because the ionic liquid phase is always in contact

with water during the phase transfer. To resolve this issue, microfluidic device is a promising apparatus to prepare emulsion-like polymersome solution by a one-pot process.[9–11] As shown in Scheme 6–2, three capillary tube are connected to each other, and three different fluids flow; ionic liquid with catalyst flows through the inner phase channel, block copolymers are provided through the middle phase, and the droplets are dispersed in the outer phase, water. After removing volatile solvent in the middle phase, monodispersed microemulsion-like polymersome can be obtained with high loading efficiency of catalyst.

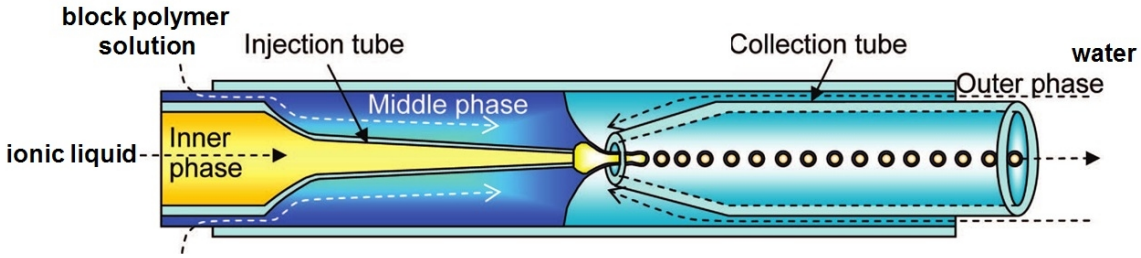

Scheme 6–2. Scheme of a microfluidic device for one-pot emulsion-like polymersome preparation with capillary tubes.(Reproduced with permission from reference 9)

6.3 References

1. Bai, Z.; Zhao, B.; Lodge, T. P. *J. Phys. Chem. B* **2012**, *116*, 8282–8289.
2. Eftink, M. R.; Ghiron, C. A. *Anal. Biochem.* **1981**, *114*, 199–227.
3. Bai, Z.; Lodge, T. P. *J. Am. Chem. Soc.* **2010**, *132*, 16265–16270.
4. Delaittre, G.; Reynhout, I. C.; Cornelissen, J. J. L. M.; Nolte, R. J. M. *Chem. Eur. J.* **2009**, *15*, 12600–12603.
5. Watanabe, K.; Takizawa, S.; Murata, S. *Chem. Lett.* **2011**, *40*, 345–347.
6. Moniruzzaman, M.; Kamiya, N.; Nakashima, K.; Goto, M. *Green Chem.* **2008**, *10*, 497–500.
7. Lan, Y.; Zhang, M.; Zhang, W.; Yang, L. *Chem. Eur. J.* **2009**, *15*, 3670–3673.
8. Wang, Z.; van Oers, M. C. M.; Rutjes, F. P. J. T.; van Hest, J. C. M. *Angew. Chem. Int. Ed.* **2012**, *51*, 10746–10750.
9. Shum, H. C.; Kim, J.-W.; Weitz, D. A. *J. Am. Chem. Soc.* **2008**, *130*, 9543–9549.
10. Thiele, J.; Chokkalingam, V.; Ma, S.; Wilson, D. A.; Huck, W. T. S. *Mater. Horiz.* **2014**, *1*, 96–101.
11. Foster, T. Dorfman, K. D.; Davis, H. T. *J. Colloid Interf. Sci.* **2010**, *351*, 140–150.

Bibliography

Adalsteinsson, T.; Dong, W.; Schönhoff, M. *J. Chem. Phys.*, **2004**, *108*, 20056–20063.

Anderson, J. L.; Ding, J.; Welton, T.; Armstrong, D. W. *J. Am. Chem. Soc.* **2002**, *124*, 14247–14254.

Anisur, R. M.; Shin, J.; Choi, H. H.; Yeo, K. M.; Kang, E. J.; Lee, I. S. *J. Mater. Chem.* **2010**, *20*, 10615–10621.

Antonietti, M.; Förster, S. *Adv. Mater.* **2003**, *15*, 1323–1333.

Appetecchi, G. B.; Scaccia, S.; Tizzani, C.; Alessandrini, F.; Passerini, S. *J. Electrochem. Soc.* **2006**, *153*, A1685–A1691.

Aranda-Espinoza, H.; Bermudez, H.; Bates, F. S.; Discher, D. E. *Phys. Rev. Lett.* **2011**, *87*, 208301-1–208301-4.

Armstrong, D. W.; He, L.; Liu, Y.-S. *Anal. Chem.* **1999**, *71*, 3873–3876.

Ashworth, A. J.; Wickham, M. D. *J. Memb. Sci.* **1987**, *34*, 225–240.

Autenrieth, B.; Frey, W.; Buchmeiser, M. R. *Chem. Eur. J.* **2012**, 18, 14069–14078.

Azzam, T.; Eisenberg, A. *Angew. Chem. Int. Ed.* **2006**, *45*, 7443–7447.

Bai, Z.; He, Y.; Lodge, T. P. *Langmuir* **2008**, *24*, 5284–5290.

Bai, Z.; He, Y.; Young, N. P.; Lodge, T. P. *Macromolecules* **2008**, *41*, 6615–6617.

Bai, Z.; Lodge, T. P. *J. Am. Chem. Soc.* **2010**, *132*, 16265–16270.

Bai, Z.; Lodge, T. P. *J. Phys. Chem. B* **2009**, *113*, 14151–14157.

Bai, Z.; Lodge, T. P. *Langmuir* **2010**, *26*, 8887–8892.

Bai, Z.; Nagy, M. W.; Zhao, B.; Lodge, T. P. *Langmuir* **2014**, *30*, 8201–8208.

Bai, Z.; Zhao, B.; Lodge, T. P. *J. Phys. Chem. B* **2012**, *116*, 8282–8289.

Bang, J.; Jain, S.; Li, Z.; Lodge, T. P.; Pedersen, J. S.; Kesselman, E.; Talmon, Y. *Macromolecules* **2006**, *39*, 1199–1208.

Battaglia, G.; Ryan, A. J. *J. Phys. Chem. B* **2006**, *110*, 10272–10279.

Battaglia, G.; Ryan, A. J. *Macromolecules* **2006**, *39*, 798–805.

Battaglia, G.; Ryan, A. J.; Tomas, S. *Langmuir* **2006**, *22*, 4910–4913.

Bermudez, H.; Brannan, A. K.; Hammer, D. A.; Bates, F. S.; Discher, D. E. *Macromolecules* **2002**, *35*, 8203–8208.

Bhargava, P.; Zheng, J. X.; Li, P.; Quirk, R. P.; Harris, F. W.; Cheng, S. Z. D. *Macromolecules* **2006**, *39*, 4880–4888.

Bhattacharyya, S.; Bagchi, B. *J. Chem. Phys.* **1997**, *106*, 1757–1763.

Blanazs, A.; Armes, S. P.; Ryan, A. J. *Macromol. Rapid Commun.* **2009**, *30*, 267–277.

Bolinger, P.; Stamou, D.; Vogel, H. *J. Am. Chem. Soc.* **2004**, *126*, 8594–8595.

Bolinger, P.-Y.; Stamou, D.; Vogel, H. *Angew. Chem. Int. Ed.* **2008**, *47*, 5544–5549.

Boon, J. A.; Levisky, J. A.; Pflug, J. L.; Wilkes, J. S. *J. Org. Chem.* **1986**, *51*, 480–483.

Brunner, G.; Ferber, E.; Resch, K. *Anal. Biochem.* **1977**, *80*, 420–429.

Cammarata, L.; Kazarian, S. G.; Salter, P. A.; Welton, T. *Phys. Chem. Chem. Phys.* **2001**, *3*, 5192–5200.

Chechick, V.; Zhao, M.; Crooks, R. M. *J. Am. Chem. Soc.* **1999**, *121*, 4910–4911.

Chen, G.; Guan, Z. *J. Am. Chem. Soc.* **2004**, *126*, 2662–2663.

Chen, Q.; Rausch, K. G.; Schönherr, H.; Vancso, G. J. *Chem. Phys. Chem.* **2010**, *11*, 3534–3540.

Chen, Q.; Schonherr, H.; Vancso, G. J. *Small* **2009**, *5*, 1436–1445.

Chen, W. Y.; Zheng, J. X.; Cheng, S. Z. D.; Li, C. Y.; Huang, P.; Zhu, L.; Xiong, H.; Ge, Q.; Guo, Y.; Quirk, R. P.; Lotz. B.; Deng, L.; Wu, C.; Thomas, E. L. *Phys. Rev. Lett.* **2004**, *93*, 028301.

Cheng, Y.; Samia, A. C.; Meyers, J. D.; Panagopoulos, I.; Fei, B.; Burda, C. *J. Am. Chem. Soc.* **2008**, *130*, 10643–10647.

Chiappe, C.; Pieraccini, D. *J. Phys. Org. Chem.* **2005**, *18*, 275–297.

Chiu, D. T.; Wilson, C. F.; Karlsson, A.; Danielsson, A.; Lundqvist, A.; Stromberg, A.;

Ryttsen, F.; Davidson, M.; Nordholm, S.; Orwar, O.; Zare, R. N. *Chem. Phys.* **1999**, *247*, 133–139.

Cho, J. H.; Lee, J.; Xia, Y.; Kim, B.; He, Y.; Renn, M. J.; Lodge, T. P.; Frisbie, C. D. *Nat. Mater.* **2008**, *7*, 900–906.

Choucair, A.; Lavigueur, C.; Eisenberg, A. *Langmuir* **2004**, *20*, 3894–3900.

Choucair, A.; Soo, P. L.; Eisenberg, A. *Langmuir* **2005**, *21*, 9308–9313.

Choudhury, R. P.; Galvosas, P.; Schönhoff, M. *J. Phys. Chem. B* **2008**, *112*, 13245–13251.

Chuanoi, S.; Anraku, Y.; Hori, M.; Kishimura, A.; Kataoka, K. *Biomacromolecules* **2014**, *15*, 2389–2397.

Clarke, R. J.; Apell, H.-J. *Biophys. Chem.* **1989**, *34*, 225–237.

Crothers, M.; Zhou, Z.; Ricardo, N. M. P. S.; Yang, Z.; Taboada, P.; Chaibundit, C.; Attwood, D.; Booth, C. *Int. J. Pharm.* **2005**, *293*, 91–100.

Cussler, E. L. *Diffusion*, 3rd ed; Cambridge University Press, New York, 2009.

Davies, T. S.; Ketner, A. M.; Raghavan, S. R. *J. Am. Chem. Soc.* **2006**, *128*, 6669–6675.

Davis, K.; Lodge, T. P.; Bates, F. S. *Macromolecules* **2008**, *41*, 8289–8291.

Delaittre, G.; Reynhout, I. C.; Cornelissen, J. J. L. M.; Nolte, R. J. M. *Chem. Eur. J.* **2009**, *15*, 12600–12603.

Discher, B. M.; Won, Y.; Ege, D. S.; Lee, J. C-M.; Bates, F. S.; Discher, D. E.; Hammer, D. A. *Science* **1999**, *284*, 1143–1146.

Discher, D. E.; Eisenberg, A. *Science* **2002**, *297*, 967–973.

Dong, R.; Liu, W.; Hao, J. *Acc. Chem. Res.* **2012**, *45*, 504–513.

Dorokhin, D.; Tomczak, N.; Han, M.; Reinhoudt, D. N.; Velders, A. H.; Vansco, G. J. *ACS Nano* **2009**, *3*, 661–667.

Doyagüez, E. G.; Rodríguez-Hernández, J.; Corrales, G.; Fernández-Mayoralas, A. *Macromolecules* **2012**, *45*, 7676–7683.

Du, J.; O'Reilly, R. K. *Chem. Soc. Rev.* **2011**, *40*, 2402–2416.

Du, J.; O'Reilly, R. K. *Soft Matter* **2009**, *5*, 3544–3561.

Dupont, J.; *J. Braz. Chem. Soc.* **2004**, *15*, 341–350.

Dzyuba, S. V.; Bartsch, R. A. *Tetrahedron Lett.* **2002**, *43*, 4657–4659.

Earle, M. J.; Esperanca, J. M. S. S.; Gilea, M. A.; Canongia Lopes, J. N.; Rebelo, L. P. N.; Magee, J. W.; Seddon, K. R.; Widegren, J. A. *Nature* **2006**, *439*, 831–834.

Earle, M.; McCormac, P. B.; Seddon, K. R. *Green Chem.* **1999**, *1*, 23–25.

Edward, J. T. *J. Chem. Educ.* **1970**, *47*, 261–270.

Edwards, E. W.; Chanana, M.; Wang, D.; Möhwald, H. *Angew. Chem. Int. Ed.* **2008**, *47*, 320–323.

Eftink, M. R.; Ghiron, C. A. *Anal. Biochem.* **1981**, *114*, 199–227.

Ehlich, D.; Sillescu, H. *Macromolecules* **1990**, *23*, 1600–1610.

Enache, D. I.; Edwards, J. K.; Landon, P.; Solsona-Espriu, B.; Carley, A. F.; Herzing, A. A.; Watanabe, M.; Kiely, C. J.; Knight, D. W.; Hutchings, G. J. *Science* **2006**, *311*, 362–365.

Florin, E.; Kjellander, R.; Eriksson, J. C. *J. Chem. Soc. Faraday Trans. 1* **1984**, *80*, 2889.

Foster, T. Dorfman, K. D.; Davis, H. T. *J. Colloid Interf. Sci.* **2010**, *351*, 140–150.

Fredlake, C. P.; Crosthwaite, J. M.; Hert, D. G.; Aki, S. N. V. K.; Brennecke, J. F. *J. Chem. Eng. Data* **2004**, *49*, 954–964.

Freire, M. G.; Carvalho, P. J.; Gardas, R. L.; Marrucho, I. M.; Santos, L. M. N. B. F.; Coutinho, J. A. P. *J. Phys. Chem. B* **2008**, *112*, 1604–1610.

Frick, T. S.; Huang, W. J.; Tirrell, M.; Lodge, T. P. *J. Polym. Sci. B Polym. Phys.***1990**, *28*, 2629–2649.

Frisken, B. J.; Asman, C.; Patty, P. J. *Langmuir* **2000**, *16*, 928–933.

Froba, A. P.; Kremer, H.; Leipertz, A. *J. Phys. Chem. B* **2008**, *112*, 12420–12430.

Garcia, B.; Lavallée, S.; Perron, G.; Michot, C.; Armand, M. *Electrochim. Acta* **2004**, *49*,

4583–4588.

Garcia, B.; Lavallée, S.; Perron, G.; Michot, C.; Armand, M. *Electrochim. Acta* **2004**, *49*, 4583–4588.

Geng, Y.; Ahmed, F.; Bhasin, N.; Discher, D. E. *J. Phys. Chem. B* **2005**, *109*, 3772–3779.

Geng, Y.; Dalhaimer, P.; Cai, S.; Tsai, R.; Tewari, M.; Minko, T.; Discher, D. E. *Nat. Nanotechnol.* **2007**, *2*, 249–255.

Geyer, U.; Johnson, W. L.; Schneider, S.; Qiu, Y.; Tombrello, T. A.; Macht, M.-P. *Appl. Phys. Lett*. **1996**, *69*, 2492–2494

Ghareh Bagh, F. S.; Mjalli, F. S.; Hashim, M. A.; Hadj-Kali, M. K. O.; Alnashef, I. M. *Ind. Eng. Chem. Res.* **2013**, *52*, 11488–11493.

Ghavre, M.; Morrissey, S.; Gathergood, N. *Ionic Liquids: Applications and Perspectives: Theory and Practice*; *Hydrogenation in Ionic Liquids*: InTech, 2011.

Gittins, D. I.; Caruso, F. *Angew. Chem. Int. Ed.* **2001**, *40*, 3001–3004.

Gonfa, G.; Bustam, M. A.; Man, Z.; Abdul Mutalib, M. I. *Asian Transactions on Engineering* **2011**, *1*, 24–34.

Gu, Y.; Cussler, E. L.; Lodge, T. P. *J. Membr. Sci.* **2012**, *423–424*, 20–26.

Guerrero-Sanchez, C.; Wouters, D.; Hoeppener, S.; Hoogenboom, R.; Schubert, U. S. *Soft Matter* **2011**, *7*, 3827–3831.

Hallet, J. P.; Welton, T. *Chem. Rev.* **2011**, *111*, 3508–3576.

Halpern, M. *Ullmann's Encyclopedia of Industrial Chemistry* **2000**, *26*, 495–501**.**

Hauschild, S.; Lipprandt, U.; Rumplecker, A.; Borchert, U.; Rank, A.; Schubert, R.; Föster, S. *Small* **2005**, *1*, 1177–1180.

He, Y.; Li, Z.; Simone, P. M.; Lodge, T. P. *J. Am. Chem. Soc.* **2006**, *128*, 2745–2750.

He, Y.; Li, Z.; Simone, P.; Lodge, T. P. *J. Am. Chem. Soc.* **2006**, *128*, 2745–2750.

He, Y.; Lodge, T. P. *J. Am. Chem. Soc.* **2006**, *128*, 12666–12667.

Heskins, M.; Guillet, J. E. *J. Macromol. Sci. A* **1968**, *2*, 1441–1455.

Hesse-Ertelt, S.; Heinze, T.; Kosan, B.; Schwikal, K.; Meister, F. *Macromol. Symp.* **2010**, *294*, 75–89.

Hiemenz, P. C.; Lodge, T. P. *Polymer Chemistry*; 2nd ed; CRC Press: Boca Raton, London, New York, 2007

Holowka, E. P.; Sun, V. Z.; Kamei, D. T.; Deming, T. J. *Nat. Mater.* **2007**, *6*, 52–57.

Hope, M. J.; Bally, M. B.; Webb, G.; Cullis, P. R. *Biochim. Biophys. Acta* **1985**, *812*, 55–65.

Horton, J. M.; Bai, Z.; Jiang, X.; Li, D.; Lodge, T. P.; Zhao, B. *Langmuir* **2011**, *27*, 2019–2027.

Huddleston, J. G.; Visser, A. E.; Reichert, W. M.; Willauer, H. D.; Broker, G. A.; Rogers, R. D. *Green Chem.* **2001**, *3*, 156–164

Hunter, D. G.; Frisken, B. J. *Biophys. J.* **1998**, *74*, 2996–3002.

Jain, S.; Bates, F. S. *Macromolecules*, **2004**, *37*, 1511–1523.

Jain, S.; Bates, F. S. *Science* **2003**, *300*, 460–464.

Jakes, J. *Collect. Czech. Chem. Commun.* **1995**, *60*, 1781–1797.

Jeong, Y.; Ryu, J.-S. *J. Org. Chem.* **2010**, *75*, 4183–4191.

Jiang, Y.; Xu, S.; Wang, C.; Shao, H.; Wang, Z.; Cui, Y. *J. Mater. Chem.* **2012**, *22*, 13469–13472.

Johnston, K. P; Haynes, C. *AIChE J.* **1987**, *33*, 2017–2026.

Kaintz, A.; Baker, G.; Benesi, A.; Maroncelli, M. *J. Phys. Chem. B* **2013**, *117*, 11697–11708.

Kang, Y.; Li, D.; Kalams, S. a.; Eid, J. E. *Biomed. Microdevices* **2008**, *10*, 243–249.

Kärger, J. *Adv. Colloid Interfac.* **1985**, *23*, 129–148.

Karlsson, M.; Davidson, M.; Karlsson, R.; Karlsson, A.; Bergenholtz, J.; Konkoli, Z.; Jesorka, A.; Lobovkina, T.; Hurtig, J.; Voinova, M.; Orwar, O. *Annu. Rev. Phys. Chem.* **2004**, *55*, 613–649.

Kesselman, E.; Talmon, Y.; Bang, J.; Abbas, S.; Li, Z.; Lodge, T. P. *Macromolecules* **2005**, *38*, 6779–6781.

Kim, K. T.; Cornelissen, J. J. L. M.; Nolte, R. J. M.; van Hest, J. C. M. *Adv. Mater.* **2009**, *21*, 2787–2791.

Kim, K. T.; Meeuwissen, S. A.; Nolte, R. J. M.; van Hest, J. C. M. *Nanoscale* **2010**, *2*, 844–858.

Kim, K. T.; Zhu, J.; Meeuwissen, S. A.; Cornelissen, J. J. M.; Pochan, D. J.; Nolte, R. J. M.; van Hest, J. C. M. *J. Am. Chem. Soc.* **2010**, *132*, 12522–12524.

Kisak, E. T.; Coldren, B.; Evans, C. A.; Boyer, C.; Zasadzinski, J. A. *Curr. Med. Chem.* **2004**, *11*, 199–219.

Kragl, U.; Eckstein, M.; Kaftzik, N. *Curr. Opin. Biotech.* **2002**, *13*, 565–571.

Krevelen, D. W. *Properties of Polymers*, 4th ed.; Elsevier: Solvonia, 2009.

Kuchel, P.W.; Chapman, B.E.; Bubb, W.A.; Hansen, P.E.; Durrant, C.J.; Hertzberg, M.P. *Concepts Magn. Reson.* **2003**, *18A*, 56–71.

Lan, Y.; Zhang, M.; Zhang, W.; Yang, L. *Chem. Eur. J.* **2009**, *15*, 3670–3673.

Le Meins, J.-F., Sandre, O.; Lecommandoux, S. *Eur. Phys. J. E* **2011**, *34*, 1–17.

Lecuyer, S.; Ristenpart, W. D.; Vincent, O.; Stone, H. A. *Appl. Phys. Lett.* **2008**, *92*, 92–94.

Lee, H.; Lee, J. S.; Ahn, B. S.; Kim, H. S. *J. Korean Ind. Eng. Chem.* **2005**, *16*, 595–602.

Lee, J. C. M.; Bermudez, H.; Discher, B. M.; Sheehan, M. A.; Won, Y. Y.; Bates, F. S.; Discher, D. E. *Biotechnol. Bioeng.* **2001**, *73*, 135–145.

Lee, S. H.; Lee, S. B. *Chem. Commun.* **2005**, 3469–3471.

Leson, A.; Hauschild, S.; Rank, A.; Neub, A.; Schubert, R.; Forster, S.; Mayer, C. *Small* **2007**, *3*, 1074–1083.

Leson, A.; Leson, A.; Hauschild, S.; Rank, A.; Neub, A.; Schubert, R.; Forster, S.; Mayer, C. *Small* **2007**, *3*, 1074–1083.

Li, D.; Dunlap, J. R.; Zhao, B. *Langmuir* **2008**, *24*, 5911–5918.

Li, D.; Zhao, B. *Langmuir* **2007**, *23*, 2208–2217.

Li, S.; Ge, Y.; Tiwari, A.; Cao, S. *Small* **2010**, *6*, 2453–2459.

Liao, C.; Chao, K.; Tsai, J. *IEEE J. Quantum Electron.* **2010**, *46*, 1268–1274.

Linders, J.; Mayer, C.; Sekine, T.; Hoffmann, H. *J. Phys. Chem. B* **2012**, *116*, 11459–11465.

Lipshutz, B. H.; Ghorai, S. *Green Chem.* **2014**, *16*, 3660–3679.

Lipshutz, B. H.; Ghorai, S. *Org. Lett.* **2009**, *11*, 705–708.

Lipshutz, B. H.; Ghorai, S.; Abela, A. R.; Moser, R.; Nishikata, T.; Duplais, C.; Krasovskiy, A. *J. Org. Chem.* **2011**, *76*, 4379–4391.

Lipshutz, B. H.; Isley, N. A.; Fennewald, J. C.; Slack, E. D. *Angew. Chem. Int. Ed.* **2013**, *52*, 10952–10958.

Lipshutz, B. H.; Taft, B. R. *Org. Lett.* **2008**, *10*, 1329–1332.

Liptay, W. *Angew. Chem.* **1969**, *81*, 161–188.

Liu, T.; Diemann, E.; Li, H.; Dress, A. W. M. *Nature* **2003**, *426*, 59–62.

Lodge, T. P. *Science* **2008**, *321*, 50–51.

LoPresti, C.; Lomas, H. Massignani, M.; Smart, T.; Battalia, G. *J. Mater. Chem.* **2009**, *19*, 3576–3590.

Loverdo, C.; Benichou, O.; Moreau, M.; Voituriez, R. *Nat. Phys.* **2008**, *4*, 134–137.

Lund, R.; Willner, L.; Richter, D.; Dormidontova, E. E. *Macromolcelus* **2006**, *39*, 4566–4575.

Luo, H. M.; Li, Y. Q.; Zheng, W. J. *Chinese Chem. Lett.* **2005**, *16*, 906–908.

Luo, L.; Eisenberg, A. *Langmuir* **2011**, *17*, 6804–6811.

Luthra, S. S.; Yang, X.; Livingston, A. G.; Freitas dos Santos, L. M.; White, L. S. *Chem. Commun.* **2001**, 1468–1469.

Mai, Y.; Eisenberg, A. *Chem. Soc. Rev.* **2012**, *41*, 5969–5985.

McEwen, A. B.; Ngo, H. L.; LeCompte, K.; Goldman, J. L. *J. Electrochem. Soc.* **1999**, *146*, 1687–1695.

McLachlan, F.; Mathews, C. J.; Smith, P. J.; Welton, T. *Organometallics* **2003**, *22*, 5350–5357.

Meeuwissen, S. A.; Kim, K. T.; Chen, Y.; Pochan, D. J.; van Hest, J. C. M. *Angew. Chem. Int. Ed.* **2011**, *50*, 7070–7073.

Meli, L.; Lodge, T. P. *Macromolecules* **2009**, *42*, 580–583

Meli, L.; Santiago, J. M.; Lodge, T. P. *Macromolecules* **2010**, *43*, 2018–2027.

Mendes, E.; Narayanan, J.; Oda, R.; Kern, F.; Candau, S. J.; Pascal, B.; Manohar, C. *J. Phys. Chem. B* **1997**, *101*, 2256–2258.

Meng, F.; Zhong, Z.; Feijen, J. *Biomacromolecules* **2009**, *10*, 197–209.

Metzger, J. O. *Angew. Chem. Int. Ed.* **1998**, *37*, 2975–2978.

Miletic, N.; Abetz, V.; Ebert, K.; Loos, K. *Macromol. Rapid. Commun.* **2010**, *31*, 71–74.

Mills, R. *J. Phys. Chem.* **1973**, *77*, 685–688.

Mok, M. M.; Lodge, T. P. *J. Polym. Sci. B Polym. Phys.***2012**, *50*, 500–515.

Moniruzzaman, M.; Kamiya, N.; Nakashima, K.; Goto, M. *Green Chem.* **2008**, *10*, 497–500.

Monteiro, M. J. *Macromolecules* **2010**, *43*, 1159–1168.

Mueller, W.; Koynov, K.; Fischer, K.; Hartmann, S.; Pierrat, S.; Basche, T.; Maskos, M. *Macromolecules* **2009**, *42*, 357–361.

Nagayasu, A.; Uchiyama, K.; Kiwada, H. *Adv. Drug Deliv. Rev.* **1999**, *40*, 75–87.

Napoli, A.; Valentini, M.; Tirelli, N.; Müller, M.; Hubbell, J. A. *Nat. Mater.* **2004**, *3*, 183–189.

Nardin, C.; Thoeni, S.; Widmer, J.; Winterhalter, M.; Meier, W. *Chem. Commun.* **2000**, 1433–1434.

Narkwiboonwong, P.; Tumcharern, G.; Potisatityuenyong, A.; Wacharasindhu, S.;

Sukwattanasinitt, M. *Talanta* **2011**, *83*, 872–878.

Nayar, R.; Hope, M. J.; Cullis, P. R. *Biochim. Biophys. Acta* **1989**, *986*, 200–206.

Noda, A.; Hayamizu, K.; Watanabe, M. *J. Phys. Chem. B* **2001**, *105*, 4603–4610.

Ochab-Marcinek, A.; Hołyst, R. *Soft Matter* **2011**, *7*, 7366–7374.

Odian, G. *Principles of Polymerization*; John Wiley & Sons: Hoboken, 2004.

Oliver-Bourbigou, H.; Magna, L.; Morvan, D. *Appl. Catal. A* **2010**, *373*, 1–56.

Orchilles, A. V.; Miguel, P. J.; Vercher, E.; Martinez-Andreu, A. *J. Chem. Eng. Data* **2008**, *53*, 2426–2431.

Ostafin, A.; Chen, Y.-C. *Kirk-Othmer Encyclopedia of Chemical Technology* **2009**, 1–18.

Ostafin, A.; Landfester, K. *Nanoreactor engineering for life sciences and medicine*; Artech House: MA, USA, 2009.

Ovalles, C.; Rogel, E.; Moir, M.; Thomas, L.; Pradhan, A. *Energy Fuels* **2012**, *26*, 549–556.

Palivan, C. G.; Fischer-Onaca, O.; Delcea, M.; Itel, F.; Meier, W. *Chemical Society Reviews* **2012**, *41*, 2800–2823.

Papaiconomou, N.; Yakelis, N.; Salminen, J.; Bergman, R.; Prausnitz, J. M. *J. Chem. Eng. Data* **2006**, *51*, 1389–1393.

Park, S.; Kazlauskas, R. J. *Curr. Opin. Biotech.* **2003**, *14*, 432–437.

Parshall, G. W. J. *Am. Chem. Soc.* **1972**, *94*, 8716–8719.

Patty, P. J.; Frisken, B. *Biophys. J.* **2003**, *85*, 996–1004.

Paula, S.; Volkov, A. G.; Deamer, D. W. *Biophys. J.* **1998**, *74*, 319–327.

Peng, J.; Shi, F.; Gu, Y.; Deng, Y. *Green Chem.* **2003**, *5*, 224–226.

Peng, L.; You, M.; Wu, C.; Han, D. Öçsoy, I.; Chen, T.; Chen, Z.; Tan, W. *ACS Nano* **2014**, 8, 2555–2561.

Pereiro, A. B.; Araújo, J. M. M.; Oliveira, F. S.; Esperança, J. M. S. S.; Canongia Lopes, J. N.; Marrucho, I. M.; Rebelo, L. P. N. *J. Chem. Thermodyn.* **2012**, *55*, 29–36.

Peters, R. J. R. W.; Marguet, M.; Marais, S.; Fraaije, M. W.; van Hest, J. C. M.; Lecommandoux, S. *Angew. Chem.* **2014**, *126*, 150–154.

Peters, R. J. R.; Louzao, I.; van Hest, J. C. M. *Chem. Sci.* **2012**, *3*, 335–342.

Plazek, D. J.; O'Rourke, V. M. *J. Polym. Sci. A–2 Polym. Phys.* **1971**, *9*, 209–243.

Popescu, M.-T.; Tasis, D.; Tsitsilianis, C. *ACS Macro Lett.* **2014**, *3*, 981–984.

Price, W. S. *Concept. Magn. Reson.* **1997**, *9*, 299–336.

Qin, B.; Zhao, Z.; Song, R.; Shanbhag, S.; Tang, Z. *Angew. Chem.* 2008, *120*, 10023–10026.

Rafelski, S. M.; Marshall, W. F. *Nature Review* **2008**, *9*, 593–602.

Raiford, D. S.; Fisk, C. L.; Becker, E. D. *Anal. Chem.* **1979**, *51*, 2050–2051.

Ramesh, N.; Davis, P. K.; Zielinski, J. M.; Danner, R. P.; Duda, J. L. *J. Polym. Sci. B Polym. Phys.***2011**, *49*, 1629–1644.

Rein, D. H.; Baddour, R. F.; Cohen, R. E. *J. Appl. Polym. Sci.* **1992**, *45*, 1223–1227.

Renggli, K.; Baumann, P.; Langowska, K.; Onaca, O.; Bruns, N.; Meier, W. *Adv. Funct. Mater.* **2011**, *21*, 1241–1259.

Renggli, K.; Baumann, P.; Langowska, K.; Onaca, O.; Bruns, N.; Meier, W. *Adv. Funct. Mater.* **2011**, *21*, 1241–1259.

Riisager, A. Wasserscheid, P. van Hal, R.; Fehmann, R. *J. Catal.* **2003**, *219*, 452–455.

Riisager, A.; Fehrmann, R.; Flicker, S.; van Hal, R.; Haumann, M.; Wasserscheid, P. *Angew. Chem. Int. Ed.* **2005**, *44*, 815–819.

Rivera-Rubero, S.; Baldelli, S. *J. Phys. Chem. B* **2006**, *110*, 15499–15505.

Rodríguez-García, R.; Mell, M.; López-Montero, I.; Netzel, J.; Hellweg, T.; Monroy, F. *Soft Matter* **2011**, *7*, 1532–1542.

Rodríguez-Hernández, J.; Lecommandoux, S. *J. Am. Chem. Soc.* **2005**, *127*, 2026–2027.

Rogers, R. D.; Seddon, K. R. *Science* **2003**, *302*, 792–793.

Rogers, R. D.; Willauer, H. D.; Griffin, S. T.; Huddleston, J. G. *J. Chromatogr. B Biomed.*

Sci. Appl. **1998**, *711*, 255–263.

Rumplecker, A.; Föster, S.; Zähres, M.; Mayer, C. *J. Chem. Phys.* **2004**, *120*, 8740–8747.

Sackmann, E. *FEBS Lett.* **1994,** *346*, 3–16.

Sanada, Y.; Akiba, I.; Sakurai, K.; Shiraishi, K.; Yokoyama, M.; Mylonas, E.; Ohta, N.; Yagi, N.; Shinohara, Y.; Amemiya, Y. *J. Am. Chem. Soc.* **2013**, *135*, 2574–2582.

Sanson, C.; Schatz, C.; Le Meins, J.-F.; Brûlet, A.; Soum, A.; Lecommandoux, S. *Langmuir* **2010**, *26*, 2751–2760.

Sarraute, S.; Gomes, M.; Pádua, A. *J. Chem. Eng. Data* **2009**, *54*, 2389–2394.

Sato, T.; Kijima, M.; Shiga, Y.; Yonezawa, Y. *Langmuir* **1991**, *7*, 2330–2335.

Schillen, K.; Brown, W.; Johnsen, R. M. *Macromolecules* **1994**, *27*, 4825–4832.

Schulze, M. W.; McIntosh, L. D., Hillmyer, M. A.; Lodge, T. P. *Nano Lett.* **2014**, *14*, 122–126.

Sekhon, B. S. *Asian J. Pharm. Biol. Res.* **2011**, *1*, 395–411.

Seo, Y. S.; Kim, M. W.; Ou-yang, D. H.; Peiffer, D. G. *Polymer* **2002**, *43*, 5629–5638.

Shannon, M. S.; Bara, J. E. *Ind. Eng. Chem. Res.* **2011**, *50*, 8665–8677.

Sharman, M.; Yashonath, S. *Diffusion Fundamentals* **2007**, *7*, 11.1–11.15.

Sheldon, R. *Chem. Commun.* **2001**, 2399–2407.

Shen, H.; Eisenberg, A. *J. Phys. Chem. B* **1999**, *103*, 9473–9487.

Shin, W. S. *News & information for chemical engineers* **2007**, *25*, 286–291.

Shum, H. C.; Kim, J.-W.; Weitz, D. A. *J. Am. Chem. Soc.* **2008**, *130*, 9543–9549.

Siano, D. B. *J. Chem. Educ.* **1972**, *49*, 755–757.

Simone, P. M.; Lodge, T. P. *Macromol. Chem. Phys.* **2007**, *208*, 339–348.

Simone, P. M.; Lodge, T. P. *Macromolecules* **2008**, *41*, 1753–1759.

Skibsted, U.; Hansen, P. E. *NMR Biomed.* **1990**, *3*, 248–258.

So, S.; Lodge, T. P. *J. Phys. Chem. C* **2014**, *118*, 21140–21147.

So, S.; Lodge, T. P. *Langmuir* **2015**, *31*, 594–601.

Soto-Figueroa, C.; Rodríguez-Hidalgo, M.-R.; Vicente, L. *Chem. Phys. Lett.* **2012**, *531*, 155–159.

Spitzer, M.; Sabadini, E.; Loh, W. *J. Braz. Chem. Soc.* **2002**, *13*, 7–9.

Spitzer, M.; Sabadini, E.; Loh, W. *J. Phys. Chem. B* **2002**, *106*, 12448–12452.

Spulber, M.; Baumann, P.; Saxer, S. S.; Pieles, U.; Meier, W.; Bruns. N. *Biomacromolecules* **2014**, *15*, 1469–1475.

Stano, P.; Luigi, P. *Reactions in Liposomes, in Molecular Encapsulation: Organic Reactions in Constrained Systems*; John Wiley & Sons, Ltd: Chichester, UK. 2010.

Starks, C. M. *J. Am. Chem. Soc.* **1971**, *93*, 196–199.

Stoimenovski, J.; MacFarlane, D. R. *Chem. Commun.* **2011**, *47*, 11429–11431.

Svaneborg, C.; Pedersen, J. S. *Macromolecules* **2002**, *35*, 1028–1037.

Thiele, J.; Chokkalingam, V.; Ma, S.; Wilson, D. A.; Huck, W. T. S. *Mater. Horiz.* **2014**, *1*, 96–101.

Thiele, J.; Steinhauser, D.; Pfohl, T.; Föster, S. *Langmuir* **2010**, *26*, 6860–6863.

Tian, H.; Chen, X.; Lin, H.; Deng, C.; Zhang, P.; Wei, Y.; Jing, X. *Chem. Eur. J.* **2006**, *12*, 4305–4312.

Tokuda, H.; Tsuzuki, S.; Susan, Md.; Hayamizu, K.; Watanabe, M. *J. Phys. Chem. B* **2006**, *110*, 19593–19600.

Tung, S.-H.; Lee, H.-Y.; Raghavan, S. R. *J. Am. Chem. Soc.* **2008**, *130*, 8813–8817.

Ud-Dean, S. M. M. *IET Nanobiotechnol.* **2009**, *3*, 65–70.

Ueki, T.; Sawamura, S.; Nakamura, Y.; Kitazawa, Y.; Kokubo, H.; Watanabe, M. *Langmuir* **2013**, *29*, 13661–13665.

Ueki, T.; Watanabe, M. *Chem. Lett.* **2006**, *35*, 964–965.

Ueki, T.; Watanabe, M. *Macromolecules* **2008**, *41*, 3739–3749.

Urbani, C. N.; Monteiro, M. J. *Macromolecules* **2009**, *42*, 3884–3886.

Wagner, A.; Vorauser-Uhl, K. *J. Drug Deliv.* **2011**, 591325.

Wang, H.; Yang, H.; Liu, H.; Yu, Y.; Xin, H. *Langmuir* **2013**, *29*, 6687–6696.

Wang, Y.; Leng, W.; Gao, Y.; Guo, J. *ACS Appl. Mater. Interfaces* **2014**, *6*, 4143–4148.

Wang, Z.; van Oers, M. C. M.; Rutjes, F. P. J. T.; van Hest, J. C. M. *Angew. Chem. Int. Ed.* **2012**, *51*, 10746–10750.

Wasserscheid, P.; Stark, A. *Handbook of Green Chemistry, Vol. 6, Ionic Liquids*; Wiley-VCH-Verlag: Weinheim, Germany, 2010.

Watanabe, K.; Takizawa, S.-Y.; Murata, S. *Chem. Lett.* **2011**, *40*, 345–347.

Wei, D.; Ivaska, A. *Anal. Chim. Acta.* **2008**, *607*, 126–135.

Welton, T. *Chem. Rev.* **1999**, *99*, 2071–2084.

Weng, G.; Bhalla, U. S.; Iyengar, R. *Science* **1999**, *284*, 92–96.

Wijmans, J. G.; Baker, R. W. *J. Membr. Sci.* **1995**, *107*, 1–21.

Wilkes, J. S.; Levisky, J. A.; Wilson, R. A.; Hussey, C. L. *Inorg. Chem.* **1982**, *21*, 1263–1264.

Williams, D. B.; Carter, C. B. *Transmission Electron Microscopy, Imaging III*; Plenum Press: New York, 1996.

Wilson, D. A; Nolte, R. J. M.; van Hest, J. C. M. *Nat. Chem.* **2012**, *4*, 268–274.

Wolfson, A.; Vankelecom, I. F. J.; Jacobs, P. A. *Tetrahedron Lett.* **2005**, *46*, 2513–2516.

Wong, B.; Boyer, C.; Steinbeck, C.; Peters, D.; Schmidt, J.; van Zanten, R.; Chmelka, B.; Zasadzinski, J. A. *Adv. Mater.* **2011**, *23*, 2320–2325.

Wong, B.; Boyer, C.; Steinbeck, C.; Peters, D.; Schmidt, J.; van Zanten, R.; Chmelka, B.;

Wu, D.; Chen, A.; Johnson, C. S. *J. Magn. Reson.* **1995**, *115*, 260–264.

Wu, J.; Eisenberg, A. *J. Am. Chem. Soc.* **2006**, *128*, 2880–2884.

Wu, Y.; Zhang, C.; Qu, X.; Liu, Z.; Yang, Z. *Langmuir* **2010**, *26*, 9442–9448.

Yang, J.; Lee, J. Y.; Ying, J. Y. *Chem. Soc. Rev.* **2011**, *40*, 1672–1696.

Yao, L.; Heubi, J. E.; Buckley, D. D.; Fierra, H.; Setchell, K. D. R.; Granholm, N. A; Tso, P.; Hui, D. Y.; Woollett, L. A. *J. Lipid Res.* **2002**, *43*, 654–660.

Yasuda, H.; Hirotsu, T. *J. Appl. Polym. Sci.* **1977**, *21*, 105–112.

Yow, H. N.; Routh, A. F. *Soft Matter* **2006**, *2*, 940–949.

Yu, K.; Zhang, L.; Eisenberg, A. *Langmuir* **1996**, *12*, 5980–5984.

Yu, S.; Azzam, T.; Rouiller, I.; Eisenberg, A. *J. Am. Chem. Soc.* **2009**, *131*, 10557–10566.

Yu, Y.; Zhang, L.; Eisenberg, A. *Macromolecules* **1998**, *31*, 1144–1154.

Zhang, L. F.; Eisenberg, A. *Polym. Adv. Technol.* **1998**, *9*, 677–699.

Zhang, M.; Wang, M.; He, S.; Qian, J.; Saffari, A.; Lee, A.; Kumar, S.; Hassan, Y.; Guenther, A.; Scholes, G.; Winnik, M. A. *Macromolecules* **2010**, *43*, 5066–5074.

Zhang, Q.; Wang, N.; Yu, Z. *J. Phys. Chem. B* **2010**, *114*, 4747–4754.

Zhang, Y.; Chen, X.; Lan, J.; You, J.; Chen, L. *Chem. Biol. Drug. Des.* **2009**, *74*, 282–288.

Zhou, Z.; Li, Z.; Ren, Y.; Hillmyer, M. A.; Lodge, T. P. *J. Am. Chem. Soc.* **2003**, *125*, 10182–10183.

Zuwei, X.; Ning, Z.; Yu, S.; Kunlan, L. *Science* **2001**, *292*, 1139–1141.

Appendix A

Exchange Rate of Poly(ethylene glycol) Through the Membranes of Ionic Liquid Filled Polymersomes Dispersed in Water

In Chapter 3, molecular exchange of the charged 1-ethyl-3-methylimidazolium ([EMIM]), 1-butyl-3-methylimidazolium ([BMIM]) and the neutral 1-butylimidazole through the bilayer membranes of nanoemulsion-like polymersomes was investigated by nuclear magnetic resonance spectroscopy (NMR) techniques. The bilayer membrane separates two immiscible fluids, namely water and the ionic liquid (IL). The exchange rate was investigated, both to and from the polymersome interiors. In Chapter 3, the molecular partitioning between the IL and water was not considered in comparing the exchange rate of the charged and neutral molecules, because the partitioning of the molecules are similar due to their similar chemical structure and molecular weight.

In general, however, the partitioning of molecules in a biphasic system is also an important parameter in addition to the molecular charge. For simple molecules such as gases and organic molecules, the permeability (p) of a membrane is a function of partition coefficient (H) (relative affinity of the molecules in the membrane to the solvent), diffusion coefficient (D), and the thickness of the membrane (d), as $p = HD/d$.[1] However, in order to elucidate the permeability of the polymersome membrane in different interior and exterior media, the partition coefficients at each interface (H_1 and H_2) should be considered. H_1 and H_2 are the partition coefficients of the molecules in the membrane to the IL, and the aqueous phase, respectively. Then, the permeability can be described in two different ways

as $p_1 = DH_1/d$ (from the interior to the aqueous medium) or $p_2 = DH_2/d$ (from the medium to the interior), and these two permeation values are equated with the partition coefficient of a tracer molecule, X ($K_P = [X]_{IL}/[X]_W = H_2/H_1$) in the biphasic system of water and IL as

$$p_1 = K_P p_2 . \quad \text{(A–1)}$$

Therefore, depending on the partitioning of molecule (K_P), the molecular permeation in one of the directions can be limited or accelerated, and in this chapter, the effect of partition coefficient on the permeation rate was investigated and compared with the results in Chapter 3.

1,2-Polybutadiene-*b*-poly(ethylene oxide) block copolymers having M_n = 9.3 kg/mol of PB and M_n = 2.5 kg/mol of PEO (PB–PEO(9–3)) were synthesized via sequential anionic polymerization. Then, PB–PEO(9–3) polymersomes in the IL, 1-ethyl-3-methyl imidazolium bis(trifluoromethylsulfonyl)imide ([EMIM][TFSI]), were prepared through the co-solvent method. By adding D_2O to the IL solution, the polymersomes with IL interiors transferred to the top aqueous phase. For the permeation study, the aqueous phase was selectively separated, and 50 mM of 200 g/mol of α- and ω-hydroxyl terminated poly(ethylene glycol) (PEG), which has similar molecular weight with [EMIM] (112 g/mol) and 1-butylimidazole (124 g/mol), was added to the solution. A Bruker Avance III 500 MHz NMR spectrometer equipped with a 5 mm Triple Resonance Broad Band (TBO) PFG probe was used for both ^{1}H NMR spectroscopy and Pulsed-Field-Gradient NMR (PFG-NMR) at 25 °C. For all PFG-NMR measurements, DOSY (Diffusion-Ordered Spectroscopy) with ^{1}H nuclei was used with the "ledbpgp2s" or "ledbpgp1s" pulse sequence (longitudinal eddy current delay experiment using bipolar gradients acquired in 2D, and 1D mode, respectively).[2] Since PEG shows the opposite partitioning behavior to

1-butylimidazole, it was selected as a tracer molecule. As shown in Figure A–1a, after contacting the IL, most of the 1-butylimidazole transferred to the IL, whereas PEG molecules stayed in the aqueous phase, as in Figure A–1b. K_P from the spectra are 13 and 0.45 for 1-butylimidazole and PEG, respectively. Therefore, at equilibrium, PEG prefers to stay in the aqueous phase, but 1-butylimidazole prefers the IL to water.

Figure A–2 shows the ^{1}H NMR spectra of PEG in IL-saturated D_2O. Proton signals from [EMIM] and PEG can be seen. Protons of [EMIM] are assigned from a to f. The CH_2 protons signal of the central part of PEO are around 3.65 ppm, and the CH_2 protons signal adjacent to the terminal hydroxyl groups are between 3.5 and 3.6 ppm. The signal from the solvent is at 4.7 ppm from the protons of H_2O and HDO.

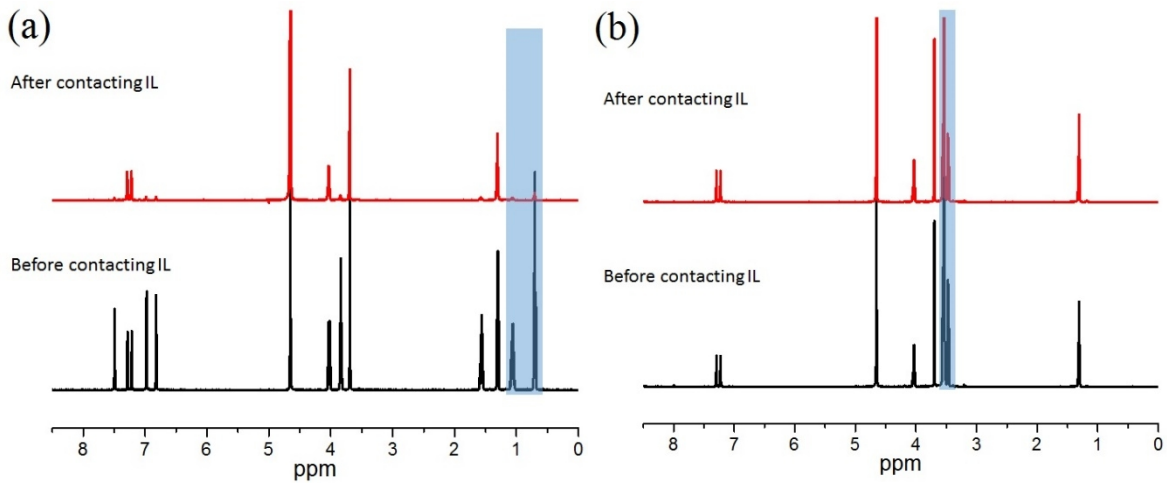

Figure A–1. ^{1}H NMR spectra of the aqueous phase with 50 mM of (a) 1-butylimidazole and (b) poly(ethylene glycol) (M_n = 200 g/mol) before and after contacting an equal volume of [EMIM][TFSI]. Highlighted region represent the representative peaks for (a) 1-butylimidazaole and (b) poly(ethylene glycol) (see Chapter 3 for the other peaks).

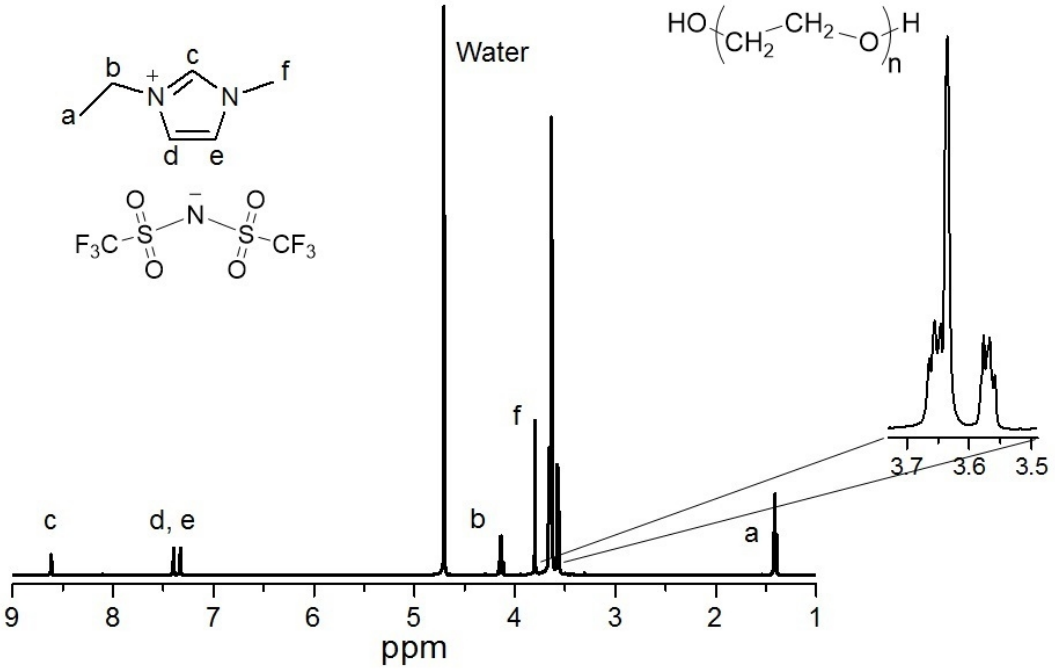

Figure A–2. ^{1}H NMR spectra of poly(ethylene glycol) in [EMIM][TFSI] saturated D_2O.

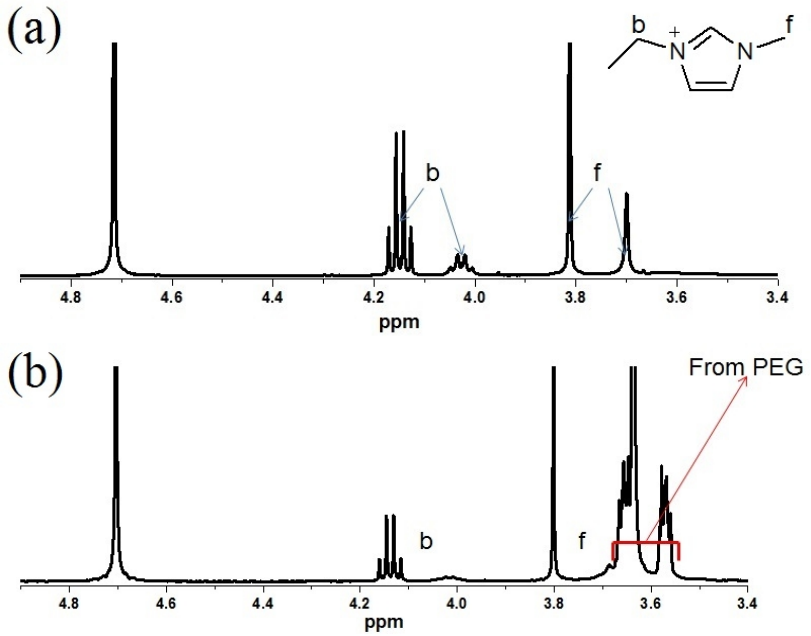

Figure A–3. ^{1}H NMR spectra of (a) IL-saturated D_2O in the presence of PB–PEO(9–3) having IL interiors and (b) poly(ethylene glycol) in the polymersome aqueous solution.

The chemical shift of ^{1}H NMR spectra in the IL domains is different within the homogeneous medium due to the magnetic susceptibility difference across the polymersome membranes (the details of the effect of magnetic susceptibility were described in Chapter 3).[3,4] As shown in Figure A–3a, there are two different sets of peaks in the presence of the PB–PEO(9–3) polymersomes. When imidazole derivatives, such as [EMIM], [BMIM], 1-butylimidazole are in the IL domains, the peaks appear slightly upfield compared to the peaks from the aqueous medium.[5] However, in the case of non-imidazole derivatives, PEG and water, their chemical shift is identical regardless of the presence of the polymersomes as shown in Figure A–3b. From ^{1}H NMR spectroscopy, the presence of polymersomes having the IL interiors can be identified, but the permeation of PEG cannot be seen due to the identical chemical shift of PEG in the IL and D_2O, unlike [BMIM] or 1-butylimidazole. K_p of PEG is less than 1, so this lower solubility in the IL can be an energy barrier to prevent the permeation of PEG into the IL interiors. Therefore, it is important to prove that PEG molecules are permeable under the condition of $K_p < 1$.

The presence of PEG molecules in the polymersome interiors was shown through PFG-NMR. In the pulse sequence of PFG-NMR experiment, the gradient strength (G) of the field gradient pulse was varied from 2% to 98% of the maximum G, 0.47 T/m, for a duration (δ). Between the two gradient pulses, there is a diffusion time (Δ) for the translation diffusion (D) of the tracer molecules. Then, the intensity (I) of detectable nuclei attenuates with time as shown in Figure A–4. The attenuation can be expressed as

$$\frac{I}{I_0} = \exp(-\gamma^2\delta^2G^2(\Delta - \delta/3)), \qquad \text{(A–2)}$$

where I_0 is peak intensity at $G = 0$, and γ is the proton gyromagnetic ratio (42.6 MHz/T), and D can be evaluated by fitting the intensity evolution with eqn A1–2.[6] The normalized attenuated intensity of PEG in the IL saturated D_2O is on the single line with various Δ, δ

as shown in Figure A–5, and D of PEG in D_2O from the fitting is 4.1×10^{-10} m^2/s. In Figure A–2, there is only one set of [EMIM] protons indicating no aggregation of the IL. These results clearly show that there is no diffusion barrier of PEG when the polymersomes are not present. However, with the polymersome having PEG molecules inside after the permeation or on the polymersome surface, there should be restricted diffusion behavior of PEG, which is much slower than the motion of free PEG molecules in water.[7] For a long enough diffusion time Δ, the diffusivity of PEG in or on the polymersomes is same as the diffusivity of polymersomes or micelles,[8] and can be obtained from the final slope of a PFG-NMR decay curve,[9] which is different to the initial decay of free PEG, whereas without polymersomes, I/I_0 decays rapidly and reaches the noise level around 0.

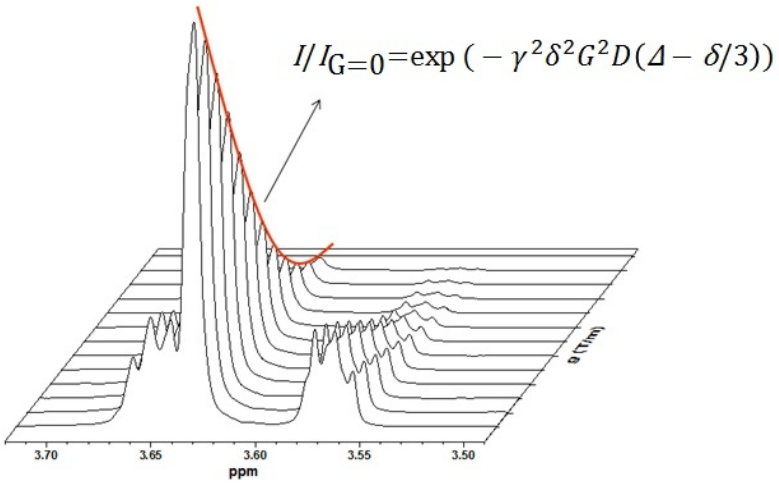

Figure A–4. 3–dimensional NMR spectra of PEG protons in [EMIM][TFSI] saturated D_2O at different gradient strength. The red line represents the intensity attenuation, and D can be evaluated by fitting with the eqn A–2.

In order to prove the permeation of PEG and the presence of adsorbed PEG molecules, four different samples were prepared: a PEG solution in D_2O, a micelle solution of PB–PEO(14–4.5) with PEG in D_2O, and two polymersome solutions with PEG in D_2O. But PEG was added to the polymersome solution in two different ways. For one sample, PEG was added to the aqueous polymersome solution, but for the other sample, PEG was loaded

during the polymersome formation process in the IL, then the PEG encapsulated polymersomes were transferred to the aqueous phase. PEG can be located in three different regions; in the medium (region A), in the interior (region B), and on the outer interface (region C), as shown in Figure A–6. As shown in Figure A–7, in micelle solution, there is no interior cargo like polymersomes. PB forms the core block, and the PEO block is solvated in the IL. So, PEG can be only in the medium (region A) or on the micelle surface (region C), but there are no IL domains. DOSY experiments were conducted under same time constants for all samples, Δ = 100 ms, δ = 8ms at 30, 50, 90 and 98% of the maximum G. At high gradient strength, the intensity is mainly affected by confined PEG, because its mobility is restricted, and slower than the free PEG molecules, but at low gradient strength the intensity attenuation is mainly from the diffusion of free PEG. The peak intensity of PEG at each G was compared to the intensity from ^{1}H NMR with 30° pulse when G = 0 T/m, and summarized in Figure A–8. The intensity of PEG in the micelle solution decreases rapidly and reaches close to 0 as the gradient strength increases, and shows the same trend with the PEG solution without any micelles and polymersomes. This result indicates that PEG molecules are freely dispersed in the medium rather than adsorbed on the micelle surface. If PEG molecules are not permeable through the PB membrane, the intensity of PEG post-added solution should show the similar decay of the micelle solution. However, with the polymersomes, both PEG pre- and post-added solutions show a similar trend, and the normalized intensity decays slowly and reaches to a certain value around 0.1 as can be seen in Figure A–8. From the PFG-NMR analysis with the equilibrated solutions at different gradient strength, we conclude that PEG molecules could permeate into the IL domains through the PB membrane even under the condition of $K_p < 1$.

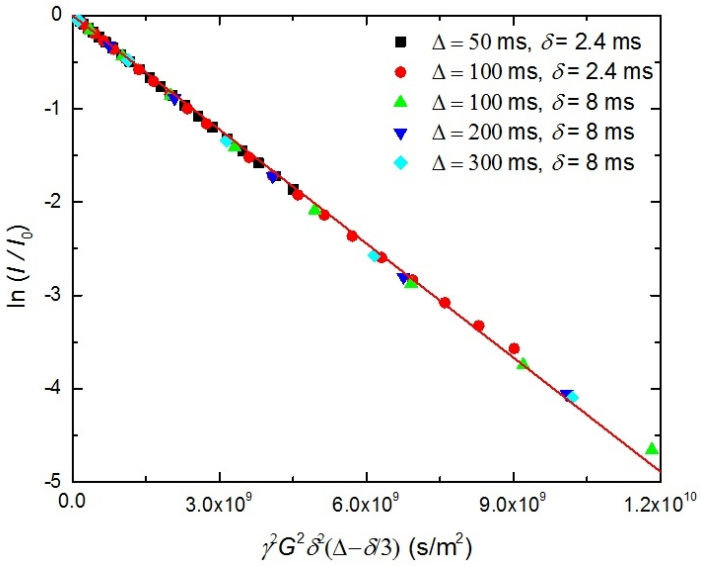

Figure A–5. The echo decay curve of 50 mM PEG in [EMIM][TFSI] saturated D_2O under variation of the field gradient strength G for different diffusion time Δ and δ.

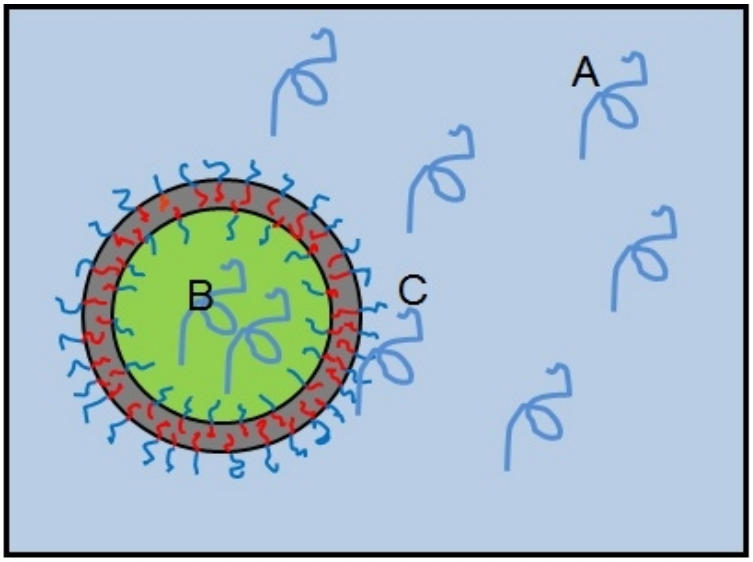

Figure A–6. Schematic illustration of possible locations of PEG chains in the polymersome solution. In region A, PEG is well dispersed in water. In region B, PEG chains are encapsulated in the polymersome interiors, and in region C, PEG chains are adsorbed on the polymersome surface.

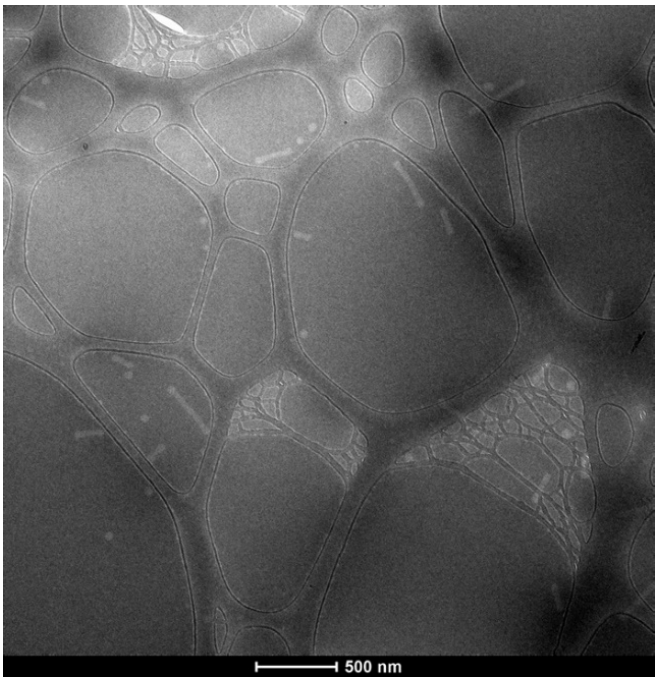

Figure A–7. Cryo-TEM image of PB–PEO(14–4.5) micelles in [EMIM][TFSI]. Bright domains represent PB core, and dark medium is the IL. The solvated PEO block cannot be seen in here. Scale bar: 500 nm.

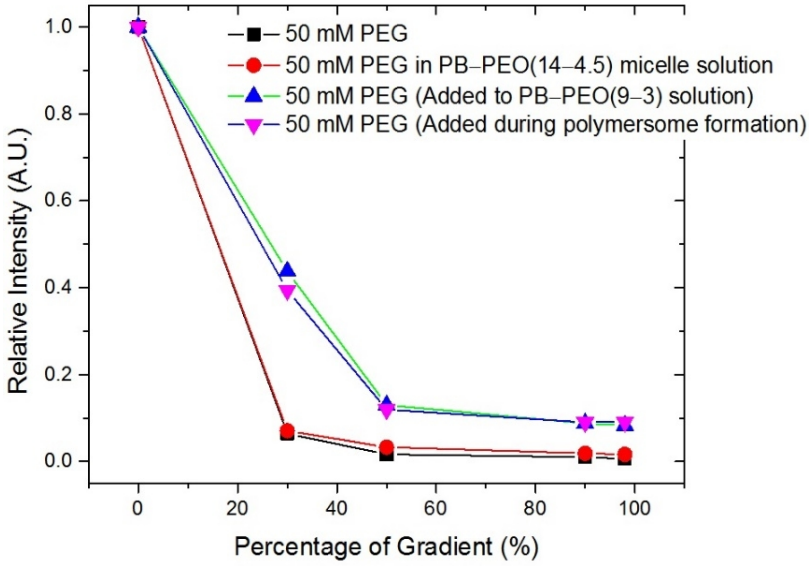

Figure A–8. Relative intensity of PEG protons at different field gradient strength, G, 30, 50, 90 and 98% of the maximum G (0.47 T/m). The DOSY experiment was conducted with the equilibrated samples with Δ = 100 ms and δ = 8ms. The intensity at 0% was from the typical ^{1}H NMR with 30° pulse.

Through the PFG-NMR experiment with PEG in four different system, it has been proven that water favorable PEG is permeable across the hydrophobic PB membrane from the aqueous phase to the IL phase. With 50 mM of PEG in PB–PEO(9–3) polymersome solution, DOSY experiments were conducted and the echo decay curves were obtained at different Δ (150, 250, 350 ms) with constant δ = 8 ms, as shown in Figure A–9. Since PEG can permeate across the polymersome membranes, the signal decay can be fitted with the two-site model described in eqn 3–4. Two apparent diffusion coefficients (D_i and D_e, which are diffusion coefficient in the interiors and exterior of polymersomes, respectively) were obtained from the initial and final slopes of the decays. D_e is 4.1×10^{-10} m^2/s, the same as the free diffusion in water, and D_i is 2.1×10^{-12} m^2/s, which is polymersome size related value and similar to that in the diffusion experiment of 1-butylimidazole and [EMIM]. According to the Stokes-Einstein equation, the hydrodynamic radius (R) of PEG and the polymersomes can be evaluated as R_{PEG} = 0.48 nm and $R_{polymersome}$ = 94 nm, respectively. From the fitting with the two-site model, the results are in Table A–1, and compared to the values of [EMIM] and 1-butylimidazole. D_i is similar to the other cases, because the apparent value, D_i is same as the size of polymersomes during long enough Δ, as discussed in Chapter 3. The population of PEG in the polymersome interiors, P_i, is 0.016 (± 0.004), and the residence time in the polymersome inside (τ_i) and outside (τ_e) are 0.3 s (± 0.1 s) and 21.9 s (± 9.0 s). At the equilibrium, water favorable PEG preferentially remains in the aqueous phase, and the permeation rate ($1/\tau$) is different than 1-butylimidazole. The rate of escape ($1/\tau_i$, Path 1 in Scheme 3–1) is close to that of neutral 1-butylimidazole, at 2.9 s^{-1}. However, the rate of entry ($1/\tau_i$, Path 2 in Scheme 3–1) is much lower than 1-butylimidazole, but similarly slow as charged [EMIM] at 0.05 s^{-1}, even though PEG does not have any molecular charge. To have relation between the exchange rate and the partitioning of tracer molecules, the experiment with the molecule having K_P = 1 is necessary, but with the comparison between two different molecules having opposite

partitioning behavior, it can be concluded that the partition coefficient is an important factor for the permeation rate in addition to the molecular charge.

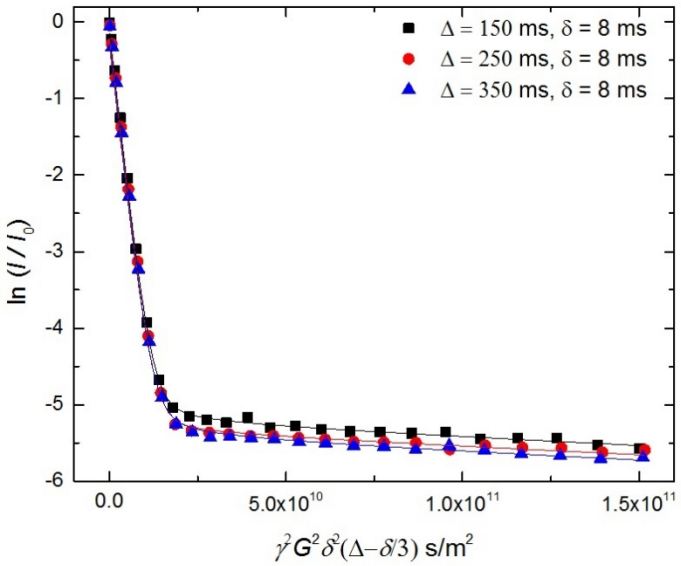

Figure A–9. Experimental data and fitted echo curve of the PEG protons in PB–PEO(9–3) polymersome solution with various *Δ*. The data were fitted using eqn 3–4. The PEG concentration was 50 mM, and the experimental temperature was 25 °C.

Table A–1. Permeation rate with two-site exchange model.

Diffuser	D_e (m^2/s)	D_i (m^2/s)	P_i	P_e	$1/\tau_i$ (1/s)	$1/\tau_e$ (1/s)
[EMIM]	7.8×10^{-10}	2.1×10^{-12}	0.20	0.80	0.17	0.04
1-Butylimidazole	5.8×10^{-10}	2.2×10^{-12}	0.07	0.93	2.5	0.18
PEG	4.1×10^{-10}	2.1×10^{-12}	0.01_6	0.99_4	2.9	0.05

In this chapter, the water favorable molecule, PEG was employed to see the effect of partitioning in the nanoemulsion-like polymersome system having two immiscible fluids. The permeability of PEG was confirmed by the combination of ^{1}H NMR and PFG-NMR techniques, then DOSY experiment was conducted to see the entry and escape rate

depending on the permeation direction. The permeation rate depending on the direction was significantly affected by partitioning of molecules in IL to water. Relatively small and neutral molecule PEG showed the fast permeation as 1-butylimidazole when the molecules permeate from the IL domains to the aqueous phase, but in the other direction, the entry rate was slow as the charged [EMIM]. This permeation study depending on the partition coefficient of molecule in two different solvents will inform the design of a nanoreactor system.

References

1. Cussler, E. L. *Diffusion*, 3rd ed; Cambridge University Press, New York, 2009.
2. Wu, D.; Chen, A.; Johnson, C. S. *J. Magn. Reson.* **1995**, *115*, 260–264.
3. Kuchel, P.W.; Chapman, B.E.; Bubb, W.A.; Hansen, P.E.; Durrant, C.J.; Hertzberg, M.P. *Concepts Magn. Reson.* **2003**, *18A*, 56–71.
4. Skibsted, U.; Hansen, P. E. *NMR Biomed.* **1990**, *3*, 248–258.
5. So, S.; Lodge, T. P. *J. Phys. Chem. C* **2014**, *118*, 21140–21147.
6. Price, W. S. *Concept. Magn. Reson.* **1997**, *9*, 299–336.
7. Linders, J.; Mayer, C.; Sekine, T.; Hoffmann, H. *J. Phys. Chem. B* **2012**, *116*, 11459–11465.
8. Ochab-Marcinek, A.; Hołyst, R. *Soft Matter* **2011**, *7*, 7366–7374.
9. Kärger, J. *Adv. Colloid Interfac.* **1985**, *23*, 129–148.

Appendix B

Modifications in Polymersome Membrane-forming Block for Permeability Control

The bilayer core membrane is the key part of the polymersome nanoreactors in terms of permeability and selectivity of molecules for reactions. As described in Appendix A, permeability (p) is a function of diffusion coefficient (D), partition coefficient (H) of diffuser, and membrane thickness (d), as shown by the equation, $p = DH/d$. One way for permeability tuning is controlling membrane fluidity, which is defined as the inverse viscosity of the bilayer membranes, to change the diffusivity of the penetrating molecules (D).[1] Lower fluidity corresponds to lower permeability. For example, Yu *et al.* reported pH-sensitive sandwiched membranes from triblock polymers composed of polystyrene (PS), poly(2-diethylaminoethyl methacrylate) (PDEA) and poly(ethylene oxide) (PEO).[2] The protonation of amino groups on PDEA block by pH change from 7.94 to 6.98 induced the change of size, which introduced swollen paths through the sandwiched layers, and then the permeability of protons from the outer medium was accelerated by three orders of magnitude. Another way for the permeability control by D is formation of physical defect for the permeation through the pores in the membrane. For instance, Kim *et al.* embedded stimuli-responsive boronic acid-containing block copolymers into the polymersomes of the PS–PEO, and by the removal of selectively soluble embedded boronic acid-containing block copolymers at high pH, increased the transportation rate of 6,8-difluoro-4-methylumbelliferyl octanoate.[3]

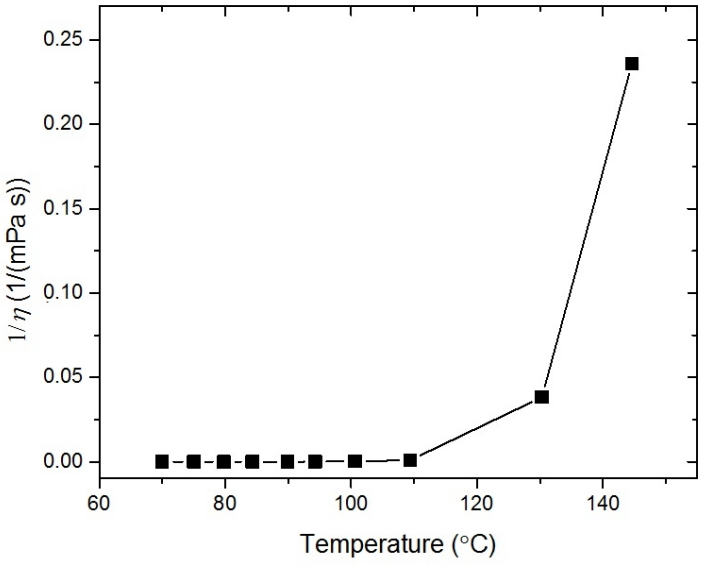

Figure B–1. Inverse viscosity ($1/\eta$) of PS (M_n = 3400 g/mol) versus temperature. (Data described in reference 5).

To control the fluidity of the membrane core, the choice of the core block with proper glass transition temperature (T_g) is a possible approach.[4] The fluidity of the membrane (~ $1/\eta$) will increase significantly above T_g. For example, the inverse viscosity ($1/\eta$) of PS showed an abrupt increase at 100 °C (see Figure B–1).[5] This temperature-induced fluidity change can provide advantages for the polymersome nanoreactor system. First, the permeability of the membrane can be controlled by temperature, since the permeability depends on the state of the membrane between glassy and rubbery limits. Second, if T_g is higher than the polymersome transfer temperature (T_t) of the polymersomes, which is around 75 °C for PB–PEO and PS–PEO polymersomes (see Chapter 1 for more details about T_t and polymersome shuttle process), the inner compartment of the polymersomes will be protected by the glassy membranes while the polymersomes move to the aqueous phase below the T_g of the membrane. However, block copolymers with T_g of the membrane blocks close to the boiling point of water (100 °C) in the biphasic system are presumably not suitable. It would be possible to use a membrane with a T_g range of 25 °C < T_g < 100 °C. For bulk polymer membrane, a good candidate is a random copolymer of glassy and

rubbery polymers for the T_g range above. But in dilute micelle solution, it has been shown that T_g of PS block itself in PS–PEO spherical micelles is lower than the bulk T_g because the PS core is in nanometer scale and some level of solvent can contribute to reduce T_g.[6] In this result, the onset glass transition temperature was around 45 °C for PS–PEO micelles having 20 kg/mol PS block, whereas the bulk T_g is around 100 °C.

The change of membrane fluidity and porosity can be controlled as described above. The porosity control can enhance the molecular transportation, but leads to leakage of the interior liquid and active species. Therefore, in this chapter, the preliminary result for the fluidity control approach is discussed with four different PS–PEO block polymers, which are expected to have the membrane T_g in the desirable range, 25 °C < T_g < 100 °C

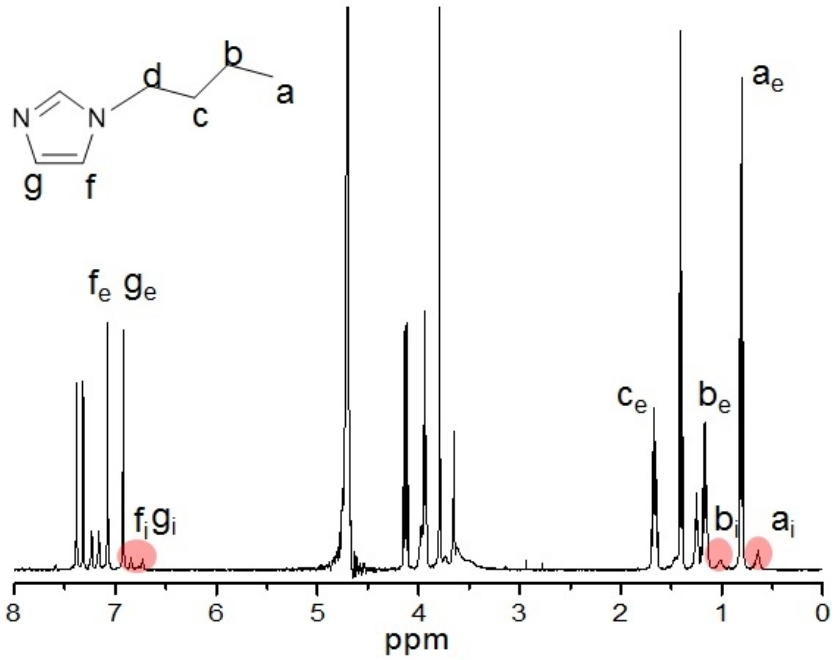

Figure B–2. Chemical structure of 1-butylimidazole, and ^{1}H NMR spectrum of 1-butylimidazole solution with PS–PEO(14–2.5) polymersome. As with [EMIM], [BMIM] shows also two sets of chemical shifts. However, many of peaks of 1-butylimidazole are not completely distinguishable due to similar chemical structure with [EMIM].

PS–PEO block polymers, PS–PEO(10–2), PS–PEO(14–2.5), PS–PEO(18–3.6), and PS–PEO(27–4) were synthesized via anionic polymerization, and the characteristics of the polymers were listed in Table 4–1. Polymersomes were prepared through the co-solvent method, as described before in Chapter 2. The final polymer concentration in the ionic liquid (IL), 1-ethyl-3-methylimidazolium bis(trifluoromethylsulfonyl)imide ([EMIM][TFSI]) was 0.5 wt %. The polymersomes were transferred to the aqueous phase with gentle stirring after adding the equal volume of D_2O to the IL solution, and the aqueous phase was taken for the permeability study. ^{1}H NMR spectroscopy and pulsed-field-gradient NMR (PFG-NMR) were used to identify the rate of exchange through the PS membranes with a Bruker Avance III 500 MHz NMR spectrometer.

In Chapter 3 and Appendix A, imidazole derivatives, such as [EMIM], 1-butyl-3-methylimidazolium ([BMIM]) and 1-butylimidazole show two sets of proton peaks in aqueous solution in the presence of the PB–PEO polymersomes having IL domains. This chemical shift, due to the magnetic susceptibility difference, can show the permeation of the molecules through the membranes directly with ^{1}H NMR spectroscopy. Figure B–2 is a ^{1}H NMR spectrum of 1-butylimidazole in PS–PEO(14–2.5) polymersome solution. Similar to the case of PB–PEO, in the presence of PS–PEO(14–2.5) polymersomes having glassy PS membranes, 1-butylimidazole also shows the shifted proton peaks slightly upfield when it is in the IL interior. The distinguishable peaks are assigned in the spectrum, Figure B–2. For example, "a_e", "a_i" represent protons at "a" position in the exterior and interiors of the polymersomes, respectively. Two sets of peaks could also be found in other PS–PEO cases. Through the ^{1}H NMR spectroscopy of 1-butylimidazole with the polymersomes, the permeation of 1-butylimidazole through the glassy PS membrane was simply demonstrated.

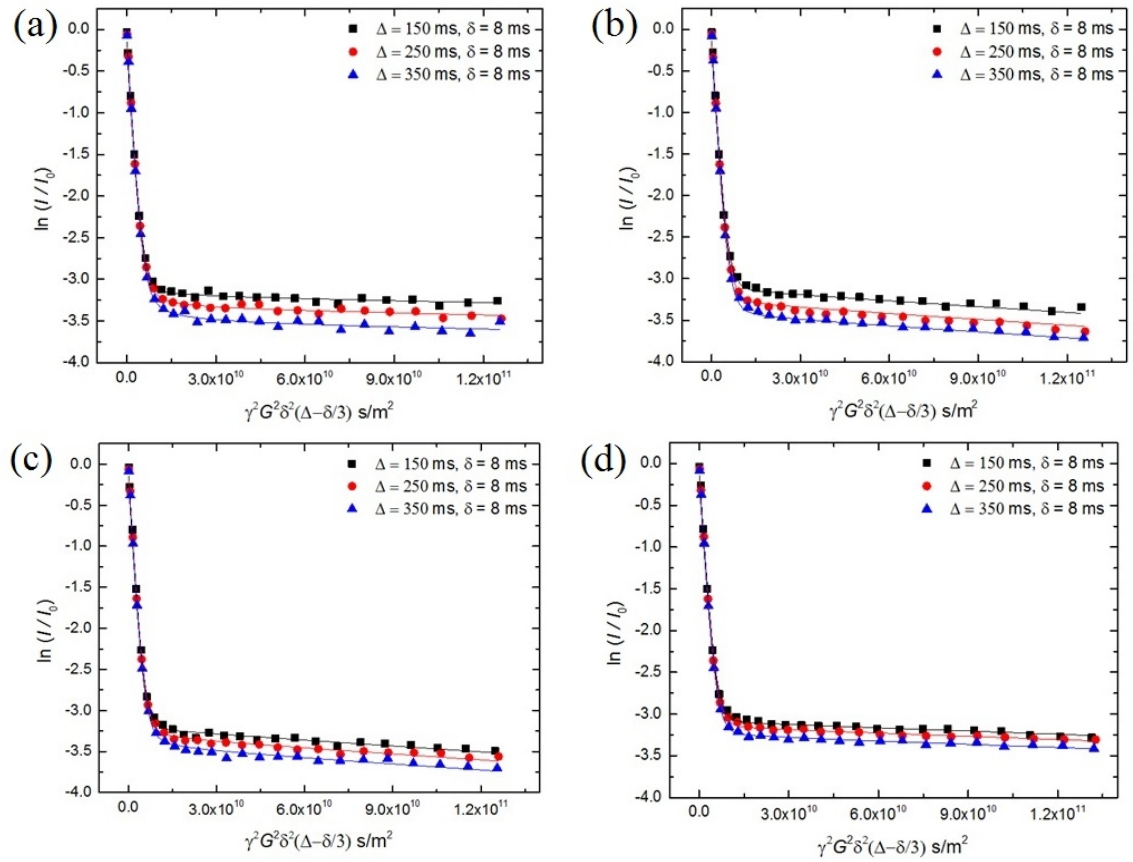

Figure B–3. Experimental data at 25 °C and fitted echo curve of the proton from 1-butylimidazole in the polymersome solution of (a) PS–PEO(10–2), (b) PS–PEO(14–3), (c) PS–PEO(18–3.6), and (d) PS–PEO(27–4) with Δ = 150, 250, 350 ms and fixed δ = 8 ms. The data were fitted using two-site exchange model.

The PFG-NMR technique DOSY (Diffusion-Ordered Spectroscopy) with the "ledbpgp2s" pulse sequence (longitudinal eddy current delay experiment using bipolar gradients acquired in 2D)[7] was used to investigate permeability changes with temperature and polymersome membrane thickness. For the NMR study, 50 mM 1-butylimidazole was added to the aqueous solution as the tracer molecule. The temperature was increased by 10 °C from 25 °C to 65 °C, and at each temperature, the NMR samples were equilibrated for at least for 30 min. The actual temperature was calibrated with the chemical shift difference between ^{1}H on -OH and -CH_2- of ethylene glycol.[8] The actual temperatures of the samples were 25 °C, 36 °C, 47 °C, 58 °C, and 69 °C. The DOSY experiments were conducted with

Δ = 150, 250 and 350 ms, and δ = 8 ms at 25 °C. At higher temperatures, however, δ was changed to 6, 4 or 3 ms to limit the measurement in the shorter range of $-\gamma^2\delta^2G^2(\Delta - \delta/3)$, where the intensity is not attenuated completely.

Figure B–3 shows echo-decays of both peaks from interiors and exteriors ("a_e", "a_i") of 1-butylimidazole at 25 °C. As expected, the difference of the final plateaus with PS–PEO polymersomes between Δ = 150 and 350 ms is much less compared to the case with PB–PEO(9–3) polymersomes having rubbery PB membranes (Figure 3–11b). With increased diffusion time Δ, the intensity contributed by the molecules in the confined polymersomes decreases. The intensity decreases as the molecules exchange more rapidly.[9] This suggests that molecular exchange is limited by the glassy PS membranes, and the diffusion barrier, which is related to the fluidity of the membrane, is the main contribution for slower exchange, given the solubility parameters of PS (δ_{PS}), PB (δ_{PB}), and 1-butylimidazole (δ_{BIm}), 18.6 $MPa^{1/2}$, 17.1 $MPa^{1/2}$, and 21 $MPa^{1/2}$, respectively.[10,11]

Using the two-site exchange model described in Chapter 3, the echo-decay curves were fitted as shown in Figure B–3, and the fitting results are summarized, and compared to PB–PEO(9–3) in Table B–1. It is known that the size of polymersome also affects the permeability. Leson *et al.* demonstrated that the exchange rate (s^{-1}) decreases with the vesicle size, however the effect was significant only for vesicles with hydrodynamic radius (R_h) smaller than 60 nm.[12] The vesicle size can be obtained by using the Stokes-Einstein equation and D_i values, which represent the diffusion coefficient of polymersome. The average R_h is around 100 nm, except for PS–PEO(10–2) (R_h ~ 330 nm) and PS–PEO(27–4) (R_h ~ 190 nm). For the precise comparison of the permeation rate ($1/\tau_i$: escape, $1/\tau_e$: entry), the polymersome size should be the same, but the result of the d dependent $1/\tau_i$ would not be changed because PS–PEO(10–2) would have a higher permeation rate when R_h is smaller.

As PS length increases, the membrane thickness (d) also increases (Figure 4–6), and both the escape and entry rates of 1-butylimidazole decrease. Membrane thickness dependent permeability has been observed in other polymer vesicles, such as PB–PEO,[13] poly(2-vinylpyridine)-*b*-poly(ethylene oxide),[12] and a series of poly(ethylene oxide)-*b*-poly(butylene oxide).[14] Even though there is no universal relationship between the p and d, p decreases as d increases. From the plot of $1/\tau_i$ versus $1/d$ in Figure B–4b, $1/\tau_i$ is proportional to $1/d$ indicating that the permeability of the polymersome membrane is a strong function of the membrane thickness.

Table B–1. Permeation rate with two-site exchange model.

Polymer	D_e (m^2/s)[a]	D_i (m^2/s)[a]	P_i[b]	P_e[b]	$1/\tau_i$ (1/s)[c]	$1/\tau_e$ (1/s)[c]
PS–PEO(10–2)	6.1×10^{-10}	7.2×10^{-13}	0.09	0.91	1.5	0.14
PS–PEO(14–2.5)	6.1×10^{-10}	2.1×10^{-12}	0.08	0.92	1.0	0.09
PS–PEO(18–3.6)	6.1×10^{-10}	2.4×10^{-12}	0.07	0.93	0.7	0.06
PS–PEO(27–4)	6.0×10^{-10}	1.3×10^{-12}	0.08	0.92	0.3	0.02
PB–PEO(9–3)	5.8×10^{-10}	2.2×10^{-12}	0.07	0.93	2.5	0.18

[a] D_e and D_i represent the diffusion coefficient (m^2/s) of a tracer molecule in the external aqueous medium and in the interiors of polymersomes, respectively. [b] P_i and P_e stand for the mole fraction of probe molecules in the encapsulated and free space ($P_i + P_e = 1$). [c] τ_i and τ_e are the residence time at each phase, and the inverse of the residence times represent the rate of escape ($1/\tau_i$) and entry ($1/\tau_e$), respectively.

It is of interest to compare the exchange rate through the glassy PS with the rubbery PB. As expected from Figure B–3 and Figure 3–10b, 1-butylimidazole exchange through glassy membrane is slower than through rubbery membrane. Especially, as shown in Figure B–4a, under the same membrane thickness, d = 21 nm (PS–PEO(18–3.6) and PB–PEO(9–3)), the exchange rate was about 3 – 4 times slower through the PS membrane at 25 °C.

For comparison, Rein and co-workers measured the permeability of Ar, CH_4 in the bulk PB and PS at different temperatures.[15] The diffusivity difference was the dominant factor for the permeability changes in PB and PS. Ar diffused 1000 times faster in PB, while the solubility, which is related to *H*, was of the same order at 20 °C. The exchange rate here shows similar trend with the bulk permeability result, and it strongly suggests that the exchange rate difference between the glassy PS and rubbery PB membranes is primarily due to the membrane fluidity difference. However, the exchange rate difference is not as significant as the difference of the bulk PS and PB polymer films. Similar solubility parameters of the IL may plasticize the PS membrane, and PEO coronas can act as hydrophobic moieties near membrane cores. Thus, we can expect that the PS membrane fluidity is enhanced in the nano-sized membrane in contact with the IL, 1-butylimidazole, and PEO coronas having low T_g, and hence the exchange rate was not reduced significantly when the membrane chemistry was changed from rubbery to glassy.

It has been shown that membrane fluidity control can effectively reduce permeation by introducing the glassy PS instead of the rubbery PB membrane. The membrane fluidity control has also been studied by Eisenberg and co-workers. They studied the effects of plasticizer amount on the permeability of molecules through the glassy membrane of polystyrene-*b*-poly(acrylic acid) polymersomes.[16,17] The plasticizer dioxane can partition into the PS membrane, and the permeability increased as the dioxane content increased. The proton diffusivity increased by an order of magnitude as the dioxane content in the solution increased from 7 to 14 vol %. Here, however, the membrane fluidity was controlled by changing the temperature in the range of 25 °C < *T* < 100 °C Then, the permeation rate changes were monitored in order to see the transition temperature of PS membrane of PS–PEO polymersome based on the Arrhenius plot of the escape rate ($1/\tau_i$).

The PFG-NMR experiments were conducted at different temperatures with PS–PEO(10–2) and PS–PEO(18–3.6). The echo-decay curves of 1-butylimidazole in PS–

PEO(18–3.6) solution are shown in Figure B–5 as an example of the temperature dependent echo-decay curve evolution. In both polymersome systems, the difference of the final plateaus increases. Since the molecules diffuse faster as the temperature increases, and lower observed molecules remain in the polymersome interior as the diffusion time, Δ, increases. Due to noise, some of data were truncated as can be seen in Figures B–5b, c, and d. Experimental data at different temperatures were also fitted with the two-site exchange model, and the Arrhenius plot of $1/\tau_i$ is shown in Figure B–6. It is clear that $1/\tau_i$ increases as the temperature increases, and at 36 °C, $1/\tau_i$ reaches 1.8 s^{-1} for PS–PEO(10–2), and 1.9 s^{-1} for PS–PEO(18–3.6) at 58 °C. Theses $1/\tau_i$ values are comparable through the rubbery PB–PEO(9–3) ($1/\tau_i$ reaches to 2.5 s^{-1}). In the Arrhenius plot, there may be suggested breakpoint, where the slope of $1/\tau_i$ becomes slightly steeper at higher temperatures. Though more experiments are required to find the relation between the breakpoint highlighted by arrows in Figure B–6 and T_g, it is interesting that the data points at 36 °C for PS–PEO(10–2) and 47 °C for PS–PEO(18–3.6) correspond well with the onset of transition temperature (~ 45 °C) of PS–PEO(20–5) micelle solutions, as measured by fluorescence spectroscopy.[6] At temperatures below the breakpoint (T_{break}), the apparent activation energy (E_a) is 10 – 20 kJ/mol, whereas above T_{break}, E_a increases to 40 – 50 kJ/mol. Assuming that the solubility of 1-butylimidazole in the PS membranes is not changed too much, the slope changes can be explained by the movement of the molecules through the free volume below T_g, where lower activation energy is necessary compared to the penetration through the rubbery chains above T_g. Extra frozen free volume increases as temperature decreases further below T_g, and leads to higher mobility of tracer molecules.[18,19] Frick *et al.* showed diffusivity of Aberchrome 540 dye (AB) through the T_g in PS/toluene solution by forced Rayleigh scattering technique. There was an abrupt change at the T_g of PS/toluene, with a jump of E_a upon heating.[19] Yasuda *et al.* also demonstrated the gas (He, CO_2, O_2, Ar, N_2) permeability through poly(acrylonitrile-*co*-methyl acrylate) film (T_g = 65 °C).[20] In the Arrhenius plot, the slope was changed for all gases except He at the T_g of the polymer from

E_a ~ 26 kJ/mol (below T_g) to E_a ~ 63 kJ/mol (above T_g). Similar Arrhenius plots of diffusivity and permeability have been observed for other small molecules.[21,22]

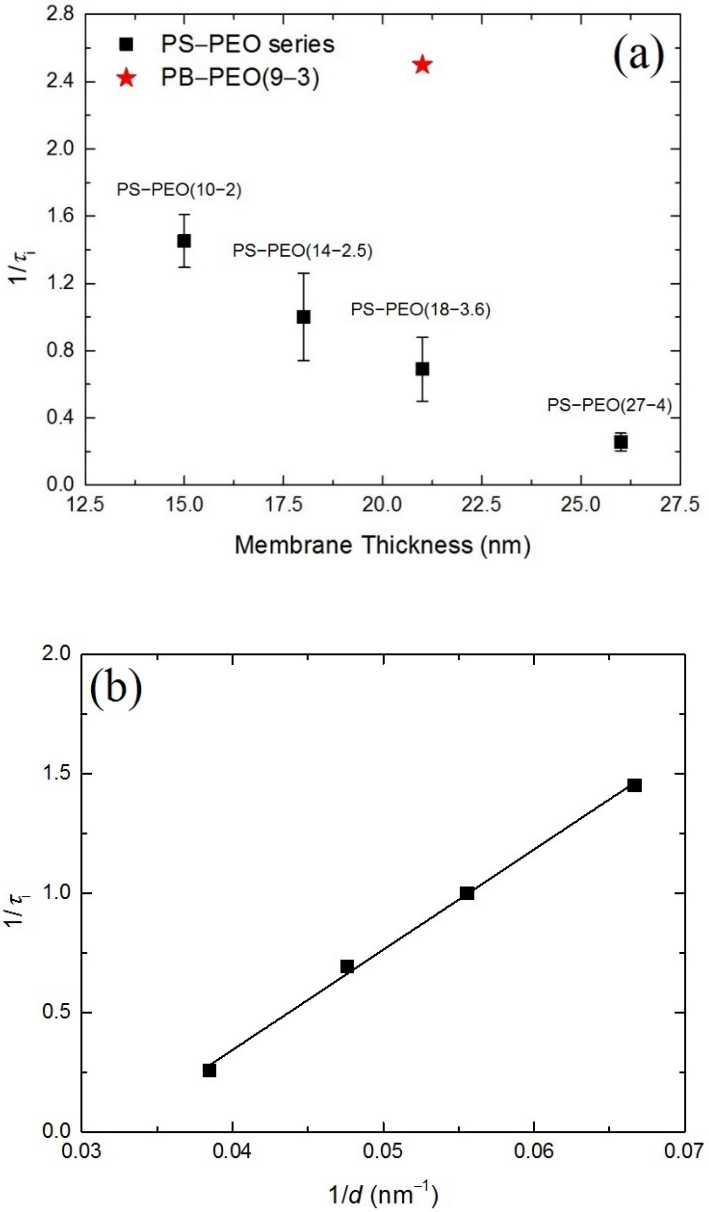

Figure B–4. (a) The membrane thickness dependence of the escape rate ($1/\tau_i$) of 1-butylimidazole through PS–PEO polymersomes at 25 °C. ■ refers to the data of PS–PEO(10–2) (d = 15 nm), PS–PEO(14–2.5) (d = 18 nm), PS–PEO(18–3.6) (d = 21 nm), and PS–PEO(27–4) (d = 26 nm), and ★ refers to the data of PB–PEO(9–3) (d = 21 nm). (b) The escape rate ($1/\tau_i$) versus $1/d$. The solid line is a linear fit ($(1/\tau_i) = 42.03 - 1.34 \times (1/d)$, $R = 1$).

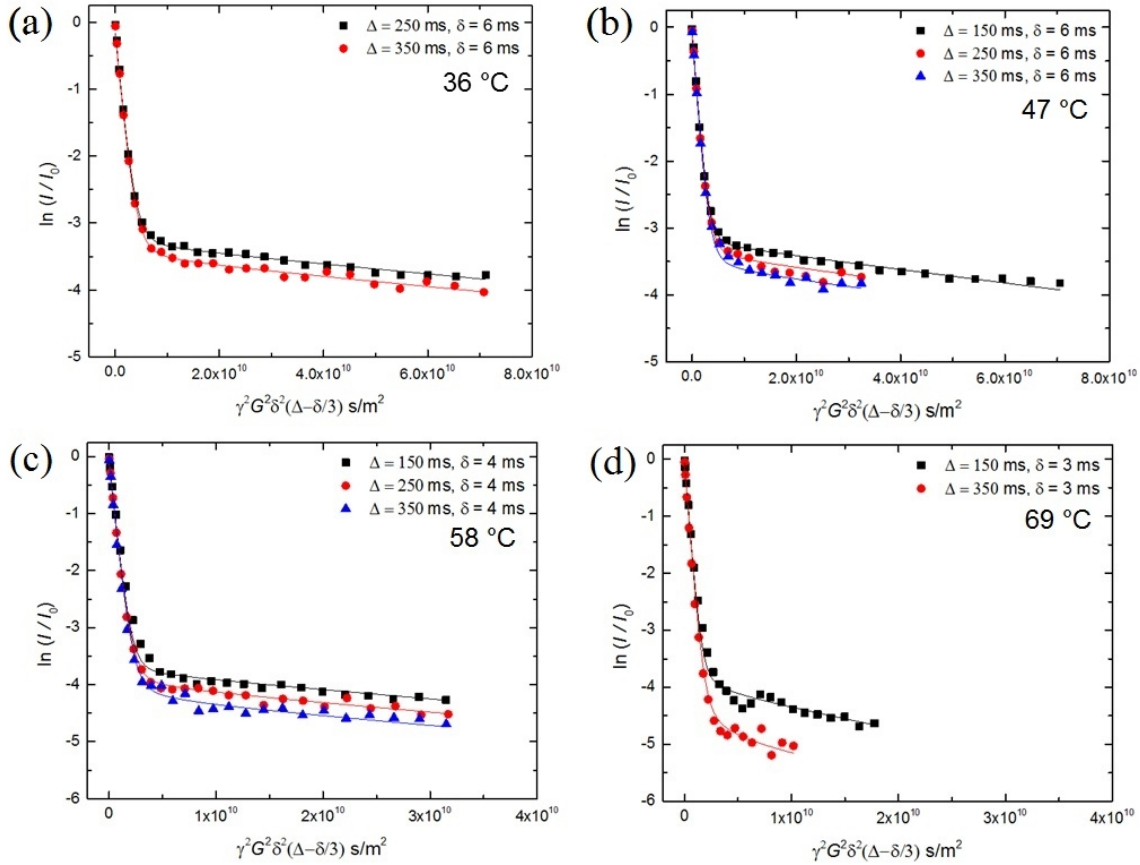

Figure B–5. Experimental data at various temperatures and fitted echo curve of the proton from 1-butylimidazole in the polymersome solution of PS–PEO(18–3.6) with Δ = 150, 250, 350 ms. The data were fitted using two-site exchange model.

In this chapter, the permeability was controlled by modifying the polymersome membrane, which can change the mobility of the membranes. The molecular exchange rate was monitored by using PFG-NMR technique. By employing glassy PS membrane, the molecular exchange was reduced by a factor of 3 for the same polymersome size and membrane thickness. However, the exchange rate through the glassy membrane can be tuned simply by changing temperature above the T_g of the membrane. T_g of the nanosize polymersome membrane was inferred from the Arrhenius plot of the escape rate of 1-butylimidazole. The Arrhenius plot showed similar trend with other permeation studies, and the transition points were well corresponded to the transition of PS–PEO micelles in

the IL. These permeability studies will provide essential information on designing polymersome reactors because the key of the polymersome nanoreactor is the molecular transport behavior. Furthermore, the membrane fluidity control can be applied to the drug delivery at a specific temperature.

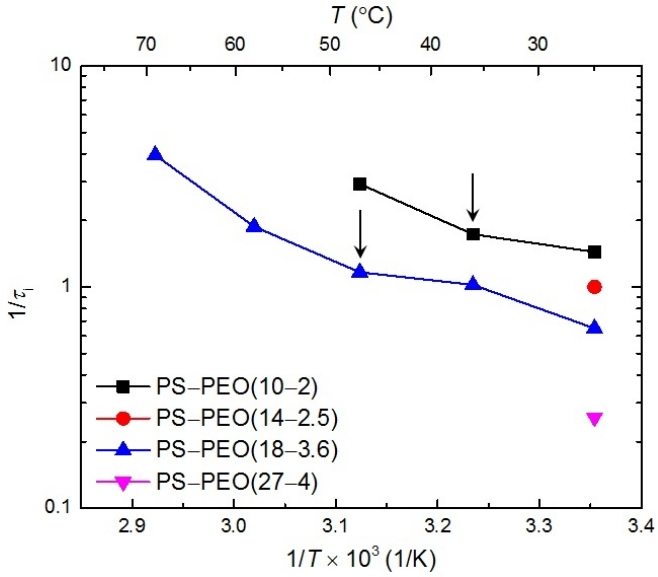

Figure B–6. Arrhenius plot of the escape rate ($1/\tau_i$) of 1-butylimidazole through PS–PEO polymersomes at 25 °C, 36 °C, 47 °C, 58 °C, 69 °C. The NMR samples were equilibrated at each temperature for 30 min before the measurement. The arrows indicate the transition points that might be related to T_g of PS membranes.

References

1. Narkwiboonwong, P.; Tumcharern, G.; Potisatityuenyong, A.; Wacharasindhu, S.; Sukwattanasinitt, M. *Talanta* **2011**, *83*, 872–878.
2. Yu, S.; Azzam, T.; Rouiller, I.; Eisenberg, A. *J. Am. Chem. Soc.* **2009**, *131*, 10557–10566.
3. Kim, K. T.; Cornelissen, J. J. L. M.; Nolte, R. J. M.; van Hest, J. C. M. *Adv. Mater.* **2009**, *21*, 2787–2791.
4. Meeuwissen, S. A.; Kim, K. T.; Chen, Y.; Pochan, D. J.; van Hest, J. C. M. *Angew. Chem. Int. Ed.* **2011**, *50*, 7070–7073.
5. Plazek, D. J.; O'Rourke, V. M. *J. Polym. Sci. A–2 Polym. Phys.* **1971**, *9*, 209–243.
6. Mok, M. M.; Lodge, T. P. *J. Polym. Sci. B Polym. Phys.***2012**, *50*, 500–515.
7. Wu, D.; Chen, A.; Johnson, C. S. *J. Magn. Reson.* **1995**, *115*, 260–264.
8. Raiford, D. S.; Fisk, C. L.; Becker, E. D. *Anal. Chem.* **1979**, *51*, 2050–2051.
9. Linders, J.; Mayer, C.; Sekine, T.; Hoffmann, H. *J. Phys. Chem. B* **2012**, *116*, 11459–11465.
10. Meli, L.; Santiago, J. M.; Lodge, T. P. *Macromolecules* **2010**, *43*, 2018–2027.
11. Shannon, M. S.; Bara, J. E. *Ind. Eng. Chem. Res.* **2011**, *50*, 8665–8677.
12. Leson, A.; Hauschild, S.; Rank, A.; Neub, A.; Schubert, R.; Forster, S.; Mayer, C. *Small* **2007**, *3*, 1074–1083.
13. Bai, Z.; Zhao, B.; Lodge, T. P. *J. Phys. Chem. B* **2012**, *116*, 8282–8289.
14. Battaglia, G.; Ryan, A. J.; Tomas, S. *Langmuir* **2006**, *22*, 4910–4913.
15. Rein, D. H.; Baddour, R. F.; Cohen, R. E. *J. Appl. Polym. Sci.* **1992**, *45*, 1223–1227.
16. Choucair, A.; Soo, P. L.; Eisenberg, A. *Langmuir* **2005**, *21*, 9308–9313.
17. Wu, J.; Eisenberg, A. *J. Am. Chem. Soc.* **2006**, *128*, 2880–2884.
18. Ramesh, N.; Davis, P. K.; Zielinski, J. M.; Danner, R. P.; Duda, J. L. *J. Polym. Sci. B Polym. Phys.***2011**, *49*, 1629–1644.

19. Frick, T. S.; Huang, W. J.; Tirrell, M.; Lodge, T. P. *J. Polym. Sci. B Polym. Phys.***1990**, *28*, 2629–2649.

20. Yasuda, H.; Hirotsu, T. *J. Appl. Polym. Sci.* **1977**, *21*, 105–112.

21. Ehlich, D.; Sillescu, H. *Macromolecules* **1990**, *23*, 1600–1610.

22. Ashworth, A. J.; Wickham, M. D. *J. Memb. Sci.* **1987**, *34*, 225–240.